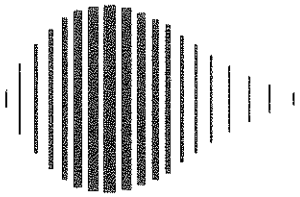

NATIONAL CENTER FOR EARTHQUAKE
ENGINEERING RESEARCH
State University of New York at Buffalo

OPTIMAL CONTROL OF NONLINEAR FLEXIBLE STRUCTURES

by

J.N. Yang, F.X. Long and D. Wong
Department of Civil, Mechanical and Environmental Engineering
The George Washington University
Washington, D.C. 20052

Technical Report NCEER-88-0002

January 22, 1988

This research was conducted at The George Washington University and was partially supported by the National Science Foundation under Grant No. ECE 86-07591.

NOTICE

This report was prepared by The George Washington University as a result of research sponsored by the National Center for Earthquake Engineering Research (NCEER) and the National Science Foundation. Neither NCEER, associates of NCEER, its sponsors, The George Washington University, nor any person acting on their behalf:

a. makes any warranty, express or implied, with respect to the use of any information, apparatus, methods, or process disclosed in this report or that such use may not infringe upon privately owned rights; or

b. assumes any liabilities of whatsoever kind with respect to the use of, or for damages resulting from the use of, any information, apparatus, method or process disclosed in this report.

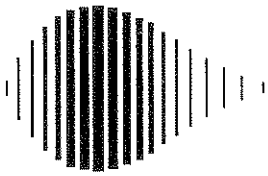

OPTIMAL CONTROL OF NONLINEAR FLEXIBLE STRUCTURES

by

J.N. Yang[1], F.X. Long[2] and D. Wong[3]

January 22, 1988

Technical Report NCEER-88-0002

NCEER Contract No. 87-2004

NSF Master Contract Number ECE 86-07591

and

NSF Grant No. ECE 85-21496

1 Professor, Dept. of Civil, Mechanical and Environmental Engineering, The George Washington University
2 Visiting Scholar, Dept. of Civil, Mechanical and Environmental Engineering, The George Washington University
3 Graduate Student, Dept. of Civil, Mechanical and Environmental Engineering, The George Washington University

NATIONAL CENTER FOR EARTHQUAKE ENGINEERING RESEARCH
State University of New York at Buffalo
Red Jacket Quadrangle, Buffalo, NY 14261

ABSTRACT

Three optimal control algorithms are proposed for reducing oscillations of flexible nonlinear structures subjected to general stochastic dynamic loads, such as earthquakes, waves, winds, etc. The optimal control forces are determined analytically by minimizing a time dependent quadratic performance index, and nonlinear equations of motion are solved using the Wilson-θ numerical procedures.

The optimal control algorithms developed for applications to nonlinear structures are referred to as the instantaneous optimal control algorithms, including the instantaneous optimal open-loop control algorithm, instantaneous optimal closed-loop control algorithm, and instantaneous optimal closed-open-loop control algorithm. These optimal algorithms are computationally efficient and suitable for on-line implementation of active control systems to realistic nonlinear structures. Numerical examples are worked out to demonstrate the applications of these optimal control algorithms to nonlinear structures. In particular, control of structures undergoing inelastic deformations under strong earthquake excitations are illustrated. The advantage of using combined passive/active control systems is also demonstrated.

ACKNOWLEDGEMENT

This research is supported by National Science Foundation Grant No. NSF-ECE-85-21496 and National Center For Earthquake Engineering Research Grant No. NCEER-87-2004.

TABLE OF CONTENTS

LIST OF FIGURES

LIST OF FIGURES (Continued)

LIST OF FIGURES (Continued)

LIST OF FIGURES (Continued)

LIST OF TABLES

I. INTRODUCTION

To improve the reliability and safety of tall buildings under strong earthquakes, the use of protective systems, such as passive or active control devices, has received considerable attention [e.g., 1-24]. These control systems have been shown theoretically and in some cases experimentally to be effective in safeguarding structural integrity. Numerous studies have been conducted for applications of passive control systems, such as lead-core rubber base isolators, tuned mass dampers, etc., and in some cases these passive control systems have been installed in representative buildings. While passive control systems are effective in some circumstances, they also suffer from a number of limitations, in particular the transient nature of strong earthquakes. As a result, active control systems, such as active mass dampers, active tendon systems, gas pulse generators, etc., whose performance depends on the supply of external energy, have been investigated intensively in the last decade mostly in the theoretical aspects. It is only until recently that experimental studies of active control systems have been realistically conducted. Likewise, the study of possible use of combined passive/active control systems is currently being initiated.

In reality, many tall buildings undergo large deformation or yielding when subjected to strong earthquake ground motions, and hence exhibit nonlinear or inelastic behavior. Consequently, active control systems may operate in the nonlinear range of motion for tall buildings. Further, for the combined use of passive/active control systems, passive devices, such as rubber base isolators, always exhibit large deformation and inelastic behavior, leading to nonlinear equations of motion for the entire structural system. Hence, the active control system should be capable of dealing with nonlinear structures.

Traditionally, active control has been applied to linear structures, and control theories for nonlinear systems are very limited. In an attempt to control nonlinear structures, active pulse control has been investigated recently in Refs. 1-3. In using active pulse control, several variables should be determined from the control algorithm, including the time at which pulses should be applied, the magnitude of each pulse, the pulse shape and duration, etc. In general, the pulse shape and duration are given because of limitations of control devices. Pulses usually are triggered when the response reaches certain levels [1-3]. The determination of pulse magnitude is important in order to achieve given control efficiency. When the pulse magnitude is too small, the effectiveness of active control will be insignificant. However, if the pulse magnitude is too large, the structure (or system) may become unstable or the structural response may be worse than that without control. In Ref. 1, the pulse magnitude is chosen to be proportional to some power of the response velocity, whereas the proportional constant is selected empirically. Given a selected proportional constant, the stability condition for the structure is examined [1]. This type of control is non-optimal.

In Ref. 2, it is assumed that the structural motion consists of stochastic components superimposed on top of a deterministic component. The pulse magnitudes are determined to minimize the deterministic component of the system response over a relatively short time segment after pulses are triggered. The optimal control algorithm is developed utilizing the model analysis of the structure, and hence it is applicable to linear structures. However, such a control algorithm can be used for control of nonlinear structures provided that reasonable equivalent linear properties can be used to represent nonlinear structures satisfactorily. In Ref. 3, the response of a SDOF nonlinear structure at every time instant t is monitored, and the

response at the next time interval $t+\Delta t$ is estimated. If the estimated response at $t+\Delta t$ exceeds a specified level, a pulse is triggered. Then, the magnitude of the pulse is estimated such that the response at $t+\Delta t$ is brought back to the specified level. The estimation of the pulse magnitude can be made using the initial conditions at time t and the specified response at $t+\Delta t$. Such a control algorithm again is non-optimal, and it is, in effect, an approximate bounded state control algorithm.

In this paper we proposed three optimal control algorithms applicable to flexible nonlinear structures, including inelastic structures, subjected to general dynamic loads, deterministic or stochastic. These include the instantaneous optimal closed-loop control algorithm, instantaneous optimal open-loop control algorithm and instantaneous optimal closed-open loop control algorithm. These optimal control algorithms are simple and reliable for on-line control operations and they are effective in mitigating structural oscillation.

Unlike pulse control, control forces considered herein are continuous in time and active control can be implemented by electrohydraulic servomechanisms along with tendons or mass dampers, referred to as active tendon control system and active mass damper, respectively. Particular emphasis is placed on the mitigation of the inelastic response of flexible tall buildings subjected to strong earthquakes. Numerical examples are worked out to demonstrate the applications of these optimal control algorithms to nonlinear structures. The advantage of using combined passive/active control systems is also illustrated.

II. FORMULATION

For simplicity, consider a one-dimensional nonlinear building structure implemented by an active tendon control system as shown in Fig. 1. The structure is idealized by an n-degree-of-freedom system and subjected to a one-dimensional earthquake ground acceleration $\ddot{X}_0(t)$. The matrix equation of motion can be expressed as

$$\underline{M}\,\ddot{\underline{Y}}(t) + \underline{C}[\dot{\underline{Y}}(t)]\,\dot{\underline{Y}}(t) + \underline{K}[\underline{Y}(t)]\,\underline{Y}(t) = -\underline{M}\,\underline{v}\,\ddot{X}_0(t) + \underline{H}\,\underline{U}(t) \qquad (1)$$

in which $\underline{Y}(t)$ is an n vector denoting the displacements of the structure relative to the moving base, $\underline{v}$ is a unit vector of order n, i.e., $\underline{v}$ = [1, 1, 1,..., 1]', $\underline{U}(t)$ is a r-dimensional control vector, and $\underline{H}$ is a (nxr) matrix denoting the location of r controllers. A super dot ($\cdot$) represents differentiation with respect to time, and an under bar denotes a vector or matrix. In Eq. (1), $\underline{M}$ is a (nxn) constant mass matrix, $\underline{C}[\dot{\underline{Y}}(t)]$ is a (nxn) nonlinear damping matrix, and $\underline{K}[\underline{Y}(t)]$ is a (nxn) nonlinear stiffness matrix. Both $\underline{C}[\dot{\underline{Y}}(t)]$ and $\underline{K}[\underline{Y}(t)]$ are general functions of velocity vector $\dot{\underline{Y}}(t)$ and displacement vector $\underline{Y}(t)$, respectively.

2.1 Solution of Nonlinear Equation of Motion

The matrix equation of motion, Eq. (1), can also be written as

$$\underline{M}\,\ddot{\underline{Y}}(t) + \underline{F}_D(t) + \underline{F}_s(t) = -\underline{M}\,\underline{v}\,\ddot{X}_0(t) + \underline{H}\,\underline{U}(t) \qquad (2)$$

in which $\underline{F}_D(t)$ is an n vector denoting the damping force and $\underline{F}_s(t)$ is an n vector denoting the stiffness restoring force, all at time t. Both $\underline{F}_D(t)$ and $\underline{F}_s(t)$ are general nonlinear functions of $\dot{\underline{Y}}(t)$ and $\underline{Y}(t)$, respectively, i.e., $\underline{F}_D(t) = \underline{F}_D[\dot{\underline{Y}}(t)]$ and $\underline{F}_s(t) = \underline{F}_s[\underline{Y}(t)]$.

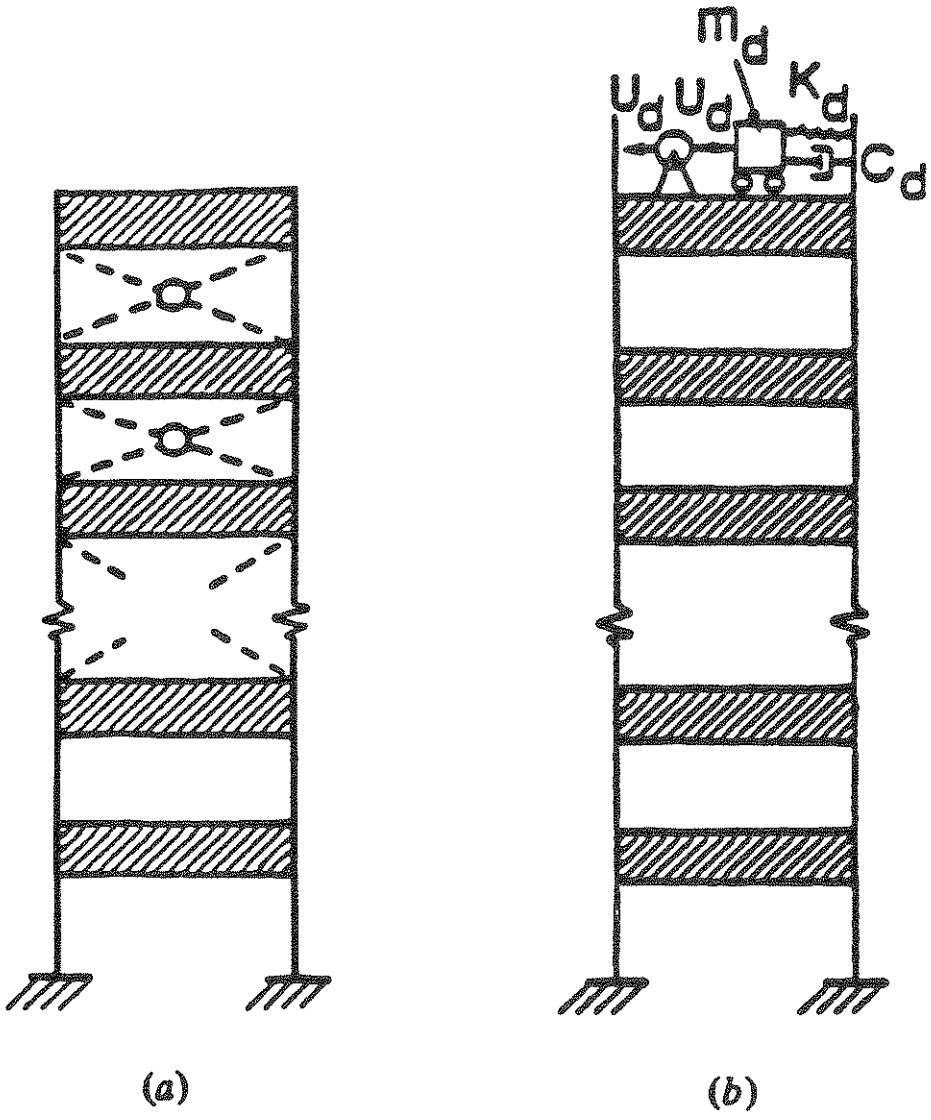

Fig. 1: Structural Model of a Multi-Story Building with Active Control System; (a) Active Tendon Control System; (b) Active Mass Damper.

For convenience of step-by-step numerical integration with a step size Δt, the nonlinear terms in Eq. (2) are approximated by

$$\left.\begin{aligned} \underset{\sim}{F}_D(t) &\approx \underset{\sim}{F}_D(t-\Delta t) + \underset{\sim}{C}^*(t-\Delta t)\,[\dot{\underset{\sim}{Y}}(t) - \dot{\underset{\sim}{Y}}(t-\Delta t)] \\ \underset{\sim}{F}_s(t) &\approx \underset{\sim}{F}_s(t-\Delta t) + \underset{\sim}{K}^*(t-\Delta t)\,[\underset{\sim}{Y}(t) - \underset{\sim}{Y}(t-\Delta t)] \end{aligned}\right\} \qquad (3)$$

in which $\underset{\sim}{C}^*(t-\Delta t)$ and $\underset{\sim}{K}^*(t-\Delta t)$ are (nxn) matrices evaluated at $t-\Delta t$. The i-jth elements of $\underset{\sim}{C}^*(t-\Delta t)$ and $\underset{\sim}{K}^*(t-\Delta t)$ matrices, denoted by $C^*_{ij}(t-\Delta t)$ and $K^*_{ij}(t-\Delta t)$, respectively, are the influence coefficients given by [e.g., 25, 26]

$$\left.\begin{aligned} C^*_{ij}(t-\Delta t) &= \frac{\partial F_{Di}(t-\Delta t)}{\partial \dot{y}_j(t-\Delta t)} \\ K^*_{ij}(t-\Delta t) &= \frac{\partial F_{si}(t-\Delta t)}{\partial y_j(t-\Delta t)} \end{aligned}\right\} \qquad (4)$$

in which $F_{Di}(t-\Delta t)$ and $F_{si}(t-\Delta t)$ are the ith elements of vectors $\underset{\sim}{F}_D(t-\Delta t)$ and $\underset{\sim}{F}_s(t-\Delta t)$, respectively, whereas $\dot{y}_j(t-\Delta t)$ and $y_j(t-\Delta t)$ are the jth element of the response vectors $\dot{\underset{\sim}{Y}}(t-\Delta t)$ and $\underset{\sim}{Y}(t-\Delta t)$, respectively. The influence coefficients, $C^*_{ij}(t-\Delta t)$ and $k^*_{ij}(t-\Delta t)$, represent the tangent damping and tangent stiffness at $t-\Delta t$, respectively, as shown in Fig. 2.

Thus, the matrix equation of motion, Eq. (2), can be expressed conveniently as

$$\underset{\sim}{M}\,\ddot{\underset{\sim}{Y}}(t) + \underset{\sim}{F}_D(t-\Delta t) + \underset{\sim}{C}^*(t-\Delta t)[\dot{\underset{\sim}{Y}}(t) - \dot{\underset{\sim}{Y}}(t-\Delta t)] + \underset{\sim}{F}_s(t-\Delta t)$$

$$+ \underset{\sim}{K}^*(t-\Delta t)\,[\underset{\sim}{Y}(t) - \underset{\sim}{Y}(t-\Delta t)] = -\underset{\sim}{M}\,\underset{\sim}{v}\,\ddot{X}_0(t) + \underset{\sim}{H}\,\underset{\sim}{U}(t) \qquad (5)$$

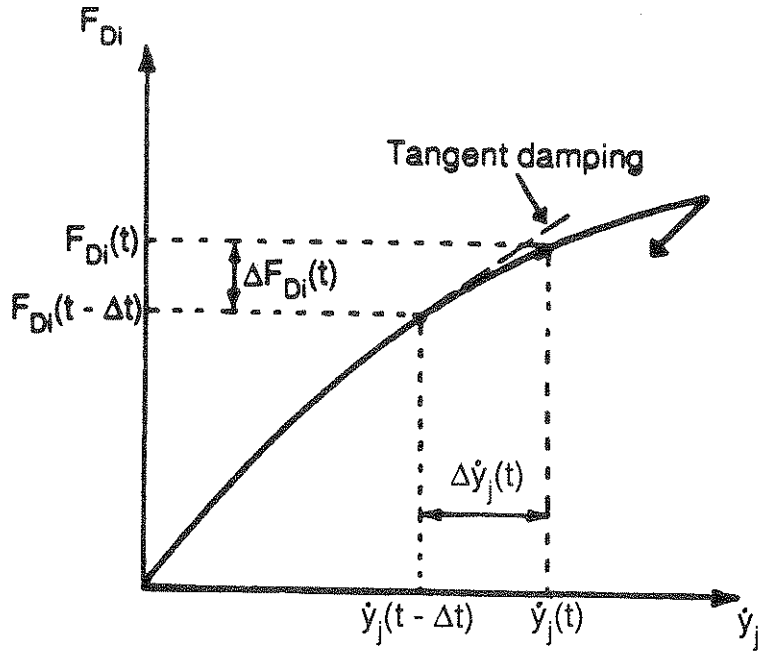

(*a*)

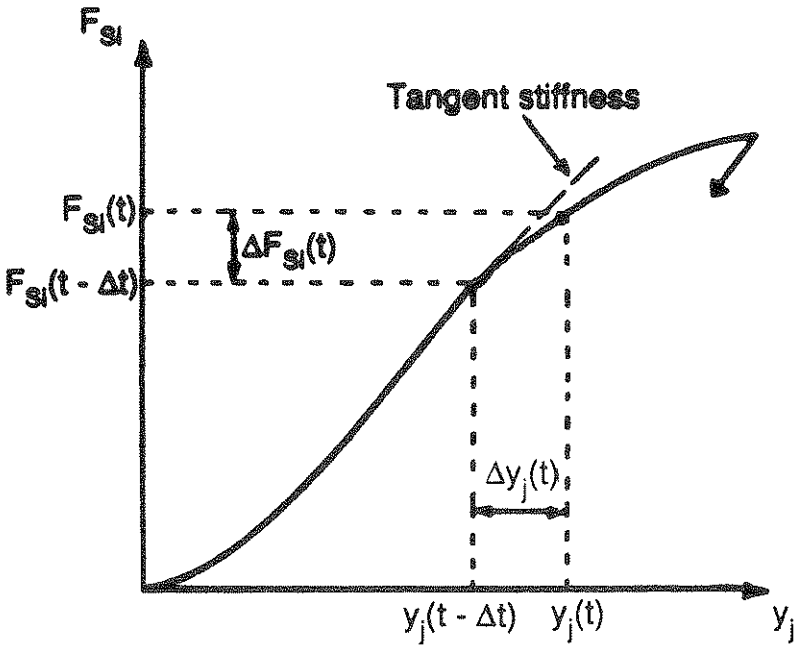

(*b*)

Fig. 2: Nonlinear Influence Coefficients: (a) Nonlinear Viscous Damping Coefficient C_{ij}^*; (b) Nonlinear Stiffness Coefficient K_{ij}^*.

Using the Wilson-θ numerical integration procedure for the solution of nonlinear equations, Eq. (5), the 2n state vector $\underset{\sim}{Z}(t)$

$$\underset{\sim}{Z}(t) = \begin{bmatrix} \underset{\sim}{Y}(t) \\ \hline \dot{\underset{\sim}{Y}}(t) \end{bmatrix} \tag{6}$$

can be expressed in terms of the response state vector $\underset{\sim}{Z}(t-\Delta t)$, nonlinear damping vector $\underset{\sim}{F}_D(t-\Delta t)$, nonlinear stiffness vector $\underset{\sim}{F}_s(t-\Delta t)$, earthquake base excitation $\ddot{X}_0(t-\Delta t)$, and the control vector $\underset{\sim}{U}(t-\Delta t)$, all at time $t-\Delta t$, as well as the control vector $\underset{\sim}{U}(t)$ and the earthquake base excitation $\ddot{X}_0(t)$ at time t as follows (see Appendix for detail derivations):

$$\underset{\sim}{Z}(t) = \underset{\sim}{D}^*(t-\Delta t) + \underset{\sim}{A}_1 \ddot{X}_0(t) + \underset{\sim}{A}_2\, \underset{\sim}{U}(t) \tag{7}$$

in which

$$\begin{aligned} \underset{\sim}{D}^*(t-\Delta t) = {} & \underset{\sim}{A}_3\, \underset{\sim}{Z}(t-\Delta t) + \underset{\sim}{A}_4[\underset{\sim}{F}_D(t-\Delta t) + \underset{\sim}{F}_s(t-\Delta t)] \\ & + \underset{\sim}{A}_5\, \ddot{X}_0(t-\Delta t) + \underset{\sim}{A}_6\, \underset{\sim}{U}(t-\Delta t) \end{aligned} \tag{8}$$

In Eqs. (7) and (8), $\underset{\sim}{A}_j$ for j=1,2,...,6 are vectors or matrices given in the following.

$$\left.\begin{aligned} \underset{\sim}{A}_1 &= \theta^{-2} \begin{bmatrix} \underset{\sim}{T}_1 \\ \hline \frac{3}{\Delta t}\, \underset{\sim}{T}_1 \end{bmatrix} \quad ; \quad \underset{\sim}{A}_2 = \theta^{-2} \begin{bmatrix} \underset{\sim}{T}_2 \\ \hline \frac{3}{\Delta t}\, \underset{\sim}{T}_2 \end{bmatrix} \\ \underset{\sim}{A}_3 &= \left[\begin{array}{c:c} \underset{\sim}{I}_1 & \theta^{-2} \underset{\sim}{E}\, \underset{\sim}{T}_3 \\ \hline \underset{\sim}{0} & \underset{\sim}{I}_1 + \theta^{-2} \underset{\sim}{E}\, \underset{\sim}{T}_4 \end{array}\right] \quad ; \quad \underset{\sim}{A}_4 = \theta^{-2} \begin{bmatrix} \underset{\sim}{E}\, \underset{\sim}{T}_5 \\ \hline \underset{\sim}{E}\, \underset{\sim}{T}_6 \end{bmatrix} \\ \underset{\sim}{A}_5 &= -\theta^{-2} \begin{bmatrix} \underset{\sim}{E}\, \underset{\sim}{T}_7 \\ \hline \underset{\sim}{E}\, \underset{\sim}{T}_8 \end{bmatrix} \underset{\sim}{M}\, \underset{\sim}{v} \quad ; \quad \underset{\sim}{A}_6 = \theta^{-2} \begin{bmatrix} \underset{\sim}{E}\, \underset{\sim}{T}_7 \\ \hline \underset{\sim}{E}\, \underset{\sim}{T}_8 \end{bmatrix} \underset{\sim}{H} \end{aligned}\right\} \tag{9}$$

in which $\underset{\sim}{I}_1$ is an (nxn) identity matrix, θ is chosen to be greater than 1.37, and

$$\left.\begin{aligned}
&\underset{\sim}{T}_1 = -\underset{\sim}{E}\,\underset{\sim}{M}\,\underset{\sim}{v},\quad \underset{\sim}{T}_2 = \underset{\sim}{E}\,\underset{\sim}{H}\ ,\quad \underset{\sim}{T}_3 = (6/\Delta t)\underset{\sim}{M} + 3\theta\underset{\sim}{C}^* + \Delta t(\theta^2-1)\,\underset{\sim}{K}^*\\
&\underset{\sim}{T}_4 = -3\,\underset{\sim}{K}^*,\qquad \underset{\sim}{T}_5 = -(3\underset{\sim}{I}_1+\underset{\sim}{S}_1),\quad \underset{\sim}{T}_6 = -(6/\Delta t)\underset{\sim}{I}_1 - \underset{\sim}{S}_2\\
&\underset{\sim}{T}_7 = 2\,\underset{\sim}{I}_1 + \underset{\sim}{S}_1,\quad \underset{\sim}{T}_8 = (3/\Delta t)\underset{\sim}{I}_1 + \underset{\sim}{S}_2\\
&\underset{\sim}{E} = \left[\frac{6}{(\theta\Delta t)^2}\,\underset{\sim}{M} + \frac{3}{\theta\Delta t}\,\underset{\sim}{C}^* + \underset{\sim}{K}^*\right]^{-1}\\
&\underset{\sim}{S}_1 = \left[\Delta t\,(1.5\theta-1)\,\underset{\sim}{C}^* + 0.5(\Delta t)^2(\theta^2-\theta)\,\underset{\sim}{K}^*\right]\underset{\sim}{M}^{-1}\\
&\underset{\sim}{S}_2 = \left[3(\theta-1)\,\underset{\sim}{C}^* + \Delta t\theta(\theta-1.5)\,\underset{\sim}{K}^*\right]\underset{\sim}{M}^{-1}
\end{aligned}\right\} \quad (10)$$

In Eq.(10), the argument $t-\Delta t$ for influence coefficient matrices $\underset{\sim}{C}^*$ and $\underset{\sim}{K}^*$ has been omitted for simplicity. For a particular case in which damping is linear viscous damping, i.e.,

$$\underset{\sim}{F}_D(t-\Delta t) = \underset{\sim}{C}\,\dot{\underset{\sim}{Y}}(t-\Delta t) \quad (11)$$

where $\underset{\sim}{C}$ is a (nxn) constant matrix, Eq. (8) becomes

$$\underset{\sim}{D}^*(t-\Delta t) = \underset{\sim}{A}_7\,\underset{\sim}{Z}(t-\Delta t) + \underset{\sim}{A}_4\,\underset{\sim}{F}_s(t-\Delta t) + \underset{\sim}{A}_5\ddot{X}_0(t-\Delta t) + \underset{\sim}{A}_6\,\underset{\sim}{U}(t-\Delta t) \quad (12)$$

in which

$$\underset{\sim}{A}_7 = \left[\begin{array}{c|c} \underset{\sim}{I}_1 & \theta^{-2}\underset{\sim}{E}\,\underset{\sim}{T}_9 \\ \hline \underset{\sim}{0} & \underset{\sim}{I}_1+\theta^{-2}\underset{\sim}{E}\,\underset{\sim}{T}_{10} \end{array}\right] \quad (13)$$

$$\underset{\sim}{T}_9 = (6/\Delta t)\underset{\sim}{M} + \left[3(\theta-1)\underset{\sim}{I}_1 - \underset{\sim}{S}_1\right]\underset{\sim}{C} + \Delta t(\theta^2-1)\underset{\sim}{K}^*(t-\Delta t)$$

$$\underset{\sim}{T}_{10} = -\left[(6/\Delta t)\underset{\sim}{I}_1 + \underset{\sim}{S}_2\right]\underset{\sim}{C} - 3\underset{\sim}{K}^*(t-\Delta t) \tag{14}$$

It follows from Eqs. (9)-(14) that $\underset{\sim}{A}_j$ for j=1,2,...,7 are functions of influence coefficient matrices $\underset{\sim}{C}^*(t-\Delta t)$ and $\underset{\sim}{K}^*(t-\Delta t)$ at time t-Δt. Hence, they are evaluated at t-Δt, i.e.,

$$\begin{aligned} &\underset{\sim}{A}_1 = \underset{\sim}{A}_1(t-\Delta t) \quad , \quad \underset{\sim}{A}_2 = \underset{\sim}{A}_2(t-\Delta t) \quad , \quad \underset{\sim}{A}_3 = \underset{\sim}{A}_3(t-\Delta t) \\ &\underset{\sim}{A}_4 = \underset{\sim}{A}_4(t-\Delta t) \quad , \quad \underset{\sim}{A}_5 = \underset{\sim}{A}_5(t-\Delta t) \quad , \quad \underset{\sim}{A}_6 = \underset{\sim}{A}_6(t-\Delta t) \\ &\underset{\sim}{A}_7 = \underset{\sim}{A}_7(t-\Delta t) \end{aligned} \tag{15}$$

Again, for simplicity of notation, the argument t-Δt for these vectors and matrices have been omitted.

2.2 Optimal Control Algorithms for Nonlinear Structures

Unlike linear systems, control theories for nonlinear structures, including inelastic structures, are not well developed [e.g., Refs. 1-3]. For linear systems, the quadratic performance index

$$J = \int_0^{t_f} [\underset{\sim}{Z}'(t)\ \underset{\sim}{Q}\ \underset{\sim}{Z}(t) + \underset{\sim}{U}'(t)\ \underset{\sim}{R}\ \underset{\sim}{U}(t)]dt \tag{16}$$

has been used to arrive at various classical optimal control theories. In Eq. (16), a prime denotes the transpose of a vector or matrix, t_f is the terminal time at which the state vector, $\underset{\sim}{Z}(t)$, will die down, and $\underset{\sim}{Q}$ and $\underset{\sim}{R}$ are weighting matrices denoting the relative importance between the response state vector $\underset{\sim}{Z}(t)$ and the control vector $\underset{\sim}{U}(t)$. Unfortunately, even for linear structures subjected to earthquake excitation, these classical

optimal control theories are not applicable as pointed out by Yang, et al [Refs. 13-15]. The reason is that these classical control theories require the prior knowledge of earthquake ground motion. Since earthquake ground acceleration is a random process, it is not known a priori.

While the earthquake ground motion is not know a priori, the base excitation of the building can be measured on-line real-time by installing sensors on the basement floor. In other words, at any particular time t, the base excitation record is available up to that time instant t. Such an important information has been utilized recently by Yang, et al to develop three new optimal control algorithms, referred to as instantaneous optimal control algorithms [Refs. 13-15]. Further, these three instantaneous optimal control algorithms have also been verified experimentally using a scale building model excited by simulated earthquakes on a shaking table [9].

A time dependent quadratic objective function J(t) was proposed to establish three instantaneous optimal control algorithms for linear structures [Refs. 13-15]

$$J(t) = \underset{\sim}{Z}'(t)\ \underset{\sim}{Q}\ \underset{\sim}{Z}(t) + \underset{\sim}{U}'(t)\ \underset{\sim}{R}\ \underset{\sim}{U}(t) \qquad (17)$$

The implication of minimizing the objective function above, Eq. (17), is that the performance index J(t) is minimized at every time instant t for all $0 \leq t \leq t_f$. Hence, the optimal control algorithms thus obtained are referred to as instantaneous optimal control algorithms [13-15].

For nonlinear structures, we propose the same time dependent objective function given in Eq. (17) with the constraints of the general equations of motion, Eq. (1) or (5). The general equations of motion for nonlinear structures have been solved numerically using the Wilson-θ method given by

Eqs. (7) and (8). Thus, we shall determine the optimal control vector $\underset{\sim}{U}(t)$ by minimizing the objective function J(t) given by Eq. (17) subjected to the constraint given by Eq. (7) as follows.

The Hamiltonian H is obtained by introducing a 2n-dimensional Lagrangian multiplier vector $\underset{\sim}{\lambda}(t)$ or co-state vector to the objective function,

$$H = \underset{\sim}{Z}'(t)\ \underset{\sim}{Q}\ \underset{\sim}{Z}(t) + \underset{\sim}{U}'(t)\ \underset{\sim}{R}\ \underset{\sim}{U}(t) + \underset{\sim}{\lambda}'\left\{\underset{\sim}{Z}(t) - \underset{\sim}{D}^{*}(t-\Delta t) - \underset{\sim}{A}_1\ \ddot{X}_0(t) - \underset{\sim}{A}_2\ \underset{\sim}{U}(t)\right\} \quad (18)$$

in which $\underset{\sim}{D}^{*}(t-\Delta t)$ is given by Eq. (8).

The necessary conditions for minimizing the performance index J(t) subjected to the constraint given by Eq. (7) are as follows

$$\frac{\partial H}{\partial \underset{\sim}{Z}} = 0 \quad , \quad \frac{\partial H}{\partial \underset{\sim}{U}} = 0 \quad , \quad \frac{\partial H}{\partial \underset{\sim}{\lambda}} = 0 \quad (19)$$

Substitution of Eq. (18) into Eq. (19) leads to the following three matrix equations

$$2\ \underset{\sim}{Q}\ \underset{\sim}{Z}(t) + \underset{\sim}{\lambda}(t) = 0 \quad (20)$$

$$2\ \underset{\sim}{R}\ \underset{\sim}{U}(t) - \underset{\sim}{A}_2'\ \underset{\sim}{\lambda}(t) = 0 \quad (21)$$

$$\underset{\sim}{Z}(t) = \underset{\sim}{D}^{*}(t-\Delta t) + \underset{\sim}{A}_1\ \ddot{X}_0(t) + \underset{\sim}{A}_2\ \underset{\sim}{U}(t) \quad (22)$$

Thus, the optimal control vector $\underset{\sim}{U}(t)$, the co-state vector $\underset{\sim}{\lambda}(t)$, and the response state vector $\underset{\sim}{Z}(t)$ can be obtained from Eqs. (20)-(22) as described in the following.

2.2.1 Instantaneous Optimal Open-Loop Control

Note that the control vector $\underset{\sim}{U}(t)$ is linearly proportional to the co-state vector $\underset{\sim}{\lambda}(t)$ at every time instant t as shown in Eq. (21). Assuming that the control vector $\underset{\sim}{U}(t)$, or the co-state vector $\underset{\sim}{\lambda}(t)$, is regulated by the measured earthquake ground motion without a feedback state vector $\underset{\sim}{Z}(t)$, i.e.,

$$\underset{\sim}{\lambda}(t) = \underset{\sim}{g}(t) \tag{23}$$

the optimal control algorithm thus obtained is referred to as the instantaneous optimal open-loop control algorithm. By use of Eq. (23), Eqs. (20)-(22) become

$$2\ \underset{\sim}{Q}\ \underset{\sim}{Z}(t) + \underset{\sim}{g}(t) = 0 \tag{24}$$

$$2\ \underset{\sim}{R}\ \underset{\sim}{U}(t) - \underset{\sim}{A}_2'\ \underset{\sim}{g}(t) = 0 \tag{25}$$

$$\underset{\sim}{Z}(t) = \underset{\sim}{D}^*(t-\Delta t) + \underset{\sim}{A}_1\ \ddot{X}_0(t) + \underset{\sim}{A}_2\ \underset{\sim}{U}(t) \tag{26}$$

The optimal control vector $\underset{\sim}{U}(t)$ can be obtained from Eqs. (24)-(26) as follows: (i) $\underset{\sim}{Z}(t)$ is eliminated by substituting Eq. (26) into Eq. (24), and (ii) the resulting $\underset{\sim}{g}(t)$ obtained from Eq. (24) is substituted into Eq. (25); with the result

$$\underset{\sim}{U}(t) = \underset{\sim}{L}\ \underset{\sim}{G}(t) \tag{27}$$

in which

$$\left.\begin{aligned} \underset{\sim}{L} &= -\left[\underset{\sim}{R} + \underset{\sim}{A}_2'\ \underset{\sim}{Q}\ \underset{\sim}{A}_2\right]^{-1}\ \underset{\sim}{A}_2'\ \underset{\sim}{Q} \\ \underset{\sim}{G}(t) &= \underset{\sim}{D}^*(t-\Delta t) + \underset{\sim}{A}_1\ \ddot{X}_0(t) \end{aligned}\right\} \tag{28}$$

As observed from Eqs. (27)-(28), the control vector at time t is regulated by the measured earthquake ground accelerations $\ddot{X}_0(t)$ and $\ddot{X}_0(t-\Delta t)$ at time t

and t-Δt, respectively, as well as the computed quantity $\underset{\sim}{D}^*(t-\Delta t)$ at time t-Δt, Eq. (8).

The response state vector $\underset{\sim}{Z}(t)$ under instantaneous optimal open-loop control is obtained by substituting Eq. (27) into Eq. (26),

$$\underset{\sim}{Z}(t) = \left[\underset{\sim}{I} - A_2 \left(\underset{\sim}{R} + \underset{\sim}{A}_2' \underset{\sim}{Q} \underset{\sim}{A}_2\right)^{-1} \underset{\sim}{A}_2' \underset{\sim}{Q} \right] \underset{\sim}{G}(t) \tag{29}$$

in which $\underset{\sim}{I}$ is a (2nx2n) identity matrix.

For the instantaneous optimal open-loop control algorithm obtained above, the response state vector $\underset{\sim}{Z}(t)$ for all time instants t is not measured, rather it is computed. It was found in the experimental program [Ref. 9] as well as analytical studies [Ref. 19] for linear structures that the control efficiency is vulnerable to system time delay. The control efficiency can be improved and the sensitivity with respective to time delay can be stabilized by measuring the response state vector $\underset{\sim}{Z}(t)$ for use in the computation of the control vector $\underset{\sim}{U}(t)$. In other words, the state vector $\underset{\sim}{Z}(t-\Delta t)$ appearing in $\underset{\sim}{D}^*(t-\Delta t)$ of Eq. (28) is measured rather than computed, see Eq. (8). In this paper, we also propose to measure the state vector $\underset{\sim}{Z}(t)$ for all t for the computation of $\underset{\sim}{D}^*(t-\Delta t)$. Such a control algorithm is referred to as the modified instantaneous optimal open-loop control algorithm.

2.2.2 Instantaneous Optimal Closed-Loop Control

For closed-loop control, the control vector $\underset{\sim}{U}(t)$, or the co-state vector $\underset{\sim}{\lambda}(t)$, is regulated by the feedback state vector $\underset{\sim}{Z}(t)$, i.e.,

$$\underset{\sim}{\lambda}(t) = \underset{\sim}{\Lambda}\ \underset{\sim}{Z}(t) \tag{30}$$

Substitution of Eq. (30) into Eq. (20) leads to the following expression,

$$(2\underset{\sim}{Q} + \underset{\sim}{\Lambda})\ \underset{\sim}{Z}(t) = 0 \tag{31}$$

For $\underset{\sim}{Z}(t) \neq 0$, the unknown matrix $\underset{\sim}{\Lambda}$ is obtained as

$$\underset{\sim}{\Lambda} = -2\underset{\sim}{Q} \tag{32}$$

Thus, the optimal closed-loop control vector $\underset{\sim}{U}(t)$ follows from Eqs. (21) and (32) as

$$\underset{\sim}{U}(t) = -\underset{\sim}{R}^{-1} \underset{\sim}{A}_2' \underset{\sim}{Q} \underset{\sim}{Z}(t) \tag{33}$$

and the response state vector is obtained by substituting Eq. (33) into Eq. (22),

$$\underset{\sim}{Z}(t) = \left[\underset{\sim}{I} + \underset{\sim}{A}_2 \underset{\sim}{R}^{-1} \underset{\sim}{A}_2' \underset{\sim}{Q} \right]^{-1} \underset{\sim}{G}(t) \tag{34}$$

in which $\underset{\sim}{G}(t)$ is given by Eq. (28). The control algorithm derived above is referred to as the instantaneous optimal closed-loop control algorithm.

It is important to notice that for the instantaneous optimal closed-loop control algorithm, the measurement of earthquake base acceleration $\ddot{X}_0(t)$ is not necessary. In other words, the control vector $\underset{\sim}{U}(t)$ is regulated only by the measured state vector $\underset{\sim}{Z}(t)$.

2.2.3 Instantaneous Optimal Closed-Open-Loop Control

Let the control vector $\underset{\sim}{U}(t)$, or the co-state vector $\underset{\sim}{\lambda}(t)$, be regulated by both the feedback response state vector $\underset{\sim}{Z}(t)$ and the measured base excitation $\ddot{X}_0(t)$, i.e.,

$$\underset{\sim}{\lambda}(t) = \tilde{\underset{\sim}{\Lambda}} \underset{\sim}{Z}(t) + \tilde{\underset{\sim}{q}}(t) \tag{35}$$

in which $\tilde{\underset{\sim}{\Lambda}}$ and $\tilde{\underset{\sim}{q}}$ are unknown matrix and vector, respectively, to be determined from Eqs. (20)-(22) as follows. Substituting Eq. (35) into Eq. (21) yields the expression for $\underset{\sim}{U}(t)$. Then, the resulting $\underset{\sim}{U}(t)$ is substituted into Eq. (22) leading to the following expression for $\underset{\sim}{Z}(t)$

$$\underline{Z}(t) = \underline{D}^{*}(t-\Delta t) + \underline{A}_1 \ddot{X}_0(t) + \frac{1}{2} \underline{A}_2 \underline{R}^{-1} \underline{A}_2' \left[\tilde{\underline{\Lambda}} \underline{Z}(t) + \tilde{\underline{g}}(t) \right] \qquad (36)$$

The term $2\underline{Q}\,\underline{Z}(t)$ in Eq. (20) is expressed as $\underline{Q}\,[\underline{Z}(t) + \underline{Z}(t)]$, and the first term of $\underline{Z}(t)$ is replaced by Eq. (36), whereas Eq. (35) is used for $\underline{\lambda}(t)$ in Eq. (20); with the result,

$$\left\{ \underline{Q} + \left[\frac{1}{2} \underline{Q} \underline{A}_2 \underline{R}^{-1} \underline{A}_2' + \underline{I} \right] \tilde{\underline{\Lambda}} \right\} \underline{Z}(t) + \left[\frac{1}{2} \underline{Q} \underline{A}_2 \underline{R}^{-1} \underline{A}_2' + \underline{I} \right] \tilde{\underline{g}}(t)$$

$$+ \underline{Q}\,\underline{G}(t) = 0 \qquad (37)$$

For $\underline{Z}(t) \neq 0$ and $\tilde{\underline{g}}(t) \neq 0$, one obtains the solutions for unknown matrix $\tilde{\underline{\Lambda}}$ and unknown vector $\tilde{\underline{g}}(t)$,

$$\tilde{\underline{\Lambda}} = -\left[\frac{1}{2} \underline{Q} \underline{A}_2 \underline{R}^{-1} \underline{A}_2' + \underline{I} \right]^{-1} \underline{Q} \qquad (38)$$

$$\tilde{\underline{g}}(t) = \tilde{\underline{\Lambda}}\,\underline{G}(t) \qquad (39)$$

Thus, the optimal control vector $\underline{U}(t)$ and the response state vector $\underline{Z}(t)$ are determined from Eqs. (21) and (22) as follows

$$\underline{U}(t) = \frac{1}{2} \underline{R}^{-1} \underline{A}_2' \tilde{\underline{\Lambda}} \left[\underline{Z}(t) + \underline{G}(t) \right] \qquad (40)$$

$$\underline{Z}(t) = \left[\underline{I} - \frac{1}{2} \underline{A}_2 \underline{R}^{-1} \underline{A}_2' \tilde{\underline{\Lambda}} \right]^{-1} \left[\underline{I} + \frac{1}{2} \underline{A}_2 \underline{R}^{-1} \underline{A}_2' \tilde{\underline{\Lambda}} \right] \underline{G}(t) \qquad (41)$$

The optimal algorithm presented above is referred to as the instantaneous optimal closed-open-loop control algorithm.

2.3 State Variable and State Vector

The state vector $\underset{\sim}{Z}(t)$ defined in Eq. (6)

$$\underset{\sim}{Z}(t) = \begin{bmatrix} \underset{\sim}{Y}(t) \\ \hline \dot{\underset{\sim}{Y}}(t) \end{bmatrix} \tag{42}$$

consists of displacement vector $\underset{\sim}{Y}(t) = [y_1(t), y_2(t), \ldots, y_n(t)]'$ and velocity vector $\dot{\underset{\sim}{Y}}(t) = [\dot{y}_1(t), \dot{y}_2(t), \ldots, \dot{y}_n(t)]'$; whereas the performance index $J(t)$ is defined in terms of the state vector $\underset{\sim}{Z}(t)$,

$$J(t) = \underset{\sim}{Z}'(t)\ \underset{\sim}{Q}\ \underset{\sim}{Z}(t) + \underset{\sim}{U}'(t)\ \underset{\sim}{R}\ \underset{\sim}{U}(t) \tag{43}$$

Both $\underset{\sim}{Z}'(t)$ and $J(t)$ are defined in terms of state variables $[y_1(t), y_2(t), \ldots, y_n(t)]$. In fact, the state variables can be defined in different forms depending on the particular situation. For instance, in the previous section the state variable $y_j(t)$ represents the relative displacement of the jth floor with respect to the moving ground. Under this circumstance, the mass matrix $\underset{\sim}{M}$, the damping matrix $\underset{\sim}{C}[\dot{\underset{\sim}{Y}}(t)]$ and the stiffness matrix $\underset{\sim}{K}[\underset{\sim}{Y}(t)]$ appearing in the matrix equation of motion, Eq. (1), are given in Appendix II.

On the other hand, the state variables can be defined as the relative displacement between adjacent floors or the deformation of each story unit, i.e.,

$$\underset{\sim}{Z}(t) = \begin{bmatrix} \underset{\sim}{X}(t) \\ \hline \dot{\underset{\sim}{X}}(t) \end{bmatrix} \tag{44}$$

in which $\underset{\sim}{X}(t) = [x_1(t), x_2(t), \ldots, x_n(t)]'$. In Eq. (44), $x_j(t)$ represents the deformation of the jth story unit, i.e., the relative displacement

between the jth floor and the j-1 th floor. The matrix equation of motion using these state variables and the corresponding mass matrix $\underset{\sim}{M}$, damping matrix $\underset{\sim}{C}[\dot{\underset{\sim}{Y}}(t)]$ and stiffness matrix $\underset{\sim}{K}[\underset{\sim}{Y}(t)]$ are shown in Appendix II.

When the structural response quantities, without active control, are all within the elastic range, the control efficiency using the two different definitions of state variables given above does not differ significantly. However, as the response quantities enter into the inelastic region, the control efficiency may differ substantially using different state variables depending on the design condition of the structure. For instance, when the optimal structural design is made such that yielding occurs in every story unit simultaneously, the state variables defined in Eq. (44) are superior to those of Eq. (42). This will be demonstrated in a numerical example presented later.

Consequently, an appropriate choice of state variables for the implementation of control systems may be important. This issue along with aspects of optimal design will be addressed in another report.

III. NUMERICAL EXAMPLES

To illustrate the effectiveness of the instantaneous optimal control algorithms developed in this paper for control of nonlinear structures, several examples are presented in the following. The structure is assumed to exhibit nonlinear material behavior and both bilinear elastic and bilinear elastic-plastic structures will be demonstrated. For simplicity, damping is assumed to be linear viscous damping. It should be mentioned that the three instantaneous optimal control algorithms result in identical structural response quantities as well as identical control force under ideal control environment. Ideal control environment refers to that without a system time delay, system uncertainty, estimation errors, etc., during the control process. This has been expected because the three instantaneous optimal control algorithms minimize the same time-dependent objective function J(t). Hence, in what follows, the instantaneous optimal closed-loop control algorithm will be used for simplicity.

Example 1: SDOF Bilinear Elastic-Plastic Structure

A conventional single-degree-of-freedom structure implemented by an active tendon control system shown in Fig. 3 is considered. The stiffness is bilinear elastic-plastic with an elastic translational stiffness $k_1 = 8.5273 \times 10^4$ kN/m and a post elastic translational stiffness $k_2 = 9.7455 \times 10^3$ kN/m as shown in Fig. 4(a). In Fig. 4(a), y denotes the lateral relative displacement and $F_s(y)$ is the stiffness restoring force. The floor mass m is 345.6 tons and the linear viscous damping coefficient C is 54.29 kN. sec/m which corresponds to a damping

ratio of 0.5%. The natural frequency of the structure is 2.5 Hz and yielding occurs at a lateral relative displacement of 2.4 cm. The angle of inclination of active tendons with respect to the ground is $\theta = 25^{\circ}$. A simulated earthquake ground acceleration time history shown in Fig. 5 is considered as the input excitation, where the maximum ground acceleration is 0.4g. Without active control, the relative displacement of the top floor and the base shear force are displayed in Figs. 6(a) and 7(a), respectively. The hysteresis loop of the inelastic restoring force is shown in Fig. 8(a), in which a significant yielding occurs in the structure. With an active tendon control system, the structural response and active control force depend on the weighting matrices $\underset{\sim}{Q}$ and $\underset{\sim}{R}$. In the present example, $\underset{\sim}{Q}$ is a (2x2) matrix, whereas $\underset{\sim}{R}$ is a (1x1) matrix. For simplicity, $\underset{\sim}{Q}$ matrix is chosen to be diagonal, i.e., $Q_{12} = Q_{21} = 0$, and the diagonal elements are identical, i.e., $Q_{11} = Q_{22} = Q_0$. The only element of $\underset{\sim}{R}$ matrix is denoted by R_0. With active tendon control for $Q_0/R_0 = 0.15 \times 10^8$, the time histories of the top floor relative displacement, the base shear force, the hysteresis loop of inelastic restoring force, and the required active control force are presented in Figs. 6(b), 7(b), 8(b) and 9(a), respectively. As observed from these figures, the maximum relative displacement is reduced by 27%; whereas the maximum base shear force is reduced by 5%. For $Q_0/R_0 = 0.8 \times 10^8$, the corresponding results are shown in Figs. 6(c), 7(c), 8(c) and 9(b), respectively. In this case, the maximum relative displacement and maximum base shear force are reduced by 63.8% and 38.5%, respectively, and the response is entirely well within the elastic range. To examine

the effect of weighting matrices on active control, the maximum floor relative displacement and maximum control force in the entire earthquake episode of 30 seconds are presented in Fig. 10 as functions of Q_0/R_0. It is observed from Figs. 6-9 that a significant reduction of structural response can be achieved through the application of an active tendon control system. It is further observed from Fig. 10 that as the ratio Q_0/R_0 increases, the structural response quantities decrease consistently; whereas the required active control force increases. Finally, the structural oscillation is completely within the elastic range when $Q_0/R_0 > 0.35 \times 10^8$. Thus, the active tendon control system is capable of preserving the structural response within the elastic range.

Example 2: SDOF Bilinear Elastic Structure

Example 1 is reconsidered in which the structure is bilinear elastic rather than bilinear elastic-plastic as shown in Fig. 4(b). The bilinear stiffnesses k_1 and k_2 are identical to that of Example 1 and the transition from k_1 to k_2 occurs at a relative displacement of 2.4 cm. Without a control system, the relative displacement and base shear force are depicted in Figs. 11(a) and 12(a), respectively. A comparison between Figs. 6(a) and 11(a) indicates that the response of a bilinear elastic structure is higher than that of a bilinear elastic-plastic structure. This has been expected because the hysteresis behavior of the elastic-plastic system dissipates energies during oscillations. With the instantaneous optimal control algorithm for $Q_0/R_0 = 0.8 \times 10^8$, the relative displacement, base shear force and

required control force are displayed in Figs. 11(b), 12(b) and 13. Again, the active control system is very effective in reducing structural oscillations. Further, as the ratio Q_0/R_0 increases, the structural response quantities reduce consistently and the active control force increases.

Example 3: Building Isolated by Rubber Bearings

A five-story building resting on lead-core rubber bearings considered in Ref. 4 has been modeled in Ref. 3 mathematically by a SDOF system in approximation as shown in Fig. 14(a). This representation seems to be reasonable since the effect of rubber bearing is to introduce a "soft story" with inelastic characteristics, whereas, in comparison, the superstructure behaves like a rigid body. As a result, we shall consider herein a representative SDOF structure resting on rubber bearings shown in Fig. 14(a). Active tendon control is introduced to limit the relative displacement of the rubber bearings to avoid instability failure as well as the relative displacement of the superstructure. The instantaneous optimal closed-loop control algorithm is most suitable for such applications. The superstructure is assumed to be linear elastic, whereas the rubber bearings exhibit bilinear elastic-plastic behavior as shown in Fig. 14(b). The structural properties are given in the following: (1) m = mass of superstructure = 153.06 tons; (2) k = translational stiffness of superstructure = 6.71×10^4 kN/m, and hence the natural frequency is 3.33 Hz; (3) C = damping coefficient of superstructure = 0; (4) k_1 = elastic stiffness of base isolators = 10,000 kN/m; (5) k_2 = post-elastic stiffness of base isolators = 2,500 kN/m; (6) y_1 =

yielding deformation of base isolators = 10.1 mm; (7) y_2 = failure deformation of base isolators = 150 mm. The angle of inclination of tendons is $\theta = 25^{\circ}$. A simulated earthquake ground acceleration shown in Fig. 15 is considered as the input excitation, where the maximum ground acceleration is 0.2g (2.05 m/sec.^{2}). The uncontrolled and controlled response quantities for two different Q_0/R_0 ratios are presented in Figs. 16-18. These include the relative displacement of the superstructure with respect to base isolators, the relative displacement of rubber isolators with respect to the ground, and the shear force in rubber isolators. The hysteresis loops of elastic-plastic restoring shear force in rubber isolators are shown in Fig. 19, whereas the required active control forces are shown in Fig. 20. To illustrate the control efficiency the maximum relative displacement of the superstructure, maximum relative displacement of rubber isolators and maximum required active control forces in 30 seconds of the earthquake episode are depicted in Fig. 21 as functions of Q_0/R_0 ratio. It is observed from Figs. 16-21 that the active tendon control system is capable of drastically reducing not only the superstructural response but also the deformation of base isolators. Likewise, both the deformations of the structure and rubber base isolators are mitigated consistently as the ratio Q_0/R_0 increases. The ability to safeguard severe damage for passive control devices against earthquakes by means of active control is quite obvious. The basic idea presented herein for the use of combined passive/active control systems is explained in the following. The base isolation system (passive) is used to absorb large deformation and dissipate input energies such that smaller

excitations are transmitted to the superstructure. However, base isolators must be protected against severe damage or instability failure. This is achieved by use of active control devices along with the optimal control algorithms developed herein. The advantage of the combined passive/active control system is clearly demonstrated.

Example 4: Eight-Story Building With Active Mass Damper

An eight-story building in which every story unit is identically constructed is considered for illustrative purposes. The stiffness of each story unit is assumed to be bilinear elastic-plastic with elastic stiffness $k_{i1} = k_1 = 3.404 \times 10^5$ kN/m, and post elastic stiffness $k_{i2} = k_2 = 10\% \; k_1 = 3.404 \times 10^4$ kN/m (i=1,2,...,8). The yielding level is identical for each story unit at a lateral deformation of 2.4 cm. The floor mass is m = 345.6 tons and the internal damping coefficient C for each story unit is C = 734.3 kN. sec/m which corresponds to a 0.5% damping ratio for the first vibrational mode of the entire building. The external damping is assumed to be zero. The computed natural frequencies are 5.79, 17.18, 27.98, 37.82, 46.38, 53.36, 58.53, and 61.69 rad/sec. The simulated earthquake shown in Fig. 5 is scaled uniformly so that the maximum ground acceleration is $\ddot{X}_{0max} = 0.3g$. The resulting earthquake time history is considered as the input excitation. Without any control system, the top floor relative displacement with respect to the ground and the base shear force of the building are shown in Figs. 22(a) and 23(a), respectively. Hysteresis loops for the shear force in each story unit are displayed in Fig. 24(a), in which "i" signifies the ith story unit. As observed from Fig. 24, yielding occurs in the lower three story units.

An active mass damper is installed on the top floor of the building as shown in Fig. 1(b). The properties of the mass damper are: m_d = mass of the damper = 36.3 tons; C_d = damping of the damper = 31.0 kN. sec./m; K_d = stiffness of the damper = 1173.0 kN/m. Note that the damper mass m_d is 10.5% of the generalized mass associated with the first vibrational mode, the frequency of the damper is 98% of the first natural frequency of the building, and the damping ratio of the damper is approximately 7.5%. Without the active control force, the mass damper is passive. With the passive mass damper, the response quantities, including the top floor relative displacement with respect to the ground and the base shear force, are shown in Figs. 22(b) and 23(b), respectively. It is observed from these two figures that the passive mass damper is not effective.

With an active mass damper, the structural response depends on the weighting matrices $\underset{\sim}{R}$ and $\underset{\sim}{Q}$. In this example, the weighting matrix $\underset{\sim}{R}$ consists of only one element denoted by R_0, whereas the dimension of the $\underset{\sim}{Q}$ matrix is (18 x 18). R_0 is chosen to be 10^{-5}. With the application of the instantaneous optimal control algorithms, the (18x18) $\underset{\sim}{Q}$ matrix is partitioned more efficiently as follows [14],

$$\underset{\sim}{Q} = \alpha \begin{bmatrix} \underset{\sim}{0} & \underset{\sim}{0} \\ \underset{\sim}{Q}_{21} & \underset{\sim}{Q}_{22} \end{bmatrix} \tag{45}$$

in which $\underset{\sim}{Q}_{21}$ and $\underset{\sim}{Q}_{22}$ are (2x9) matrices. The following values are assigned to elements of these two matrices for illustrative purposes:

$$\underset{\sim}{Q}_{21} = \begin{bmatrix} -33.5 & -67. & -100.5 & -134. & -167.5 & -201. & -234.5 & -268. & -375.6 \\ -33.5 & -67. & -100.5 & -134. & -167.5 & -201. & -234.5 & -268. & 32.2 \end{bmatrix}$$

$$Q_{22} = \begin{bmatrix} 67.5 & 135.0 & 202.5 & 270.0 & 338.5 & 405.0 & 472.5 & 540.0 & 32.2 \\ 5.8 & 11.6 & 17.6 & 23.2 & 29.0 & 34.7 & 40.5 & 46.3 & 5.7 \end{bmatrix}$$

A value of 5.12 is chosen for α, such that the top floor relative displacement with respect to the ground is reduced approximately by 58.3% and all the response quantities are well within the elastic limit. The response quantities and the required active control force from the controller are presented in Figs. 22(c), 23(c) and 25(a). The relative displacement of the mass damper with respect to the top floor is displayed in Fig. 25(b). Also, hysteresis loops for the shear force in each story unit are depicted in Fig. 24(b). Within 30 seconds of the earthquake episode, the maximum response quantities, including the relative displacement of each floor with respect to the ground, $y_i (i=1,2,\ldots,8)$, the deformation of each story unit or the relative displacement between adjacent floors, $x_i (i=1,2,\ldots,8)$, and the shear force, S_i, in each story unit are presented in Table 1 for comparison. The maximum control force is 820.7 kN. It is observed from Figs. 22-25 that with an active mass damper the response of the entire building is well within the elastic range.

In the example above, yielding in the lower three story units is moderate without control. Let us consider the case in which a large scale yielding occurs and the structure would have failed without control. Suppose the earthquake time history shown in Fig. 5 is scaled up uniformly so that the maximum ground acceleration is $\ddot{X}_{0max} = 0.55g$. Such a severe earthquake is considered as the input excitation. The

top floor relative displacement with respect to the ground, the base shear force and hysteresis loops for the shear force in each story unit for the building with and without active mass damper are shown in Figs. 26, 27 and 28. The required active control force and the relative displacement of the mass damper with respect to the top floor are depicted in Fig. 29. Within 30 seconds of the earthquake episode, the maximum floor relative displacement with respect to the ground, $y_i (i = 1,2,\ldots,8)$, the maximum interstory relative displacement, $x_i (i = 1,2,\ldots,8)$, and the maximum interstory shear force are summarized in Table 2 for comparison. The maximum active control force is 1505 kN. The following observations are made from Figs. 26-28 and Table 2: (i) The building may have failed without an active control system and structural failure can be prevented using an active mass damper, and (ii) a large scale yielding and severe inelastic damage can be reduced significantly using an active mass damper. Further numerical results indicate that the response of the entire building can be brought back to the elastic range with an increase of the control force.

Example 5: Eight-Story Building With Active Tendon Control System

The same eight-story building subjected to the same earthquake ground acceleration input illustrated in Example 4 is considered herein. Instead of installing an active mass damper on the top floor, four active tendon controllers are installed in the lowest story units and the angle of inclination of tendons with respect to the floor is 25° as shown in Fig. 1(a). In the present example, the dimension of the weighting matrices $\underset{\sim}{Q}$ and $\underset{\sim}{R}$ are (16x16) and (4x4), respectively. With the application of the instantaneous optimal control algorithm,

the weighting matrix $\underset{\sim}{R}$ is chosen to be a diagonal matrix with elements $R_{ii} = 10^{-4}$ (i=1,2,3,4). The (16x16) weighting matrix $\underset{\sim}{Q}$ is again partitioned as shown in Eq. (45), in which $\underset{\sim}{Q}_{21}$ and $\underset{\sim}{Q}_{22}$ are (8x8) matrices and α is a constant. Note that $\underset{\sim}{Q}_{11}$ and $\underset{\sim}{Q}_{12}$ do not contribute to the active control forces and, hence, they are chosen to be zero [14-15]. The choice of $\underset{\sim}{Q}_{21}$ and $\underset{\sim}{Q}_{22}$ requires some considerations as discussed in Ref. 14. For simplicity, $\underset{\sim}{Q}_{21}$ and $\underset{\sim}{Q}_{22}$ are chosen to be equal, i.e., $\underset{\sim}{Q}_{21} = \underset{\sim}{Q}_{22} = \underset{\sim}{Q}^*$. The elements of $\underset{\sim}{Q}^*$, denoted by $Q^*(i,j)$, are given in the following; $Q^*(i,j,) = j$ for $i \leq 4$ and $Q^*(i,j) = 0$ for $i > 4$. For a 47% reduction of the building response, a value of 2500 is used for α. Under the earthquake with a maximum ground acceleration of 0.3g, Fig. 5, time histories of the top floor relative displacement with respect to the ground and the base shear force are presented in Figs. 30 and 31, respectively. Hysteresis loops for the shear force in each story unit are shown in Fig. 32, whereas the required active control forces from the first controller (in the lowest story unit) and the fourth controller are depicted in Fig.33. The response quantities with or without active control are shown in these figures for comparison. Within 30 seconds of the earthquake episode, the maximum response quantities and maximum control forces are summarized in Table 3. It is observed from Figs. 30-32 and Table 3 that all the response quantities of the structure are well within the elastic range when the active tendon control system is used.

To examine the effectiveness of active tendon control for a large scale yielding in the structure, the earthquake with a maximum ground acceleration of 0.55g is considered as the input excitation. The

response quantities and required active control forces corresponding to Figs. 30-33 are presented in Figs. 34-37. In these figures, α = 2500 and 5500, respectively, are considered. The results corresponding to Table 3 are shown in Table 4. It is observed from Figs. 34-37 and Table 4 that while the active tendon control system is effective in alleviating severe structural damages and for the case α = 5500 all the structural response quantities are within the elastic range, the required active control forces are too big to be practical.

Example 6: Optimal Design For Eight-Story Building With Active Mass Damper

An eight-story building with identical stiffness for each story unit is considered in Examples 4 and 5 for illustrating the application of the proposed instantaneous optimal control algorithms. As observed from these examples for the case without control, severe yielding takes place in the lower story units, whereas the upper story units are within the elastic range. From the standpoint of optimal design, a building may be designed with variable stiffness so that yielding occurs simultaneously for each story unit. Such a building will be examined.

The properties of the eight-story building considered herein are as follows: (i) the mass for each floor is identical with $m_i = m =$ 345.6 tons, (ii) the stiffness for each story unit is bilinear elastic-plastic, with the elastic stiffnesses $k_{i1} = 3.404\text{x}10^5$, $3.257\text{x}10^5$, $2.849\text{x}10^5$, $2.686\text{x}10^5$, $2.430\text{x}10^5$, $2.073\text{x}10^5$, $1.687\text{x}10^5$, $1.366\text{x}\ 10^5$ kN/m, and the post elastic stiffnesses $k_{i2} = 0.1\ k_{i1}$, for i = 1,2,...,8, and (iii) the internal damping coefficients for each story

unit are C_i = 490, 467, 410, 386, 349, 298, 243 and 196 kN. sec./m, respectively. The damping coefficients given above result in a classically damped structure with a damping ratio of 0.38% for the first vibrational mode. The natural frequencies are 5.24, 13.99, 22.55, 30.22, 36.89, 43.06, 49.54 and 55.96 rad./sec. Note that the stiffness of each story unit of the structure is weaker than that of the structure considered in Examples 4 and 5, and hence the natural frequencies are lower. The yielding levels for each story unit vary with respect to the stiffness. Hence, the yielding levels given in term of the deformation of each story unit, x_{yi} (i = 1,2,...,8), are 2.4, 2.3, 2.2, 2.1, 2.0, 1.9, 1.7 and 1.5 cm. The simulated earthquake time history shown in Fig. 5 with a maximum ground acceleration of 0.3g is considered as the input excitation.

The properties of the active mass damper installed on the top floor are given in the following: m_d = mass of the damper = 36.3 tons; k_d = stiffness of the damper = 957.5 kN/m; C_d = damping coefficient of the damper = 27.97 kN. sec./m. Hence, the mass ratio of the damper with respect to the first generalized mass is 10.5%, the damping ratio of the damper is 7.5% and the frequency of the damper is 98% of the fundamental frequency of the building. As in the previous examples, the state variables (y_1, y_2,...,y_n) are used, and the weighting matrices $\underset{\sim}{R}$ and $\underset{\sim}{Q}$ are identical to those given in Example 4.

Without control, the top floor relative displacement with respect to the ground, the base shear force and the hysteresis loops for the shear force in each story unit are displayed in Figs. 38(a), 39(a) and

40(a), respectively. Within 30 seconds of the earthquake episode, the maximum relative displacement of each floor with respect to the moving ground, y_i (i = 1,2,...,8), the maximum interstory deformation, x_i (i = 1,2,...,8), and the maximum shear force in each story unit, S_i (i = 1,2,...,8), are summarized in Table 5. As observed from Fig. 40(a) and x_i in Table 5, yielding takes place in each story unit. With an active mass damper and α = 9.6, the corresponding response quantities are shown in Figs. 38(b), 39(b) and 40(b) as well as Table 5 for comparison. Further, the required active control force and the relative displacement of the mass damper with respect to the top floor are shown in Figs. 41(a) and 42(a), respectively. It is observed from Fig. 40(b) and x_i in Table 5 that the response of each story unit is brought back to the elastic range except the top story unit. This is due to the fact that the top floor is subjected to the active damper force. Thus, the stiffness of the top story unit should be reinforced.

The results presented above are based on the state variables (y_1, y_2,...,y_n) representing the relative displacement of each floor with respect to the moving ground. In fact, the state variables (y_1, y_2,...,y_n) put more weight on the lower story units than the upper story units. In other words, the reduction of the deformation for the lower story units is more important than that for the upper story units. On the other hand, however, the state variables, (x_1, x_2,...,x_n) put equal weight for the deformation of each story unit. Consequently, the state variables, (x_1, x_2,...,x_n), representing the deformation of each story unit, may be more beneficial for use in the optimal control formulation as described in Section 2.3. This is

particularly true for the optimally designed structure in which the yielding resistance for each story unit is almost identical, i.e., yielding for each story unit takes place simultaneously, such as the present example.

Now, the state variables, $(x_1, x_2,\ldots,x_n)$, representing the interstory deformations will be used in the proposed instantaneous optimal control algorithms. Because of the nature of such state variables, the weighting matrix Q given by Eq. (45) will be used in which Q_{21} and Q_{22} matrices are given in the following

$$Q_{21} = \begin{bmatrix} -1, & -1, & -1, & -1, & -1, & -1, & -1.59, & -2.68, & 0.0125 \\ -1, & -1, & -1, & -1, & -1, & -1, & -1.59, & -2.68, & 0.0107 \end{bmatrix}$$

$$Q_{22} = \begin{bmatrix} 2 & 2 & 2 & 2 & 2 & 2 & 2 & 2 & 0.0107 \\ 0.173 & 0.173 & 0.173 & 0.173 & 0.173 & 0.173 & 0.173 & 0.173 & 0.0107 \end{bmatrix}$$

With the active mass damper and $\alpha = 1040$, the response quantities, the required active control force and the relative displacement of the mass damper are shown in Figs. 38(c), 39(c), 40(c), 41(b) and 42(b), respectively. In 30 seconds of the earthquake episode, the maximum response quantities are summarized in Table 5 for comparison. It is observed from Fig. 40(c) and Tables 5 that the response of each story unit is well within the elastic range. Likewise, the maximum relative displacement x_d of the mass damper with respect to the top floor is much smaller when the state variables $(x_1, x_2,\ldots,x_n)$ are used. Hence, the use of state variables $(x_1, x_2,\ldots,x_n)$ is superior than the state variables $(y_1, y_2,\ldots,y_n)$.

Suppose the earthquake time history shown in Fig. 5 is scaled up uniformly so that the maximum ground acceleration is $\ddot{X}_{0max} = 0.55g$. Such a severe earthquake resulting in a large scale yielding and possible structural failure is considered as the input excitation. The hysteresis loops for the shear force in each story unit are displayed in Fig. 43 and the maximum response quantities within 30 seconds of the earthquake episode are summarized in Table 6. In Table 6 and Fig. 43, $\alpha = 4000$ is used for the formulation with state variables $(x_1, x_2,\ldots,x_n)$, whereas $\alpha = 10.5$ is used for the formulation with state variables $(y_1, y_2,\ldots,y_n)$. From Table 6, although the use of state variables $(y_1, y_2,\ldots,y_n)$ results in a significant reduction for inelastic damage in lower story units, failure occurs in the top story unit. Therefore, the hysteresis loops are not presented in Fig. 43 for state variables $(y_1, y_2,\ldots,y_n)$. It is observed from Table 6 that the use of the state variables $(x_1, x_2,\ldots,x_n)$ is superior.

TABLE 1: Maximum Response Quantities (0.3g Earthquake) : y_i = maximum relative displacement of ith floor with respect to the ground; x_i = maximum interstory deformation of ith story unit; S_i = maximum shear force in ith story unit; x_d = maximum relative displacement of mass damper; Umax = maximum control force.

FLOOR	WITHOUT CONTROL			PASSIVE MASS DAMPER x_d = 0.60 m			ACTIVE MASS DAMPER Umax = 820.7 kN x_d = 1.64 m		
NO. (i)	y_i (cm)	x_i (cm)	S_i (kN)	y_i (cm)	x_i (cm)	S_i (kN)	y_i (cm)	x_i (cm)	S_i (kN)
1	3.89	3.89	8677	2.99	2.99	8369	1.62	1.62	5529
2	7.04	3.22	8447	5.32	2.47	8195	3.11	1.48	5042
3	9.26	2.49	8200	7.44	2.21	7509	4.41	1.32	4497
4	11.16	2.30	7812	9.22	1.79	6089	5.52	1.27	4310
5	12.84	2.11	7184	10.49	1.48	5026	6.55	1.14	3877
6	14.28	1.84	6274	11.30	1.30	4426	7.45	0.93	3169
7	15.36	1.45	4951	11.82	0.99	3360	8.11	0.68	2327
8	16.00	0.80	2722	12.26	0.53	1810	8.46	0.60	2043

TABLE 2: Maximum Response Quantities (0.55g Earthquake) : y_i = maximum relative displacement of ith floor with respect to the ground; x_i = maximum interstory deformation of ith story unit; S_i = maximum shear force in ith story unit; x_d = maximum relative displacement of mass damper; Umax = maximum control force.

FLOOR	WITHOUT CONTROL			PASSIVE MASS DAMPER x_d = 1.01 m			ACTIVE MASS DAMPER Umax = 1505 kN x_d = 2.79 m		
NO. (i)	y_i (cm)	x_i (cm)	S_i (kN)	y_i (cm)	x_i (cm)	S_i (kN)	y_i (cm)	x_i (cm)	S_i (kN)
1	5.32	5.32	9164	5.30	5.30	9156	4.25	4.25	8800
2	8.97	3.90	8681	9.10	3.84	8659	6.76	2.66	8257
3	11.64	4.03	8725	11.41	2.57	8227	8.82	2.41	8174
4	13.83	3.48	8536	13.24	2.45	8186	10.49	2.32	7896
5	15.64	3.06	8395	14.80	2.32	7907	12.00	2.09	7106
6	16.68	2.93	8350	16.07	2.04	6934	13.66	1.71	5808
7	17.54	2.19	7456	17.01	1.54	5229	14.86	1.22	4135
8	18.21	1.24	4206	17.53	0.86	2915	15.50	0.94	3193

TABLE 3: Maximum Response Quantities (0.3g Earthquake) : y_i = maximum relative displacement of ith floor with respect to ground; x_i = maximum interstory deformation of ith story unit; S_i = maximum shear force in ith story unit; U_i = maximum control force from ith controller.

FLOOR No. (i)	WITHOUT CONTROL			ACTIVE TENDONS			
	y_i (cm)	x_i (cm)	S_i (kN)	y_i (cm)	x_i (cm)	S_i (kN)	U_i (kN)
1	3.89	3.89	8677	1.78	1.78	6051	1725
2	7.04	3.22	8447	3.29	1.51	5134	1722
3	9.26	2.49	8200	4.48	1.26	4298	1677
4	11.16	2.30	7812	5.39	1.33	4537	1126
5	12.84	2.11	7184	6.20	1.45	4938	0
6	14.28	1.84	6274	7.11	1.25	4269	0
7	15.36	1.45	4951	7.92	1.03	3499	0
8	16.00	0.80	2722	8.38	0.56	1900	0

TABLE 4: Maximum Response Quantities (0.55g Earthquake) : y_i = maximum relative displacement of ith floor with respect to the ground; x_i = maximum interstory deformation of ith story unit; S_i = maximum shear force in ith story unit; U_i = maximum control force from ith controller.

FLOOR	WITHOUT CONTROL			ACTIVE TENDONS α = 2500				ACTIVE TENDONS α = 5500			
NO. (i)	y_i (cm)	x_i (cm)	S_i (kN)	y_i (cm)	x_i (cm)	S_i (kN)	U_i (kN)	y_i (cm)	x_i (cm)	S_i (kN)	U_i (kN)
1	5.32	5.32	9164	3.68	3.68	8604	3129	2.29	2.29	7781	5136
2	8.97	3.90	8681	5.99	2.51	8206	3123	4.07	1.84	6262	5125
3	11.64	4.03	8725	8.04	2.23	7593	3043	5.37	1.61	5488	4994
4	13.83	3.48	8536	9.65	2.31	7876	2043	6.26	1.83	6217	3353
5	15.64	3.06	8395	11.55	2.94	8352	0	7.42	2.23	7576	0
6	16.68	2.93	8350	13.21	2.31	7873	0	8.92	1.80	6126	0
7	17.54	2.19	7456	14.55	1.90	6452	0	9.92	1.58	5377	0
8	18.21	1.24	4206	15.36	1.03	3504	0	10.36	0.91	3104	0

TABLE 5: Maximum Response Quantities (0.3g Earthquake) : y_i = maximum relative displacement of ith floor with respect to the ground; x_i = maximum interstory deformation of ith story unit; S_i = maximum shear force in ith story unit; Umax = maximum control force; x_{yi} = yielding level of ith story unit; x_d = maximum relative displacement of mass damper.

FLOOR No. (i)	x_{yi} (cm)	WITHOUT CONTROL			ACTIVE MASS DAMPER					
					$\underline{Z} = [\underline{Y}', \dot{\underline{Y}}']'$ Umax = 1370 kN x_d = 2.444 m			$\underline{Z} = [\underline{X}', \dot{\underline{X}}']'$ Umax = 1359 kN x_d = 1.158 m		
		y_i (cm)	x_i (cm)	s_i (kN)	y_i (cm)	x_i (cm)	s_i (kN)	y_i (cm)	x_i (cm)	S_i (kN)
1	2.4	2.94	2.94	8353	1.46	1.46	4980	1.40	1.40	4765
2	2.3	5.75	2.83	7663	2.76	1.31	4250	2.69	1.36	4431
3	2.2	8.32	3.33	6589	3.89	1.27	3630	4.07	1.53	4360
4	2.1	9.97	2.96	5872	4.78	1.48	3969	5.47	1.54	4123
5	2.0	12.34	2.61	5007	5.88	1.43	3463	6.88	1.50	3637
6	1.9	15.33	3.00	4165	7.08	1.22	2534	8.18	1.48	3064
7	1.7	17.75	2.75	3044	8.21	1.46	2464	9.30	1.57	2641
8	1.5	18.58	2.37	2167	9.37	2.33	2162	10.25	1.46	1994

TABLE 6: Maximum Response Quantities (0.55g Earthquake): y_i = maximum relative displacement of ith floor with respect to the ground; x_i = maximum interstory deformation of ith story unit; S_i = maximum shear force in ith story unit; Umax = maximum control force; x_{yi} = yielding level of ith story unit; x_d = maximum relative displacement of mass damper.

FLOOR No. (i)	x_{yi} (cm)	WITHOUT CONTROL			ACTIVE MASS DAMPER					
					$\underline{Z} = [\underline{Y}', \dot{\underline{Y}}']'$ Umax = 3485 kN x_d = 5.882 m			$\underline{Z} = [\underline{X}', \dot{\underline{X}}']'$ Umax = 3904 kN x_d = 2.808 m		
		y_i (cm)	x_i (cm)	s_i (kN)	y_i (cm)	x_i (cm)	s_i (kN)	y_i (cm)	x_i (cm)	S_i (kN)
1	2.4	4.40	4.40	8852	2.14	2.14	7290	2.39	2.39	8141
2	2.3	7.54	3.18	7779	3.98	1.97	6426	4.65	2.32	7499
3	2.2	10.75	3.86	6741	5.72	2.07	5892	7.00	2.94	6478
4	2.1	12.99	3.22	5942	7.11	2.23	5676	9.17	2.35	5706
5	2.0	15.33	3.64	5258	8.87	1.97	4787	11.23	2.45	4968
6	1.9	17.94	3.84	4341	10.27	1.99	3957	13.21	2.43	4049
7	1.7	21.45	4.79	3388	11.39	3.37	3149	14.87	2.83	3058
8	1.5	22.20	3.65	2343	12.83	9.07	3083	16.30	2.02	2120

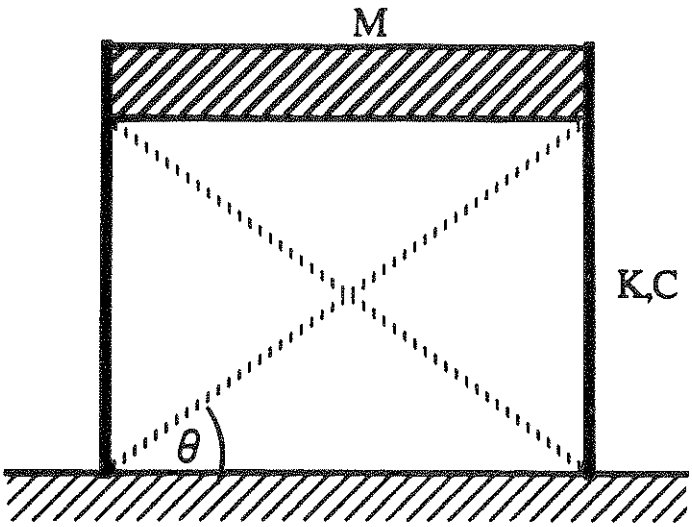

Fig. 3: A SDOF Structural Model With an Active Tendon Control System.

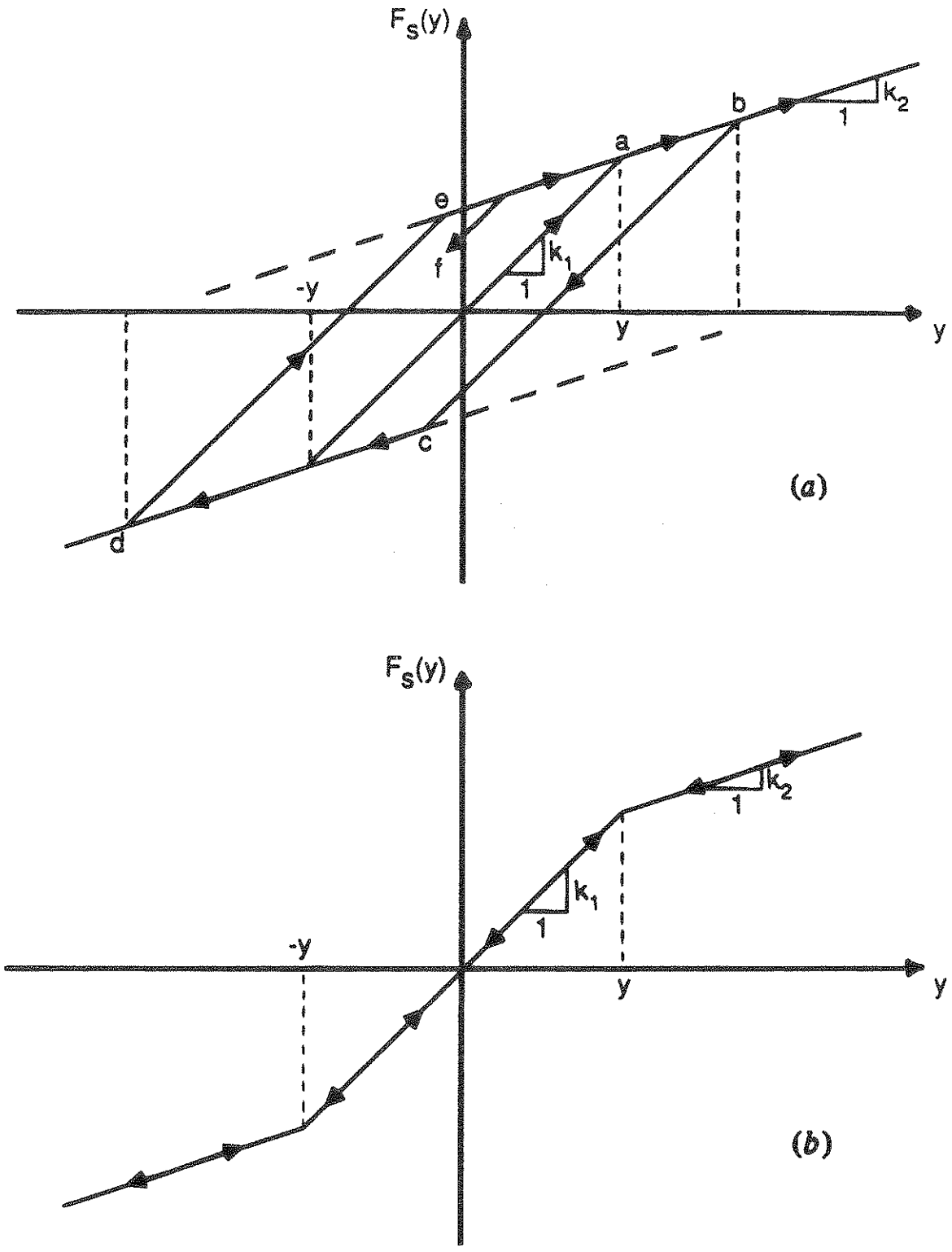

Fig. 4: Nonlinear Stiffness Characteristics: (a) Bilinear Elastic-Plastic Stiffness; (b) Bilinear Elastic Stiffness.

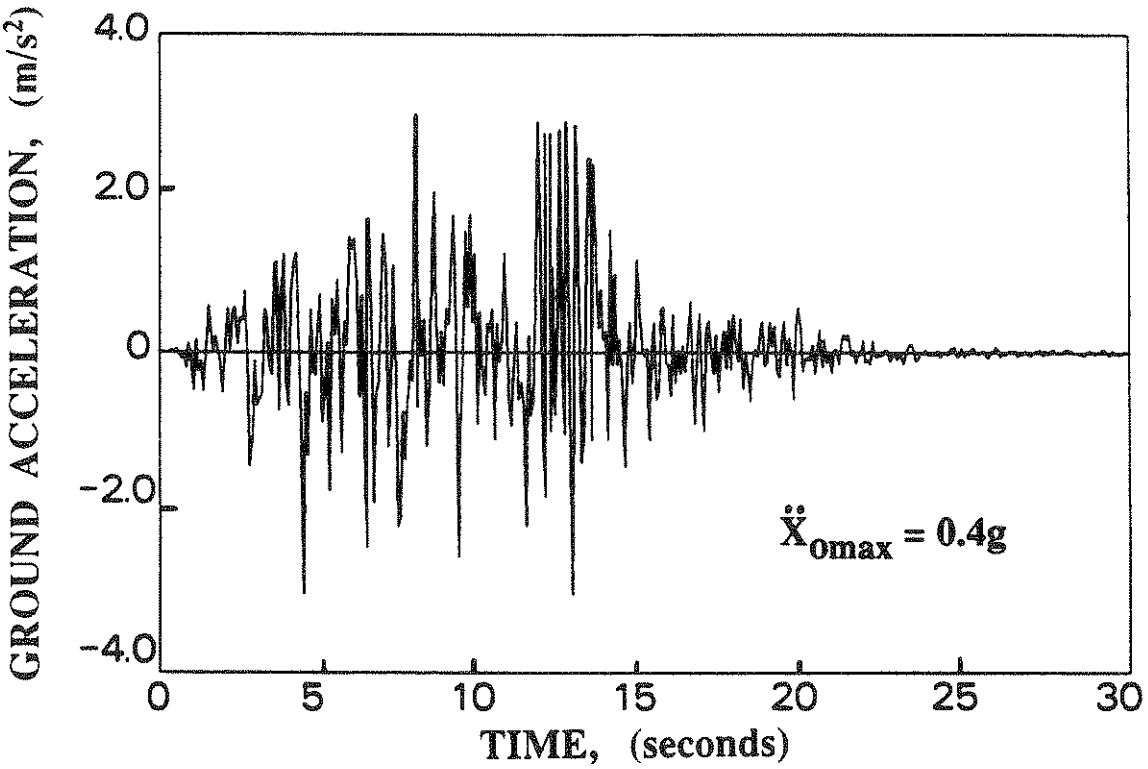

Fig. 5: A Simulated Earthquake Ground Acceleration.

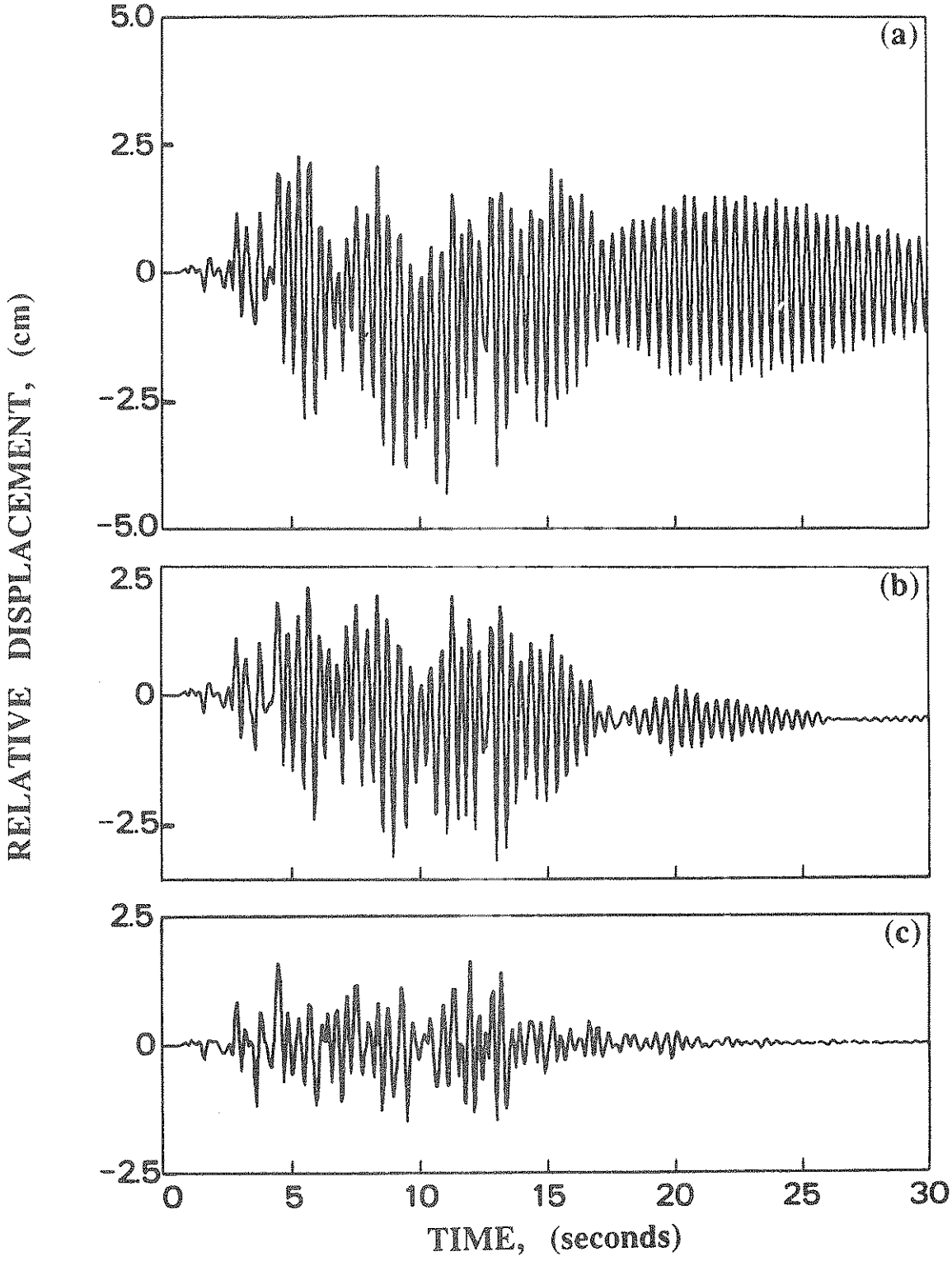

Fig. 6: Floor Relative Displacement of Bilinear Elastic-Plastic Structure; (a) Without Control; (b) $Q_o/R_o=0.15\times10^8$; (c) $Q_o/R_o=0.8\times10^8$.

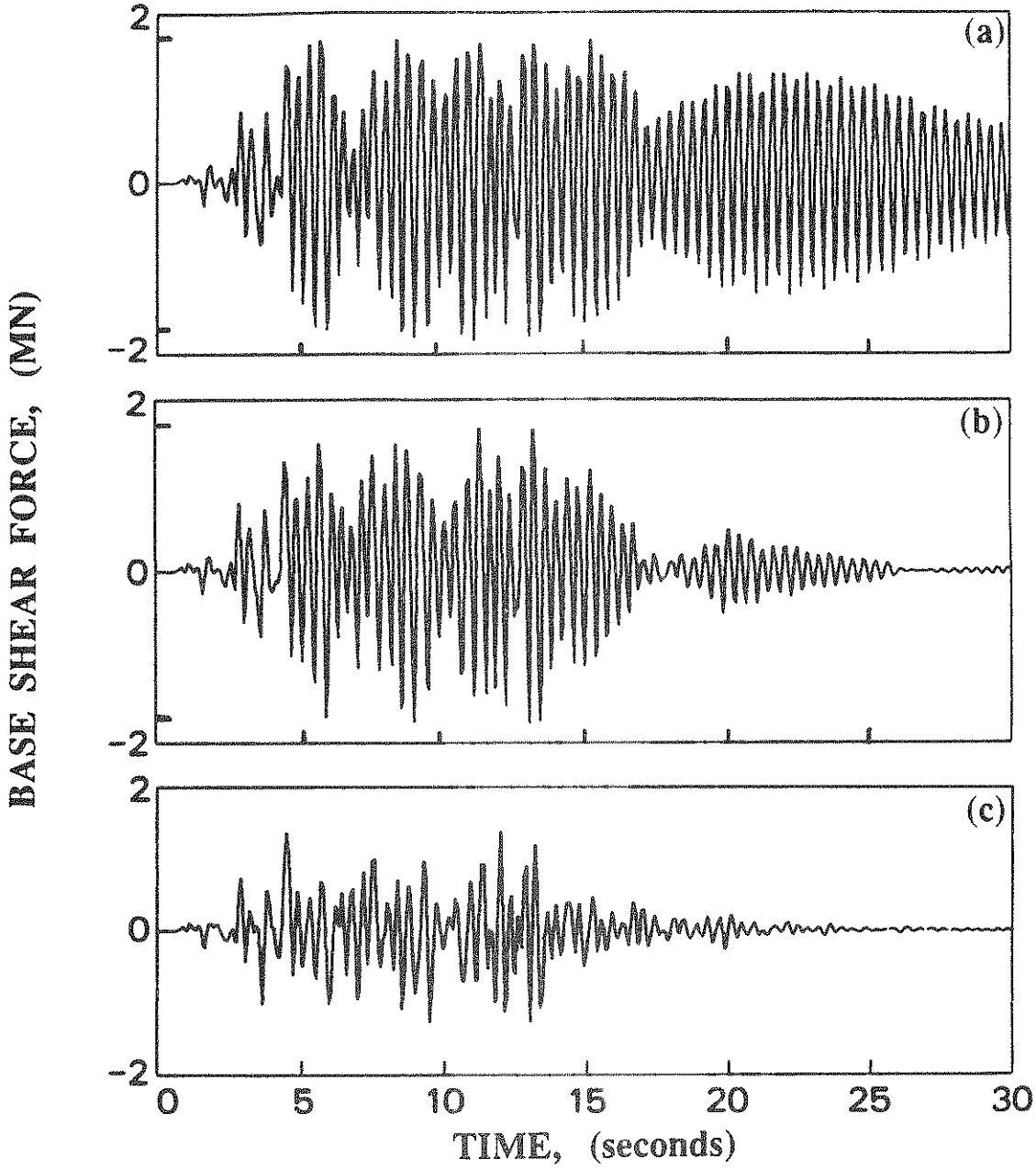

Fig. 7: Base Shear Force of Bilinear Elastic-Plastic Structure; (a) Without Control; (b) $Q_o/R_o=0.15\times10^8$; (c) $Q_o/R_o=0.8\times10^8$.

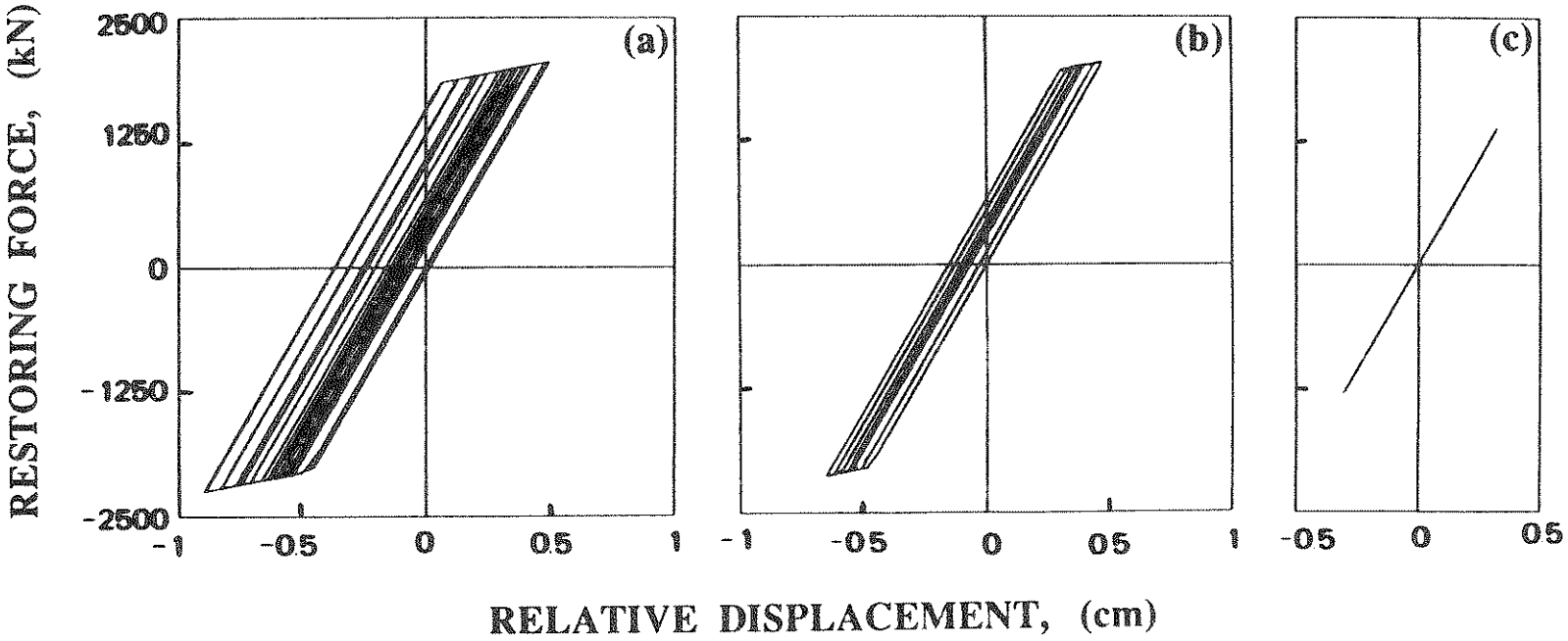

Fig. 8: Hysteresis Loop of Inelastic Restoring Force; (a) Without Control; (b) $Q_o/R_o=0.15\times10^8$; (c) $Q_o/R_o=0.8\times10^8$.

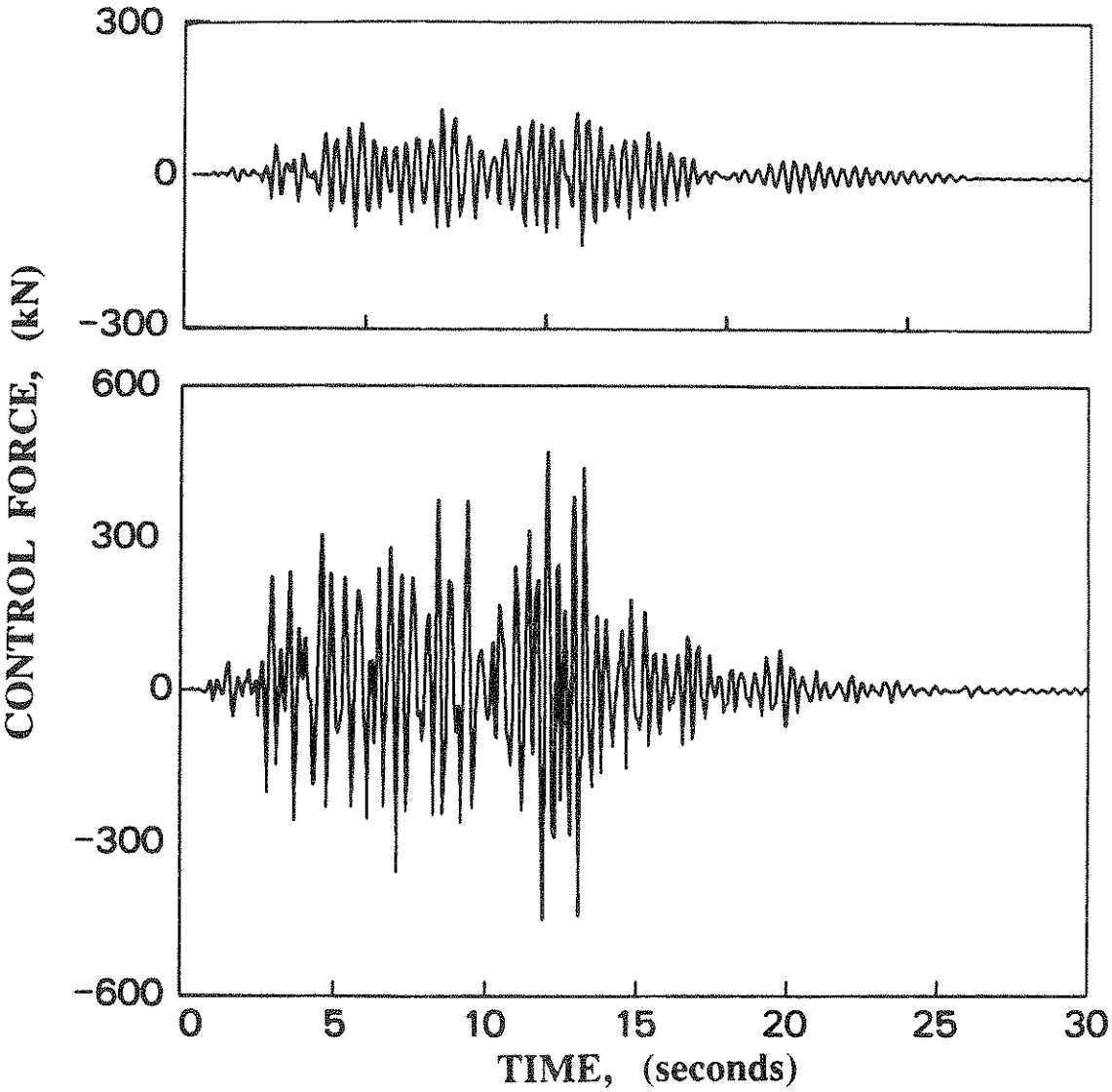

Fig. 9: Required Active Control Force; (a) $Q_o/R_o=0.15x10^8$; (b) $Q_o/R_o=0.8x10^8$.

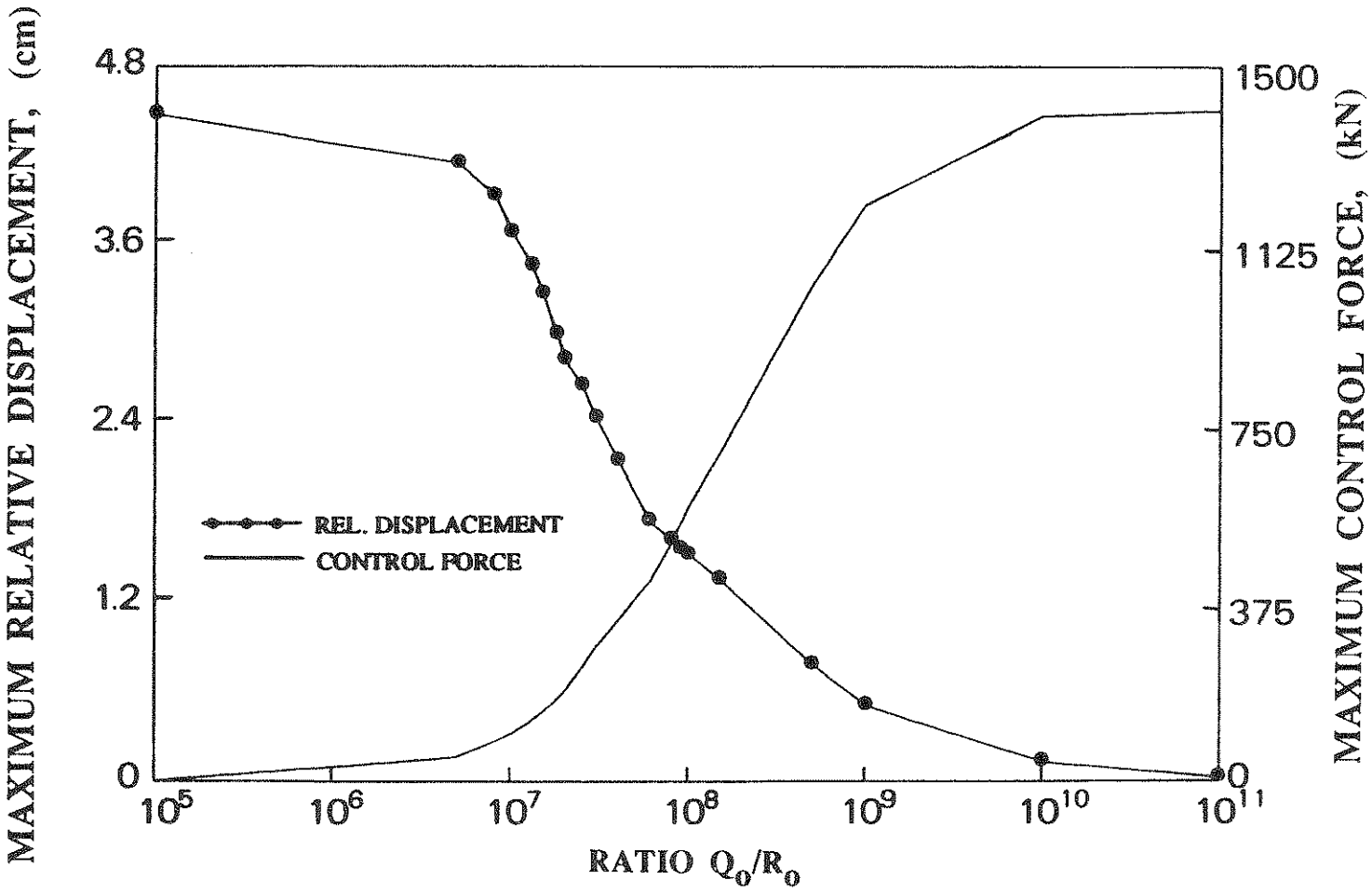

Fig. 10: Maximum Floor Relative Displacement and Control Force as Functions of Q_o/R_o Ratio.

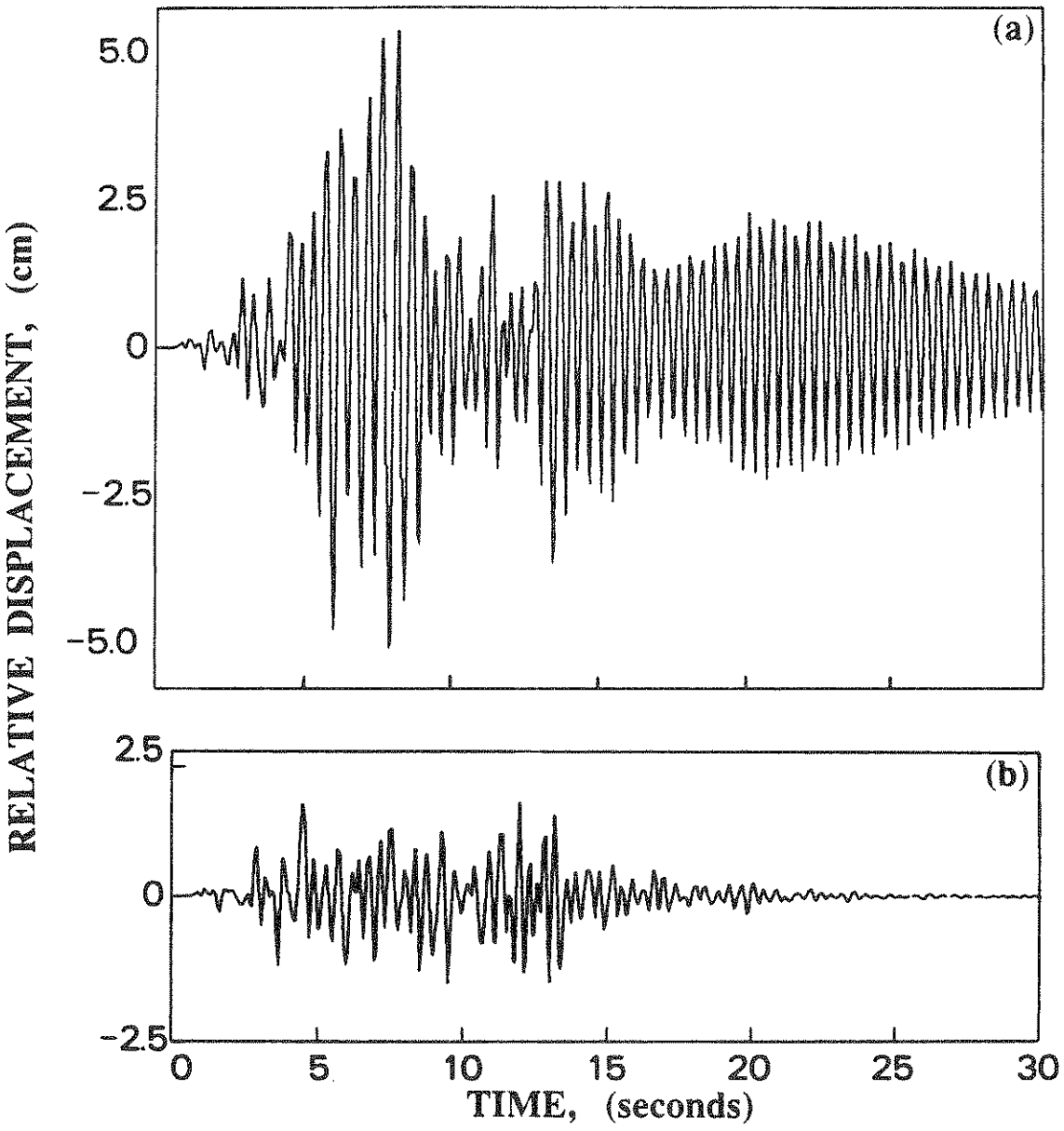

Fig. 11: Floor Relative Displacement of Bilinear Elastic Structure; (a) Without Control; (b) With Active Control $Q_o/R_o=0.8x10^8$.

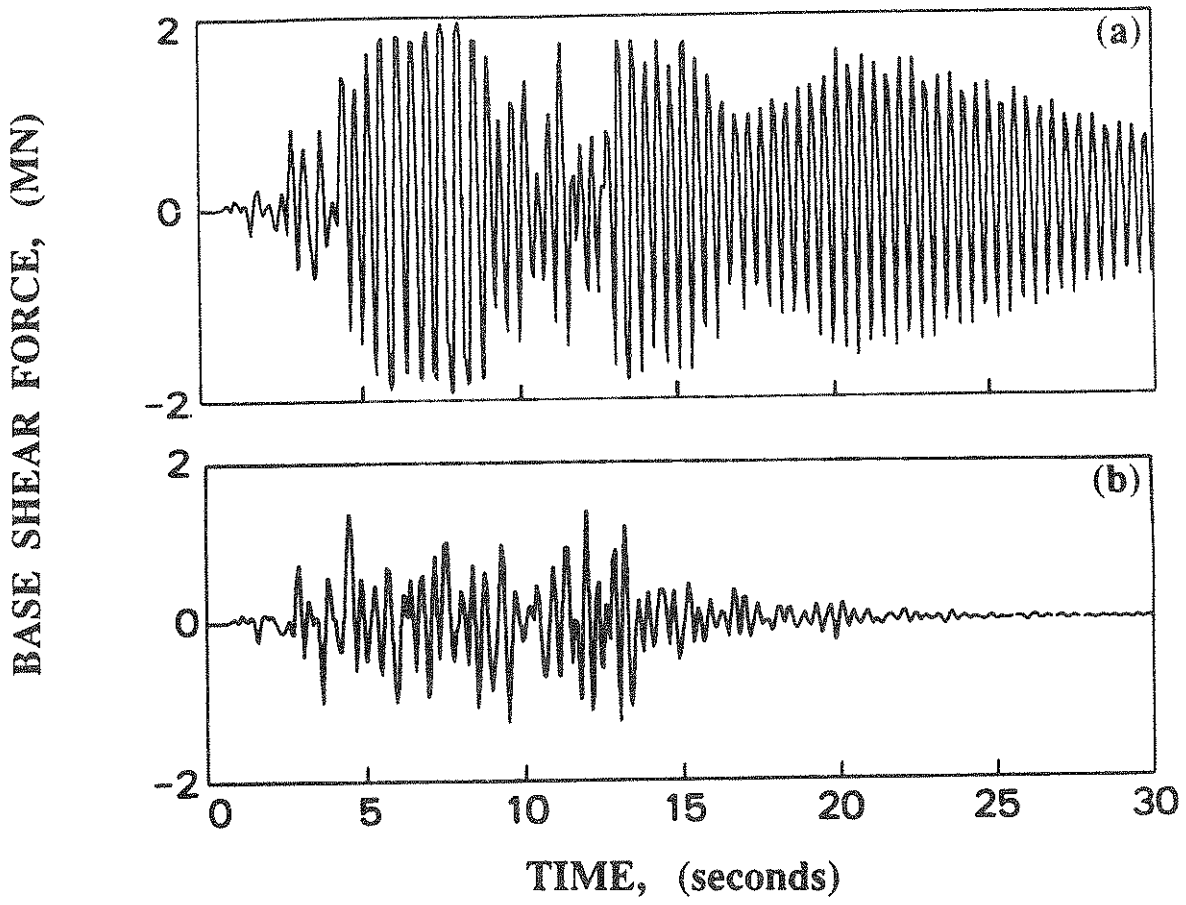

Fig. 12: Base Shear Force of Bilinear Elastic Structure; (a) Without Control; (b) With Active Control $Q_o/R_o=0.8x10^8$.

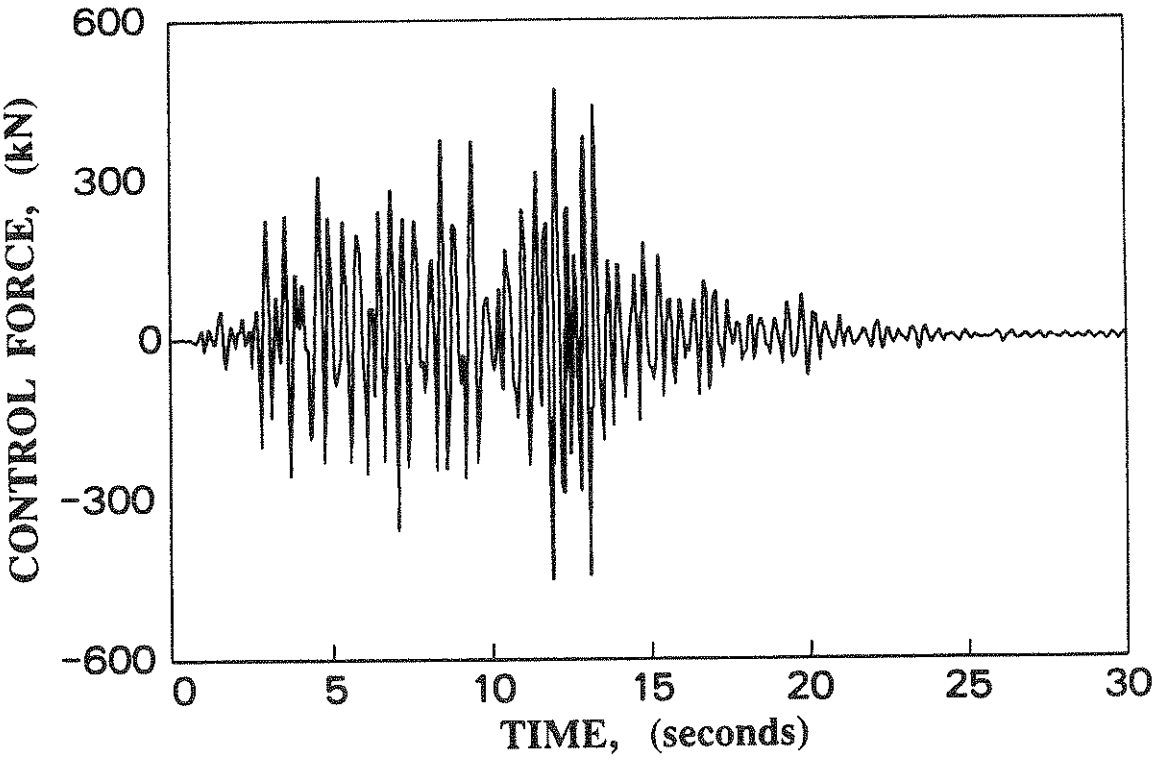

Fig. 13: Required Active Control Force for Bilinear Elastic Structure with $Q_o/R_o=0.8x10^8$.

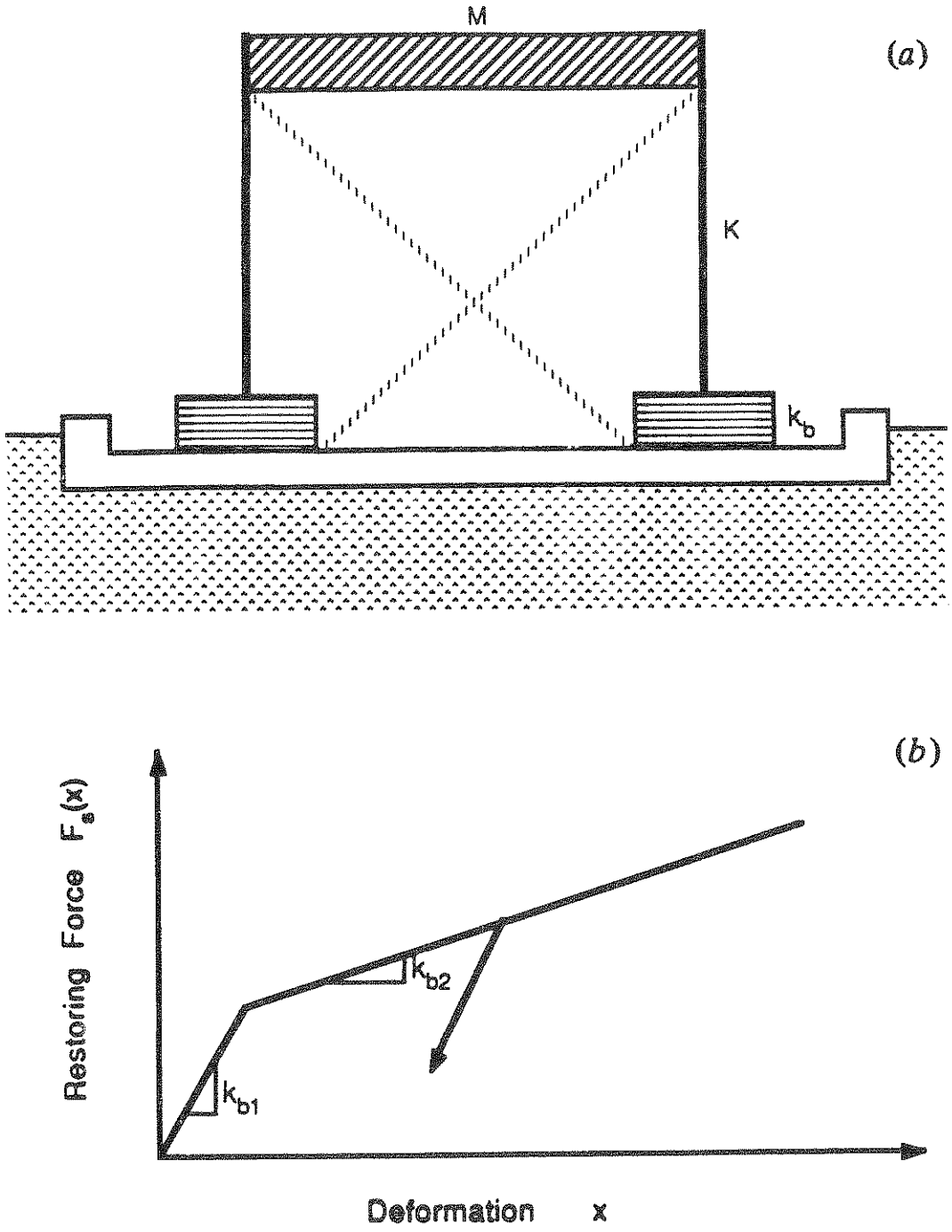

Fig. 14: Structural Model and Characteristics of Restoring Force; (a) SDOF Model with Base Isolators and Active Tendon System; (b) Bilinear Elastic-Plastic Restoring Force.

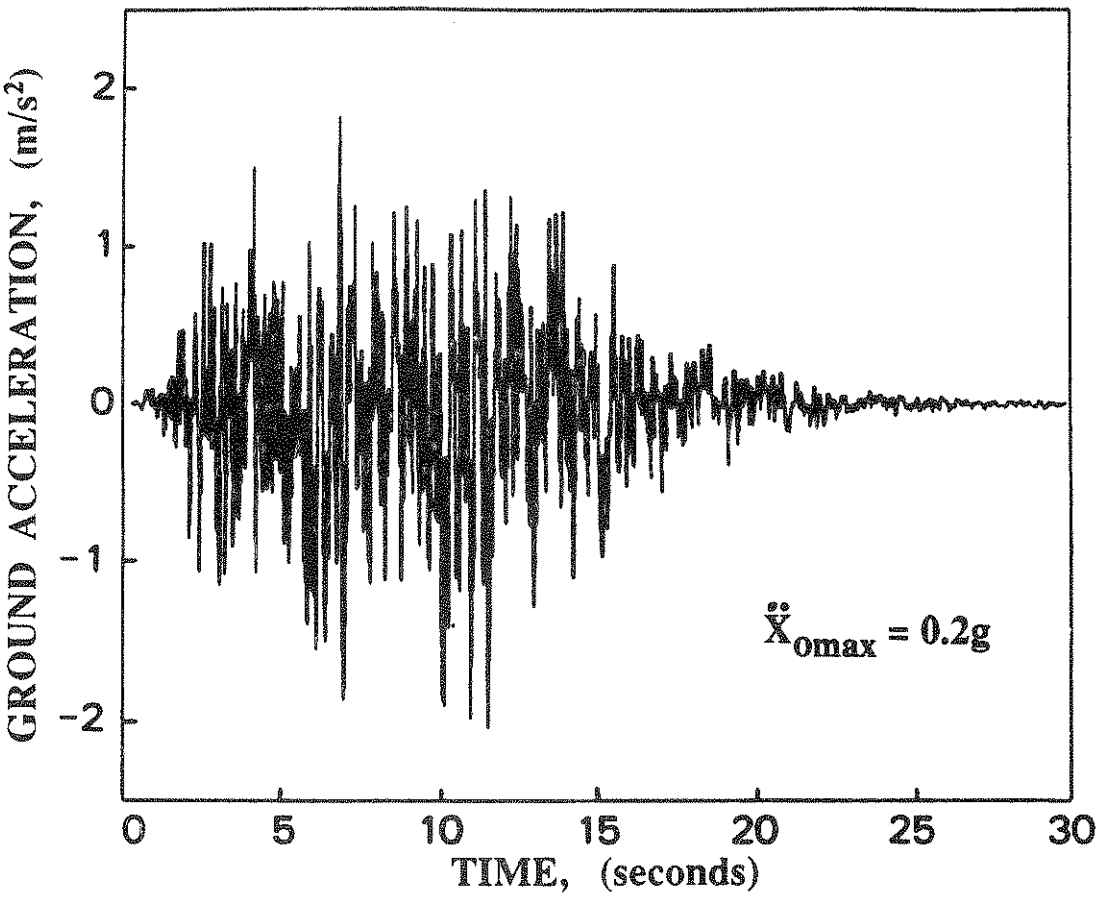

Fig. 15: A Simulated Earthquake Ground Acceleration.

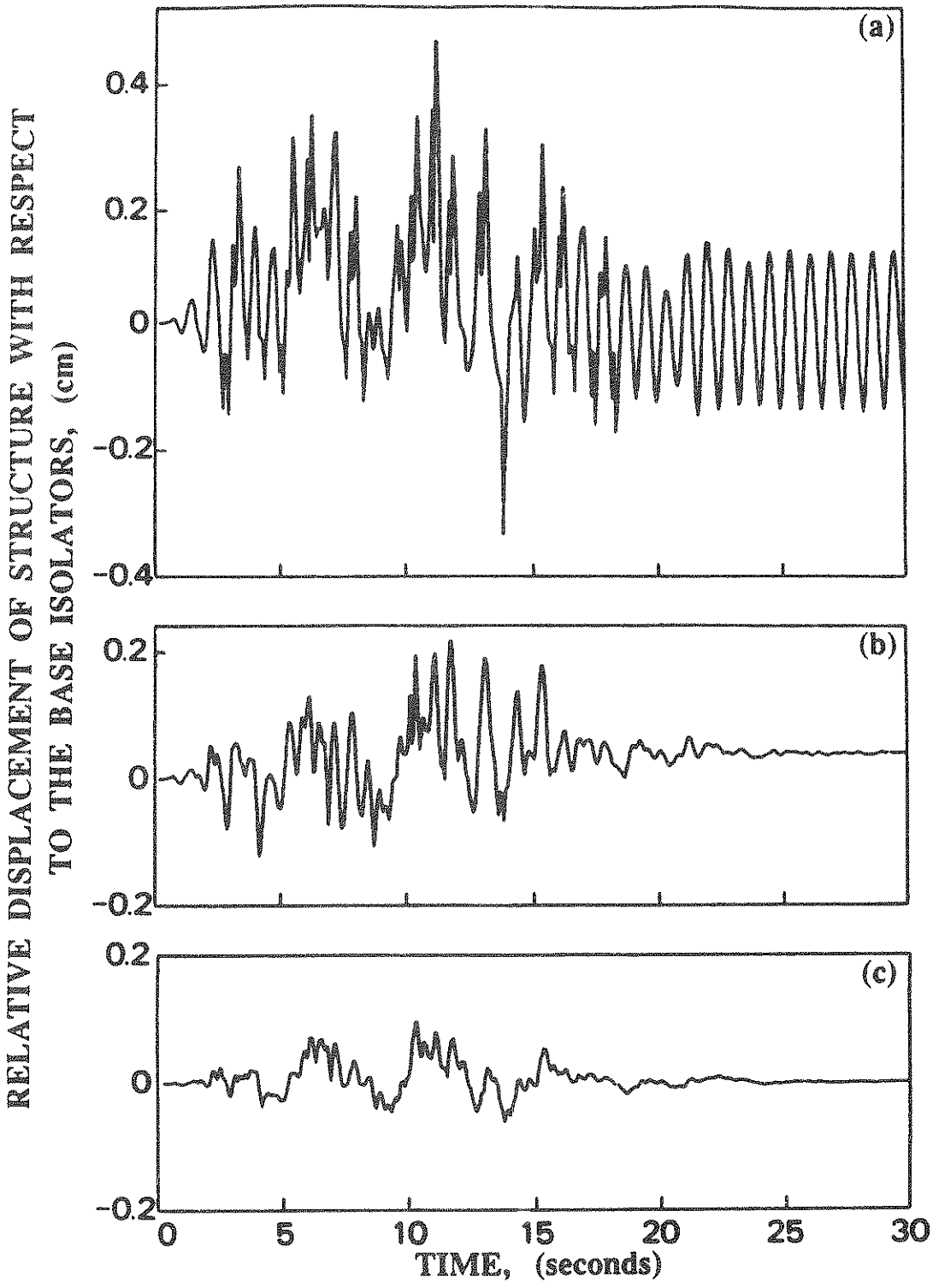

Fig. 16: Relative Displacement of Superstructure with Respect to Base Isolators; (a) Without Control; (b) $Q_o/R_o=2x10^7$; (c) $Q_o/R_o=9x10^7$.

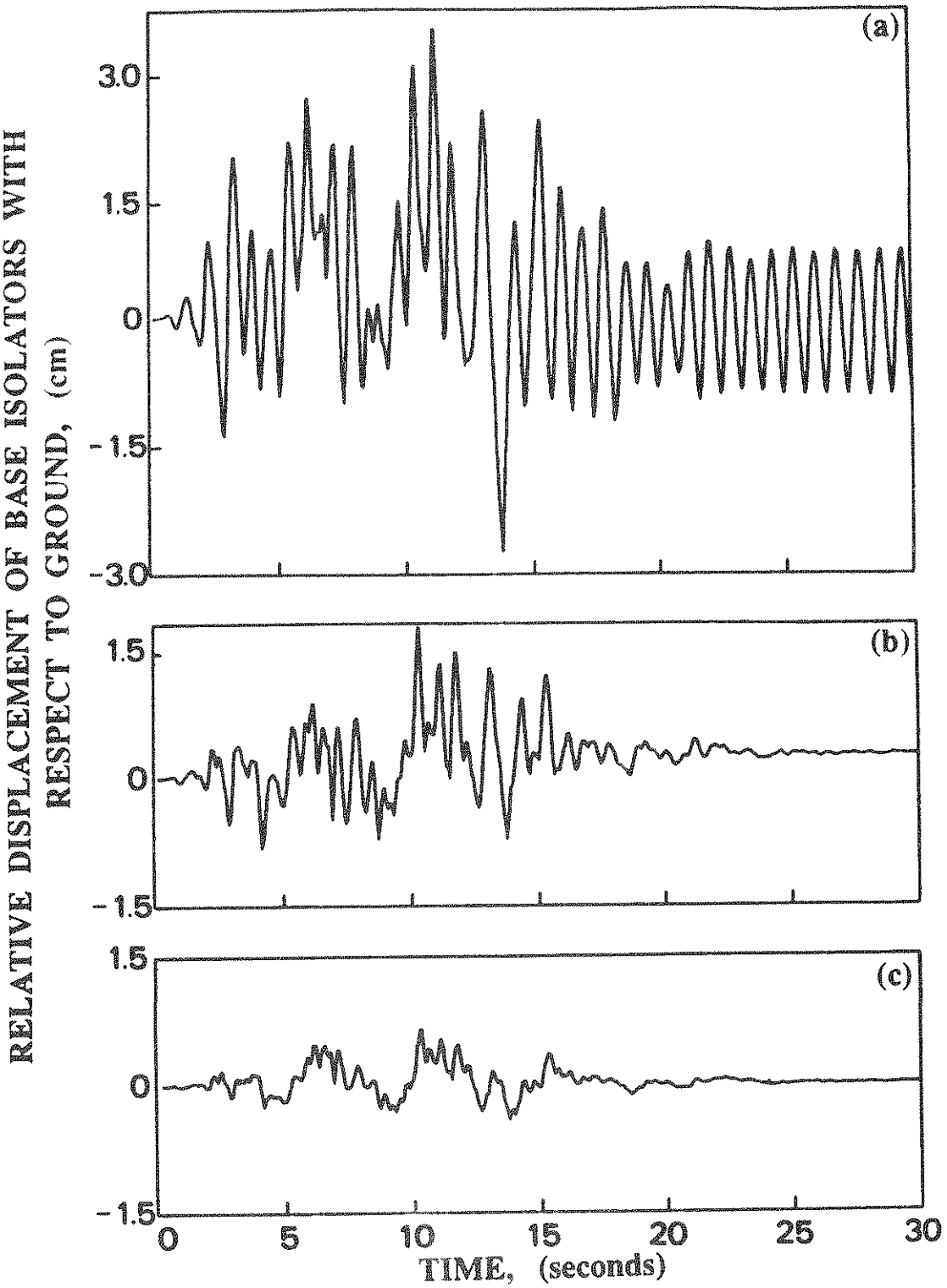

Fig. 17: Relative Displacement of Base Isolators with Respect to Ground; (a) Without Control; (b) $Q_o/R_o=2x10^7$; (c) $Q_o/R_o=9x10^7$.

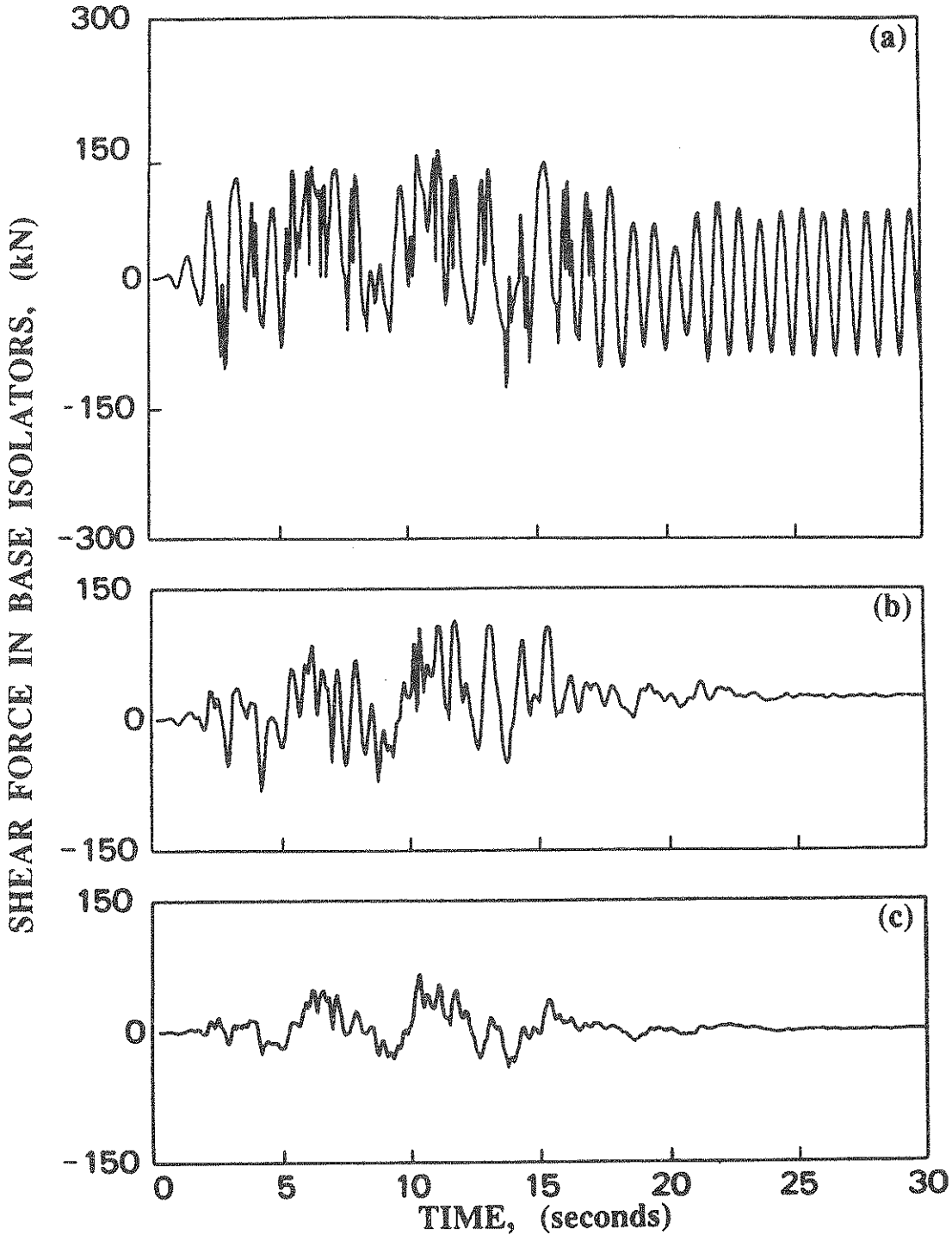

Fig. 18: Shear Force in Rubber Base Isolators; (a) Without Control; (b) $Q_o/R_o=2x10^7$; (c) $Q_o/R_o=9x10^7$.

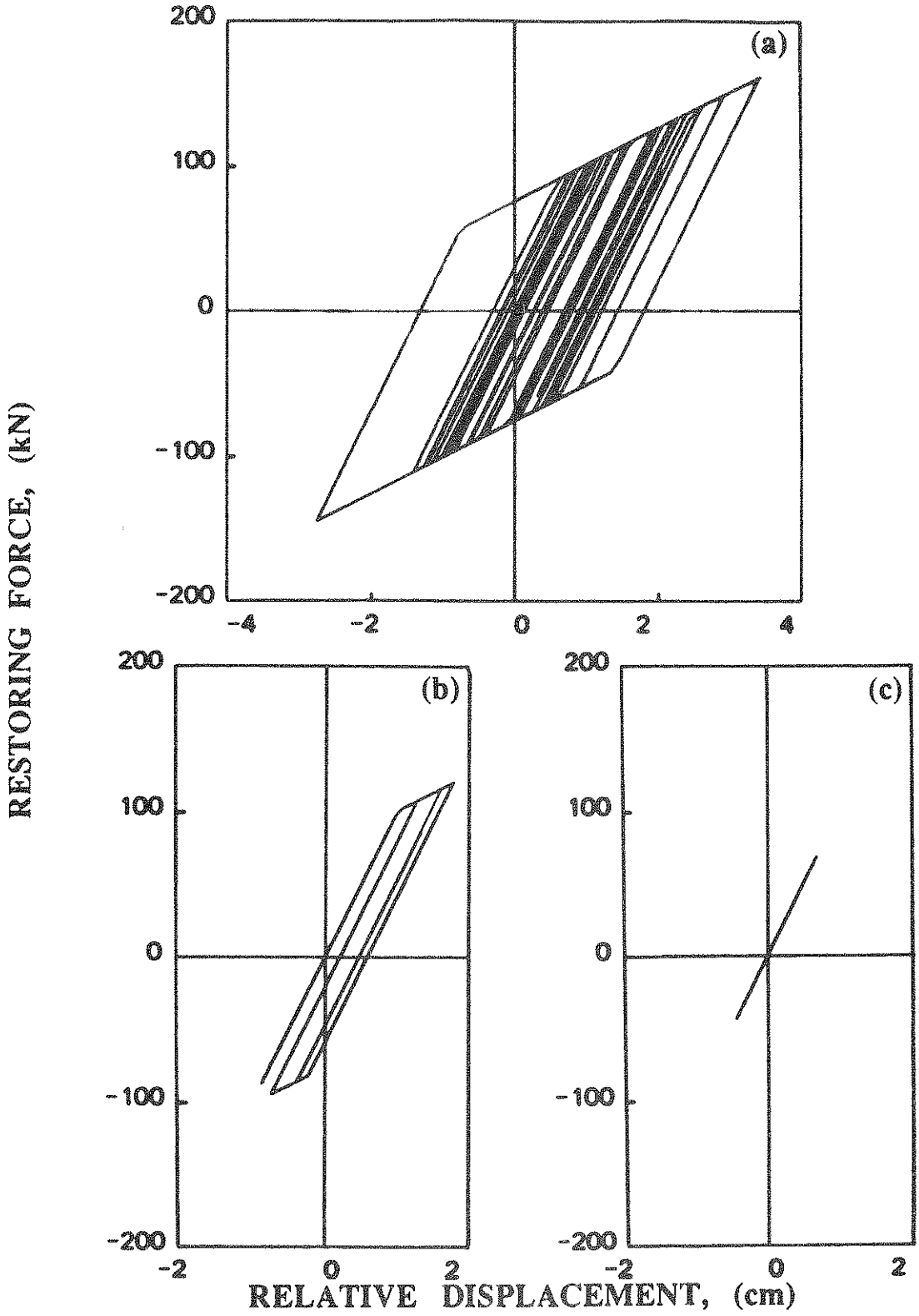

Fig. 19: Hysteresis Loop of Inelastic Shear Force in Rubber Isolators; (a) Without Control; (b) $Q_o/R_o=2x10^7$; (c) $Q_o/R_o=9x10^7$.

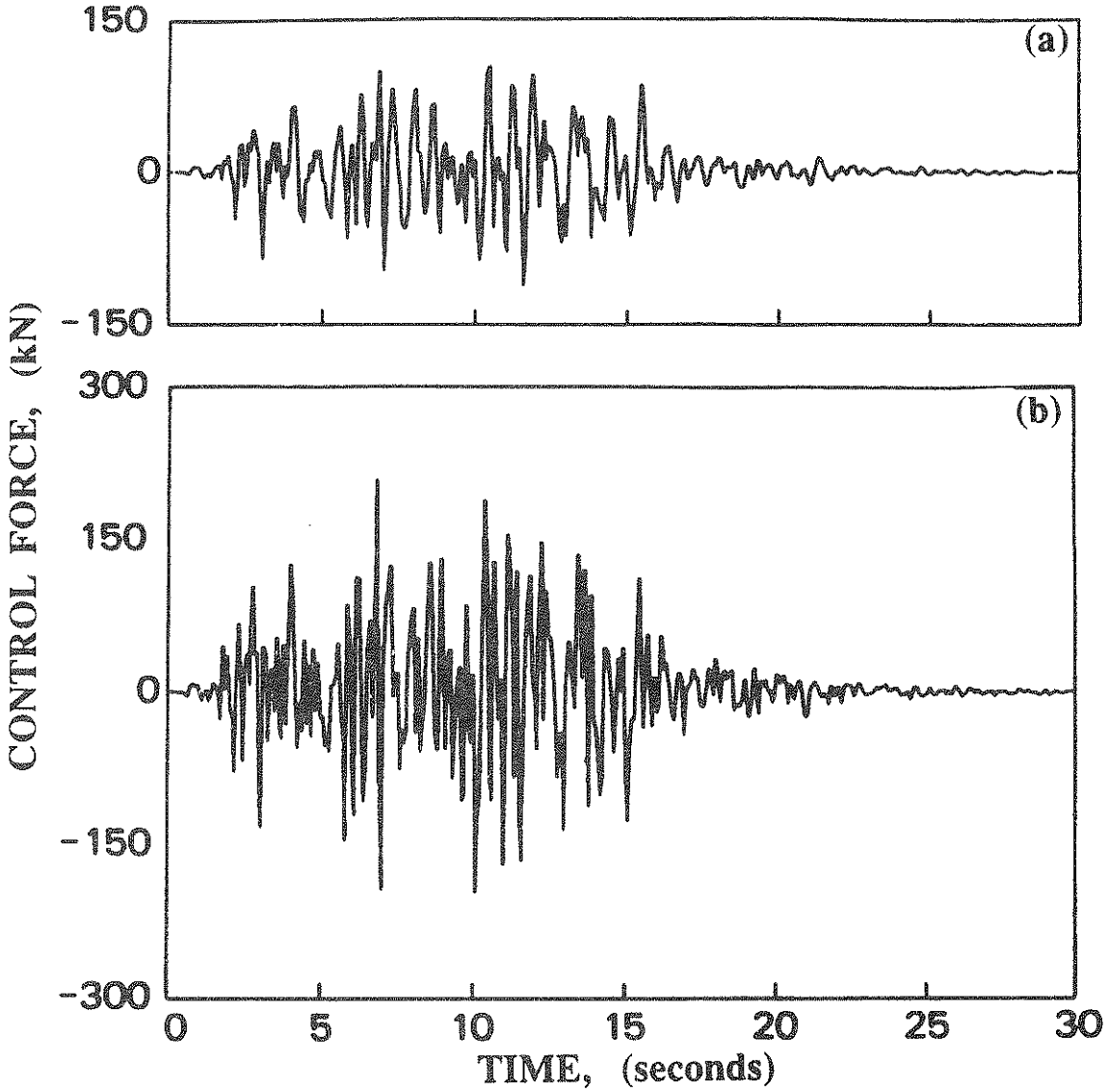

Fig. 20: Active Control Force; (a) $Q_o/R_o=2x10^7$; (b) $Q_o/R_o=9x10^7$.

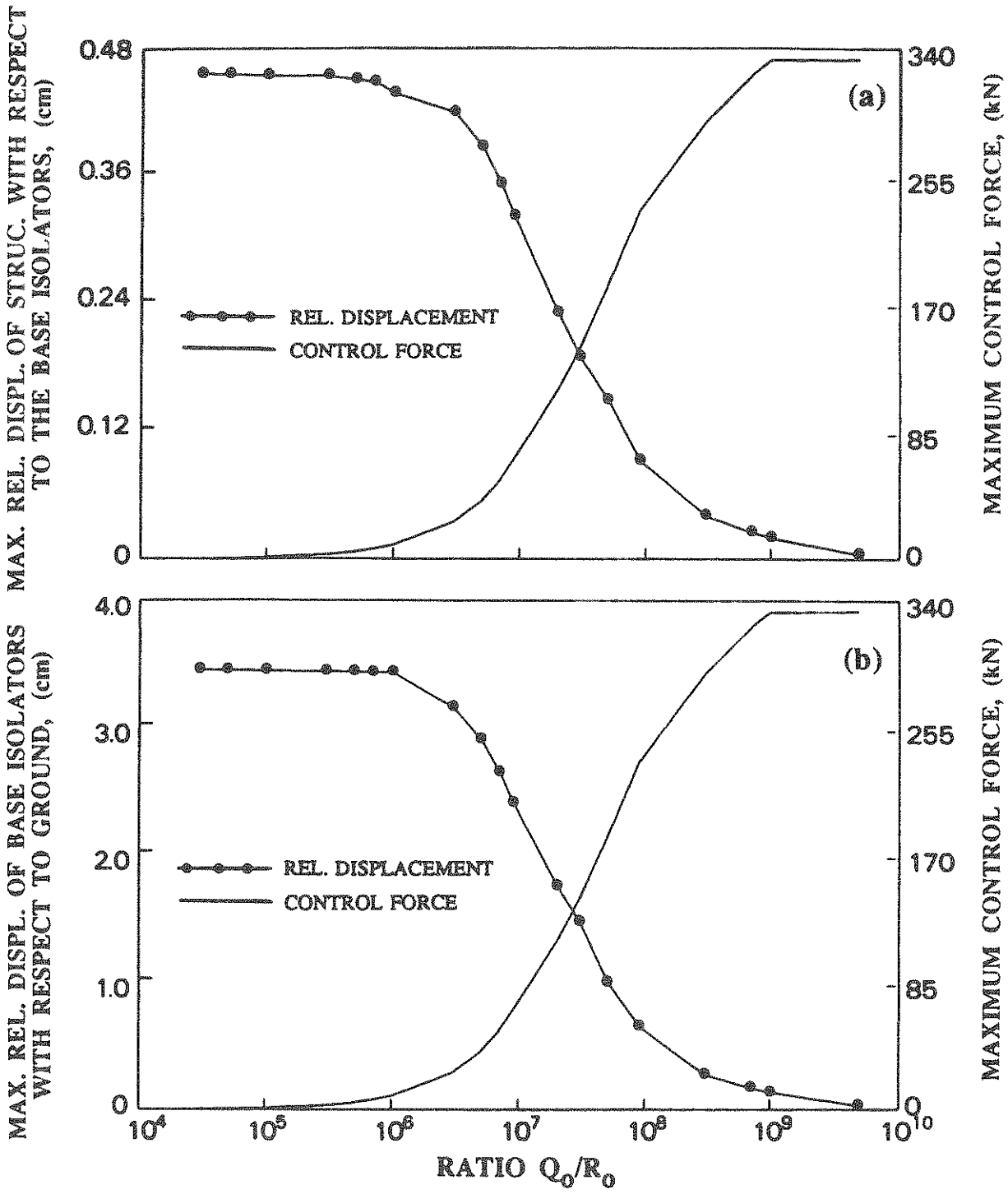

Fig. 21: Maximum Response Quantities and Control Force as Functions of Q_o/R_o Ratio; (a) Maximum Relative Displacement of Superstructure and Maximum Control Force; (b) Maximum Relative Displacement of Rubber Base Isolators and Maximum Control Force.

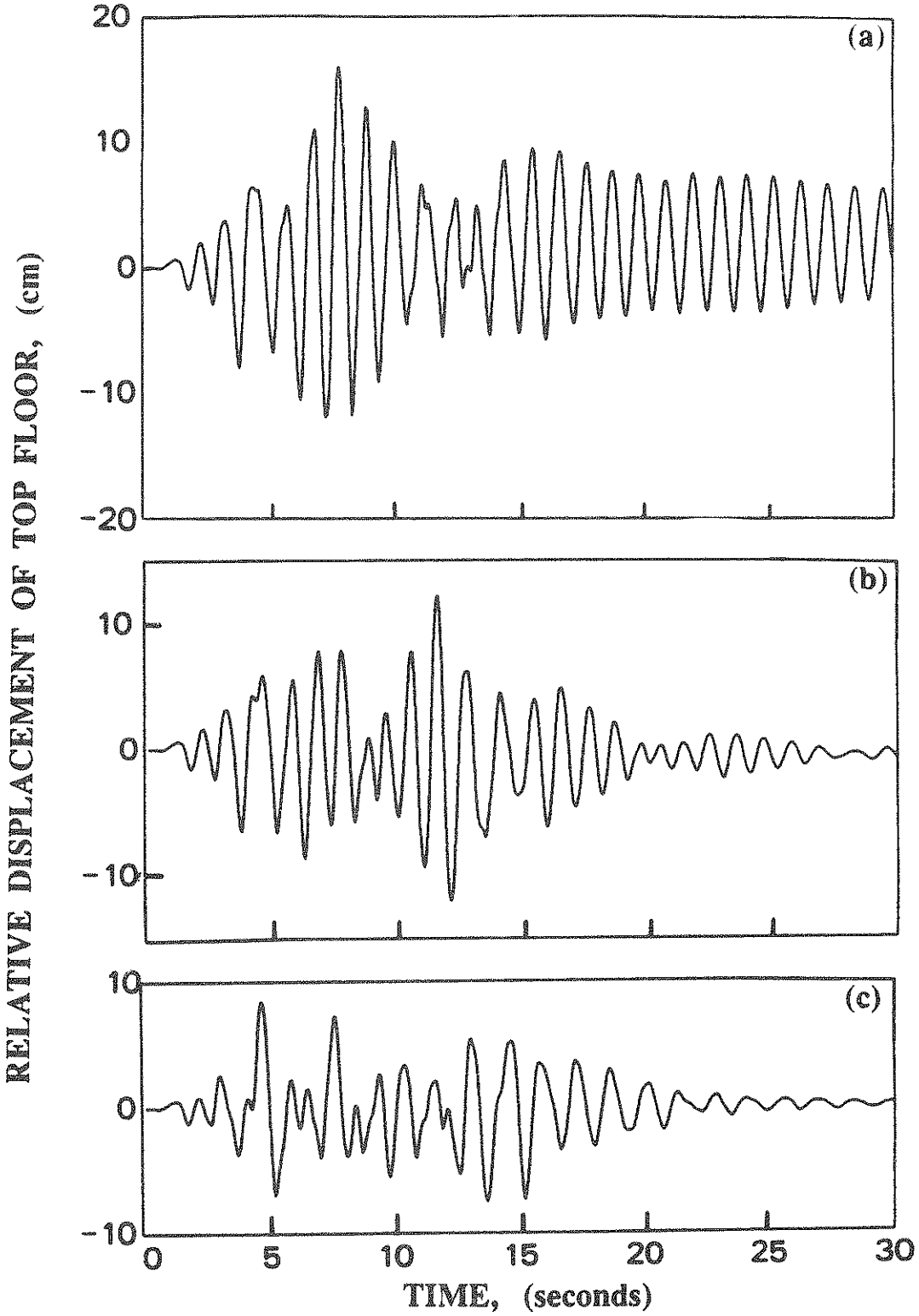

Fig. 22: Top Floor Relative Displacement With Respect to Ground (0.3g Earthquake): (a) Without Control; (b) With Passive Mass Damper; (C) With Active Mass Damper.

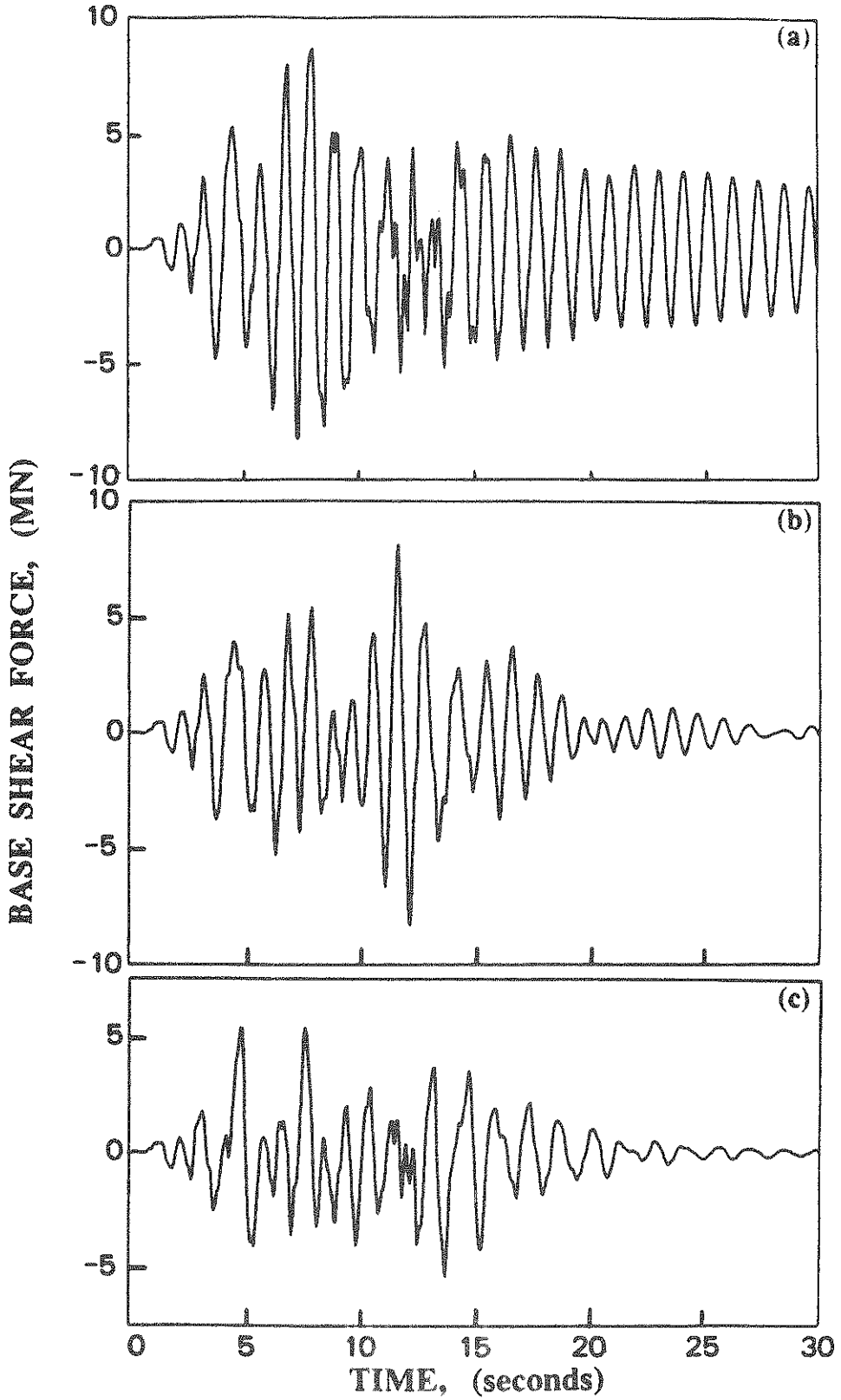

Fig. 23: Base Shear Force (0.3g Earthquake): (a) Without Control; (b) With Passive Mass Damper; (c) With Active Mass Damper.

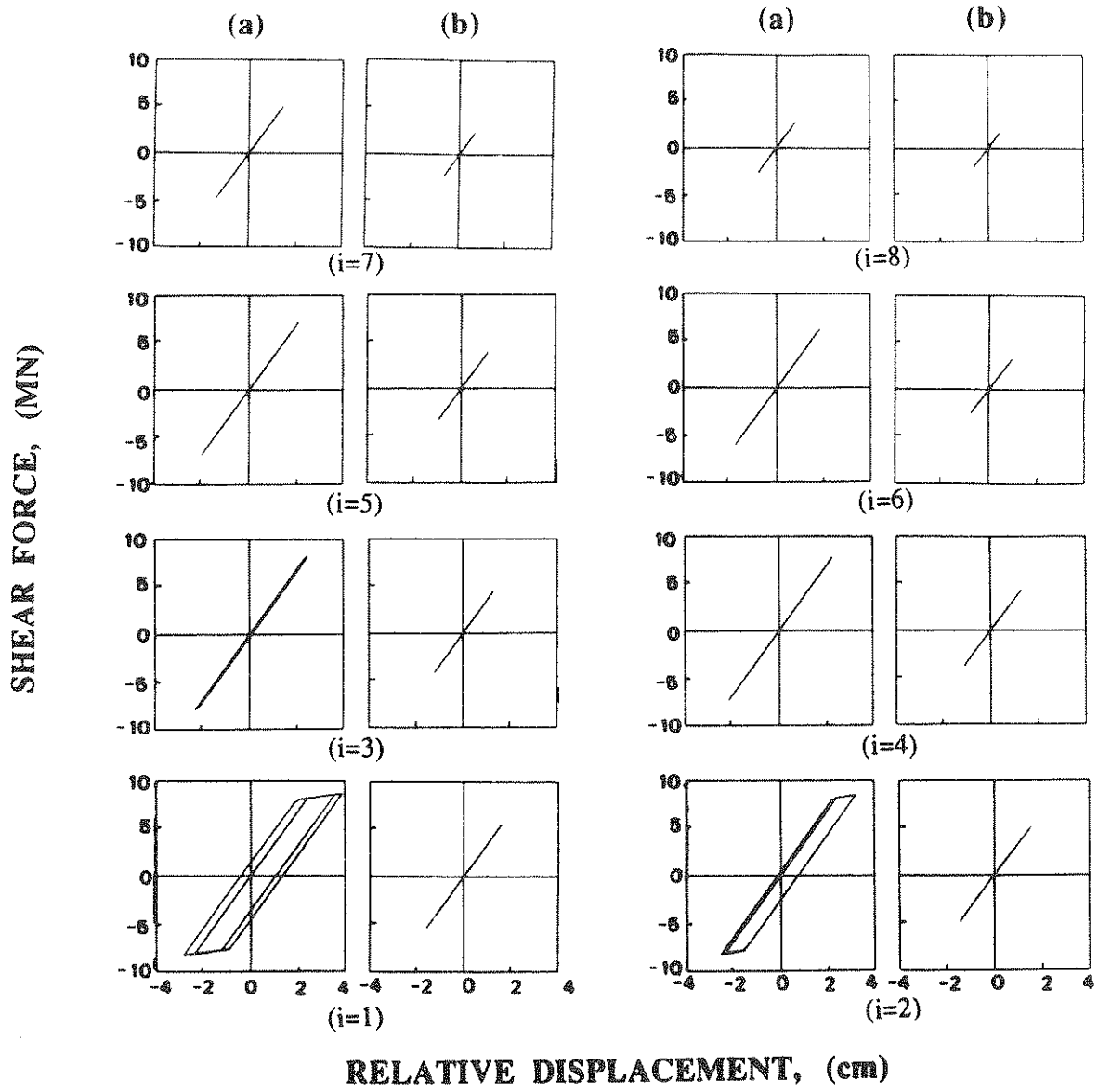

Fig. 24: Hysteresis Loops For Shear Force in Each Story Unit (0.3g Earthquake): (a) Without Control; (b) With Active Mass Damper.

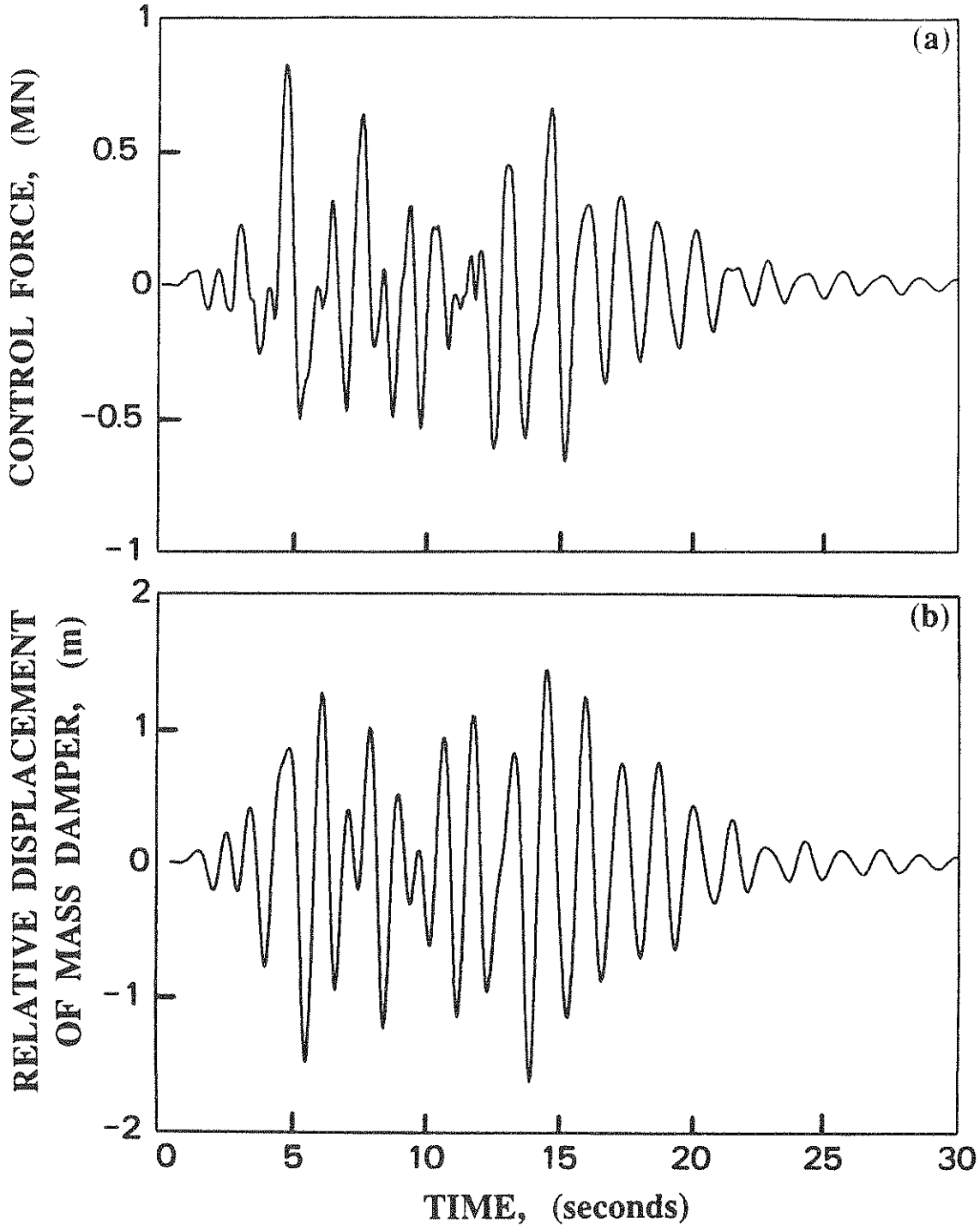

Fig. 25: Required Active Control Force and Relative Displacement of Mass Damper With Respect to Top Floor (0.3g Earthquake): (a) Active Control Force; (b) Relative Displacement of Mass Damper.

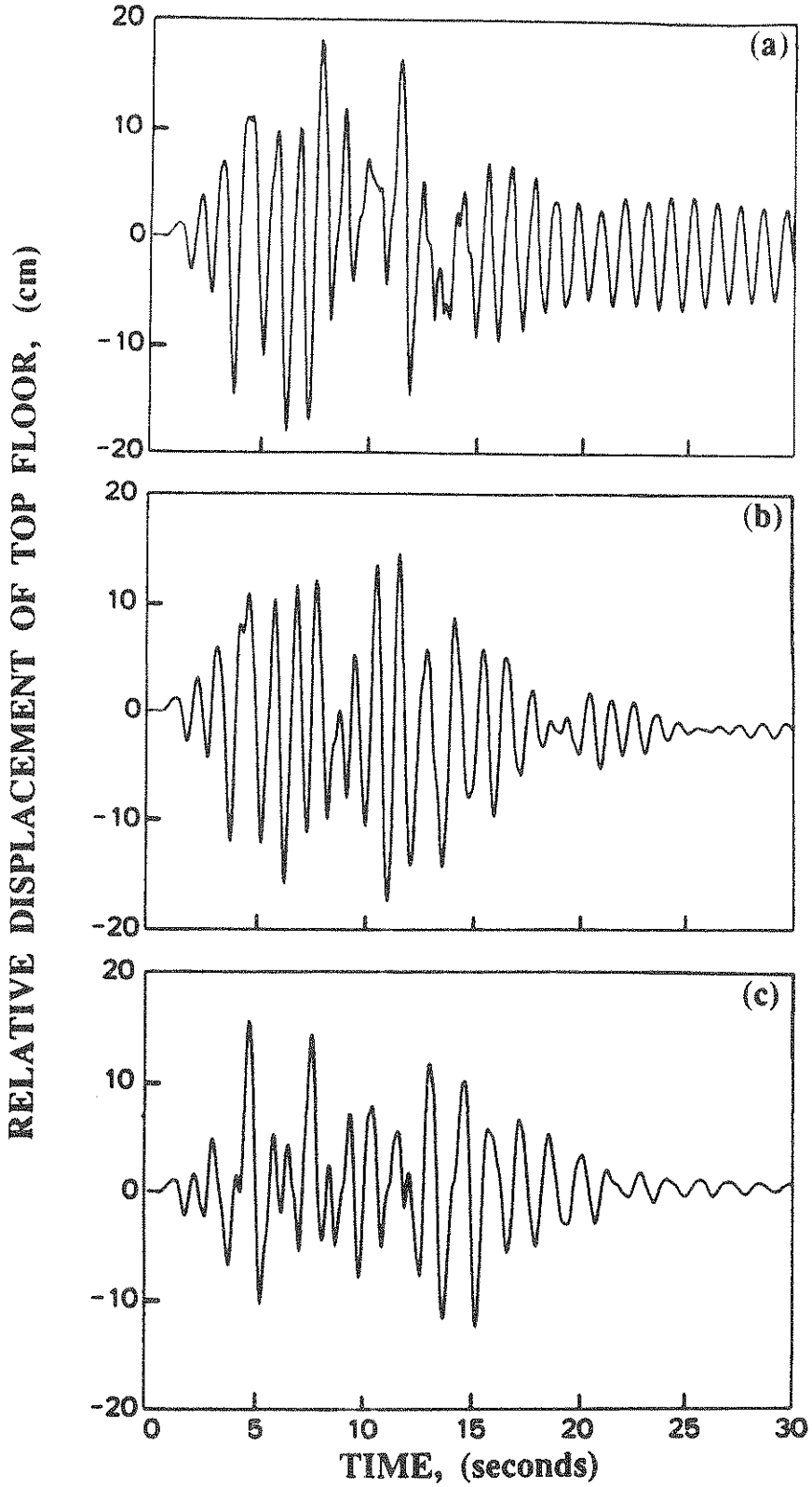

Fig. 26: Top Floor Relative Displacement With Respect to Ground (0.55g Earthquake): (a) Without Control; (b) With Passive Mass Damper; (c) With Active Mass Damper.

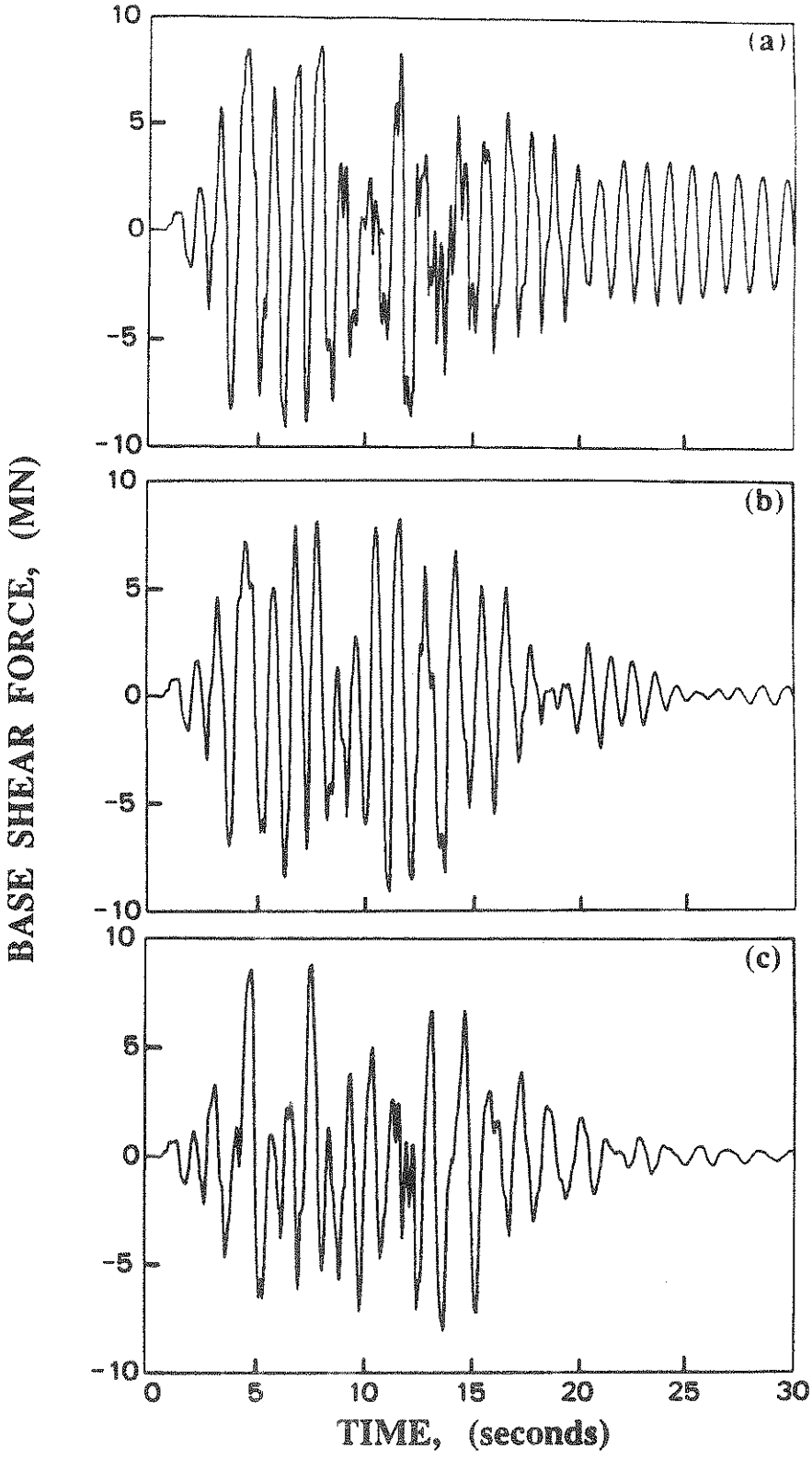

Fig. 27: Base Shear Force (0.55g Earthquake): (a) Without Control; (b) With Passive Mass Damper; (c) With Active Mass Damper.

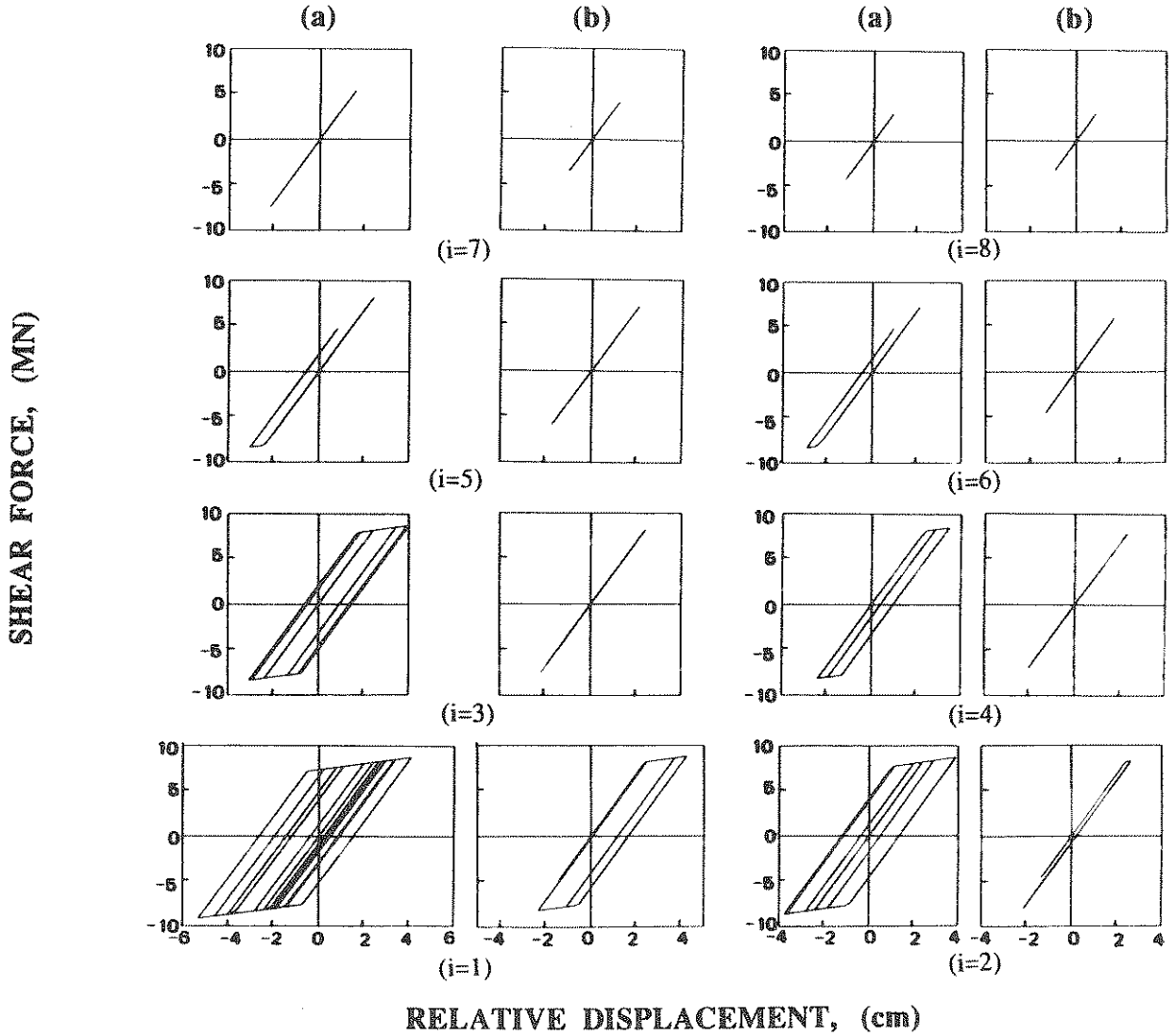

Fig. 28: Hysteresis Loops For Shear Force in Each Story Unit (0.55g Earthquake): (a) Without Control; (b) With Active Mass Damper.

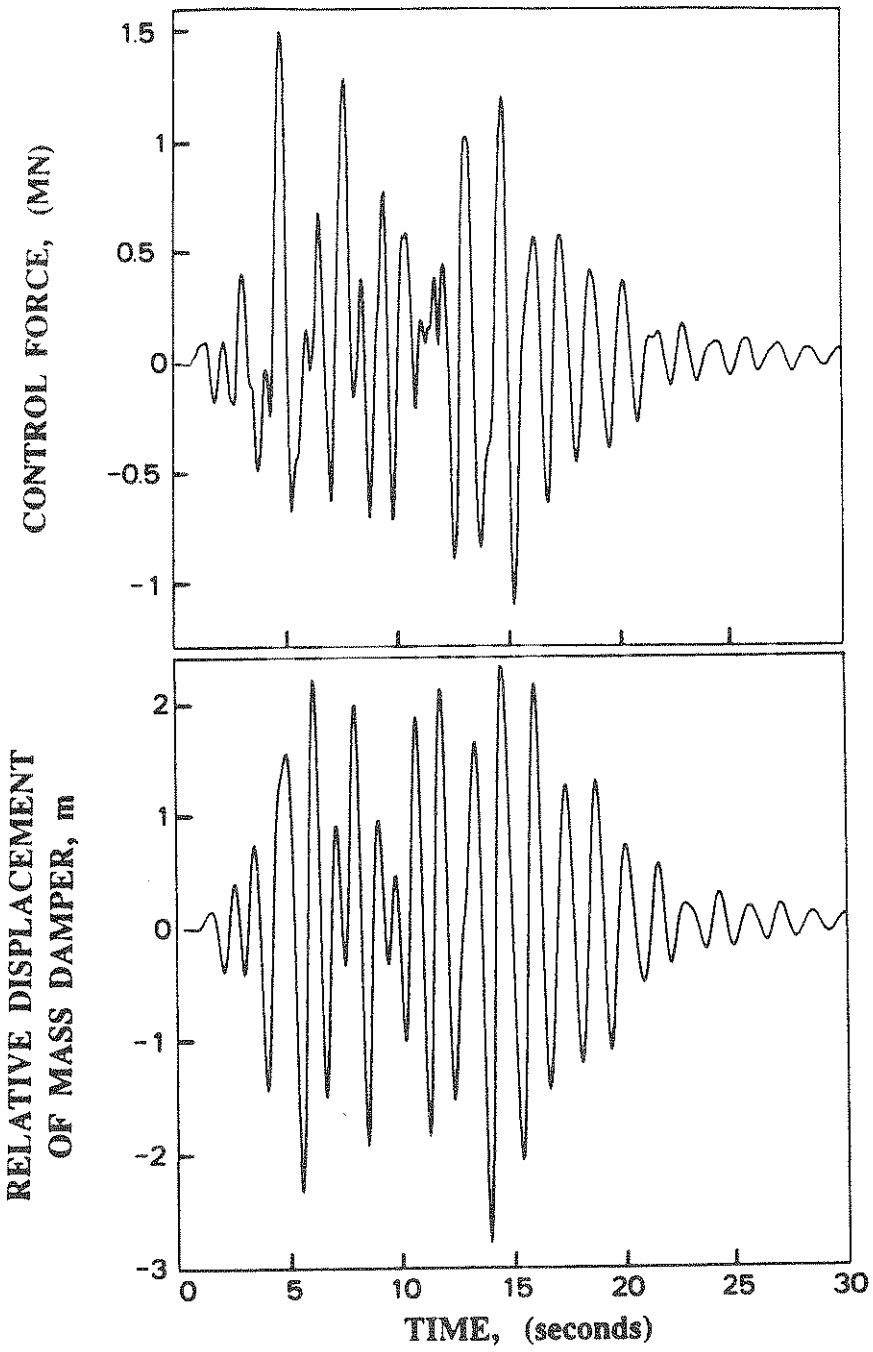

Fig. 29: Required Active Control Force and Relative Displacement of Mass Damper With Respect to Top Floor (0.55g Earthquake): (a) Active Control Force; (b) Relative Displacement of Mass Damper.

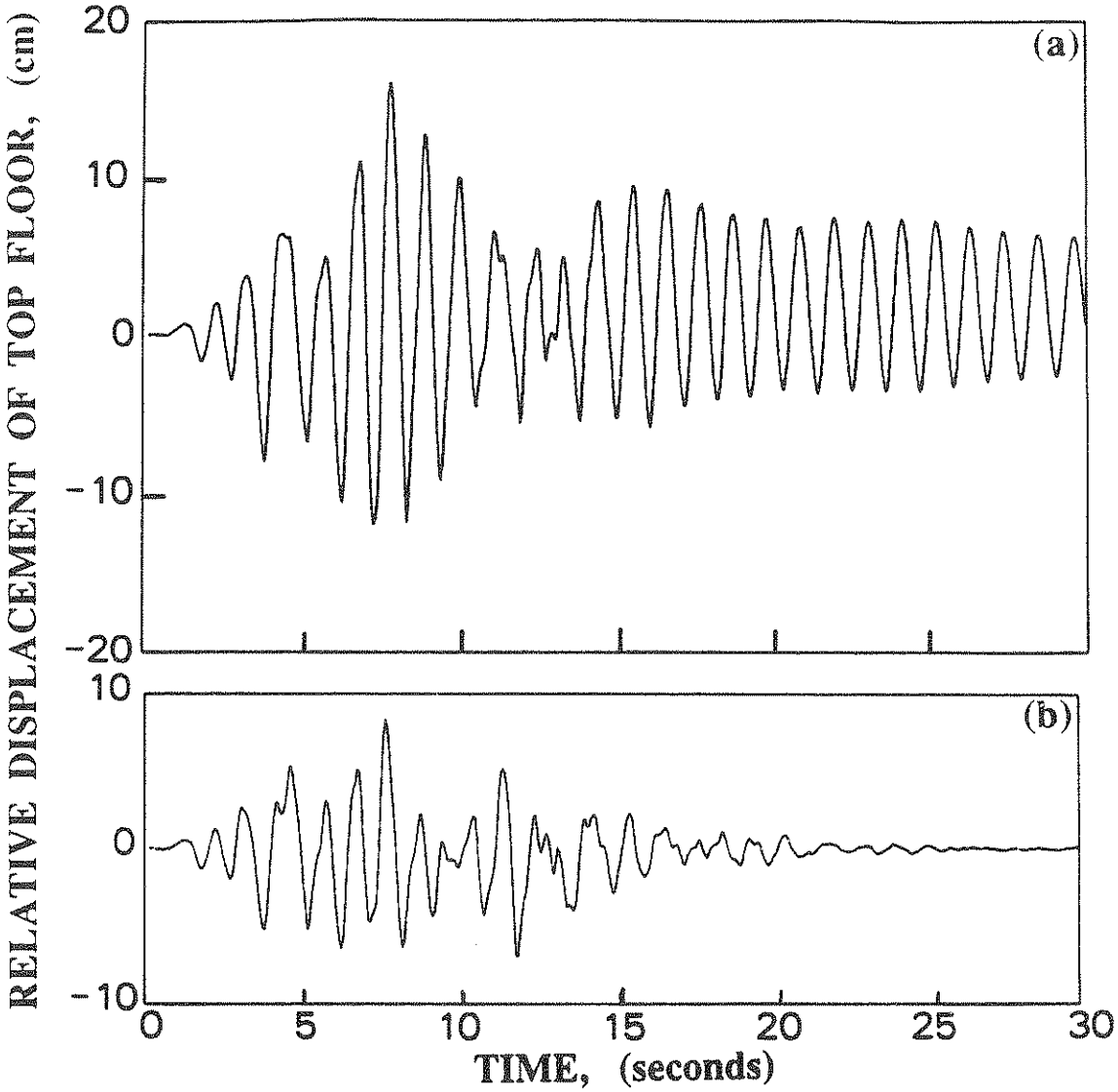

Fig. 30: Top Floor Relative Displacement With Respect to Ground (0.3g Earthquake): (a) Without Control; (b) With Active Tendon Control.

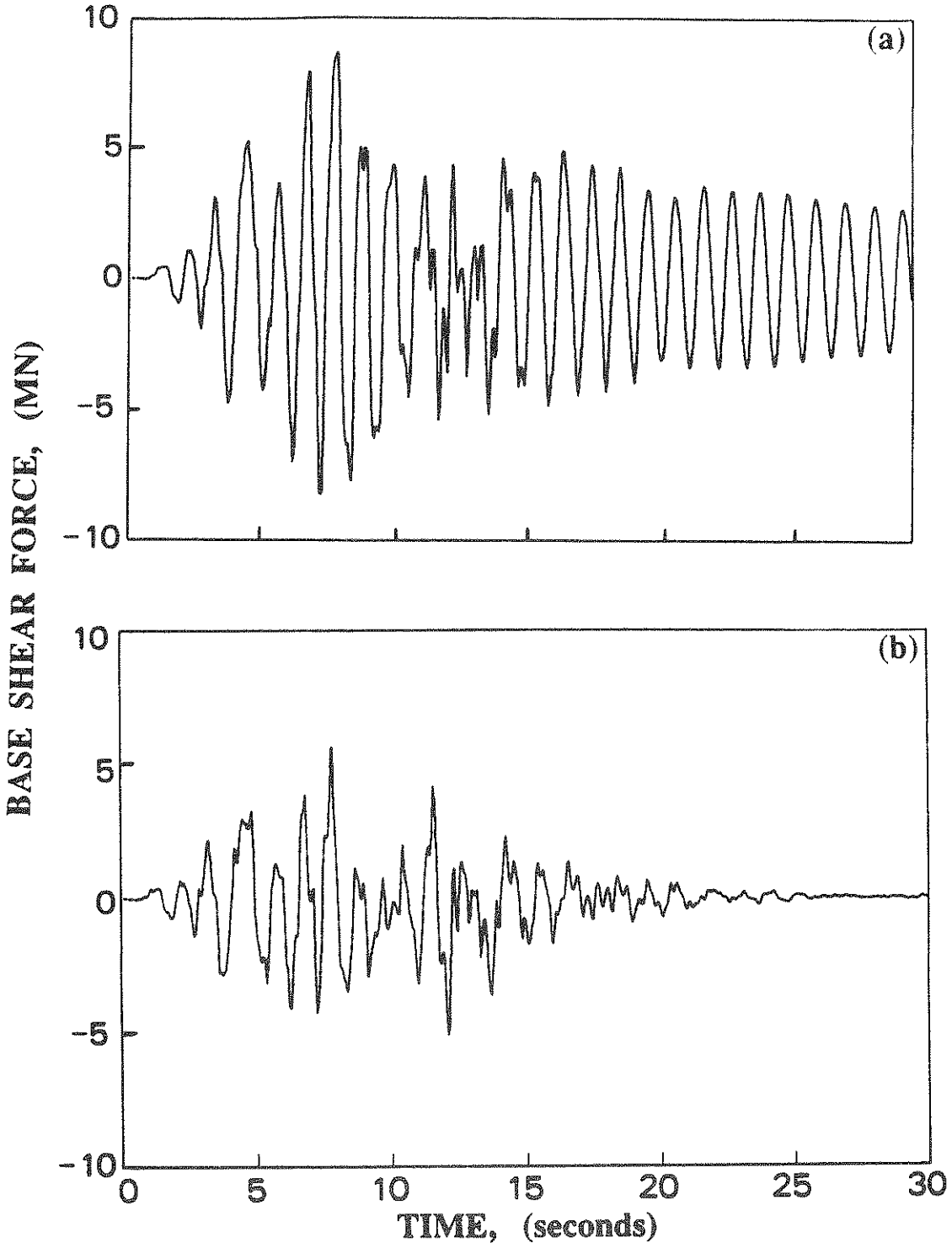

Fig. 31: Base Shear Force (0.3g Earthquake): (a) Without Control; (b) With Active Tendon Control.

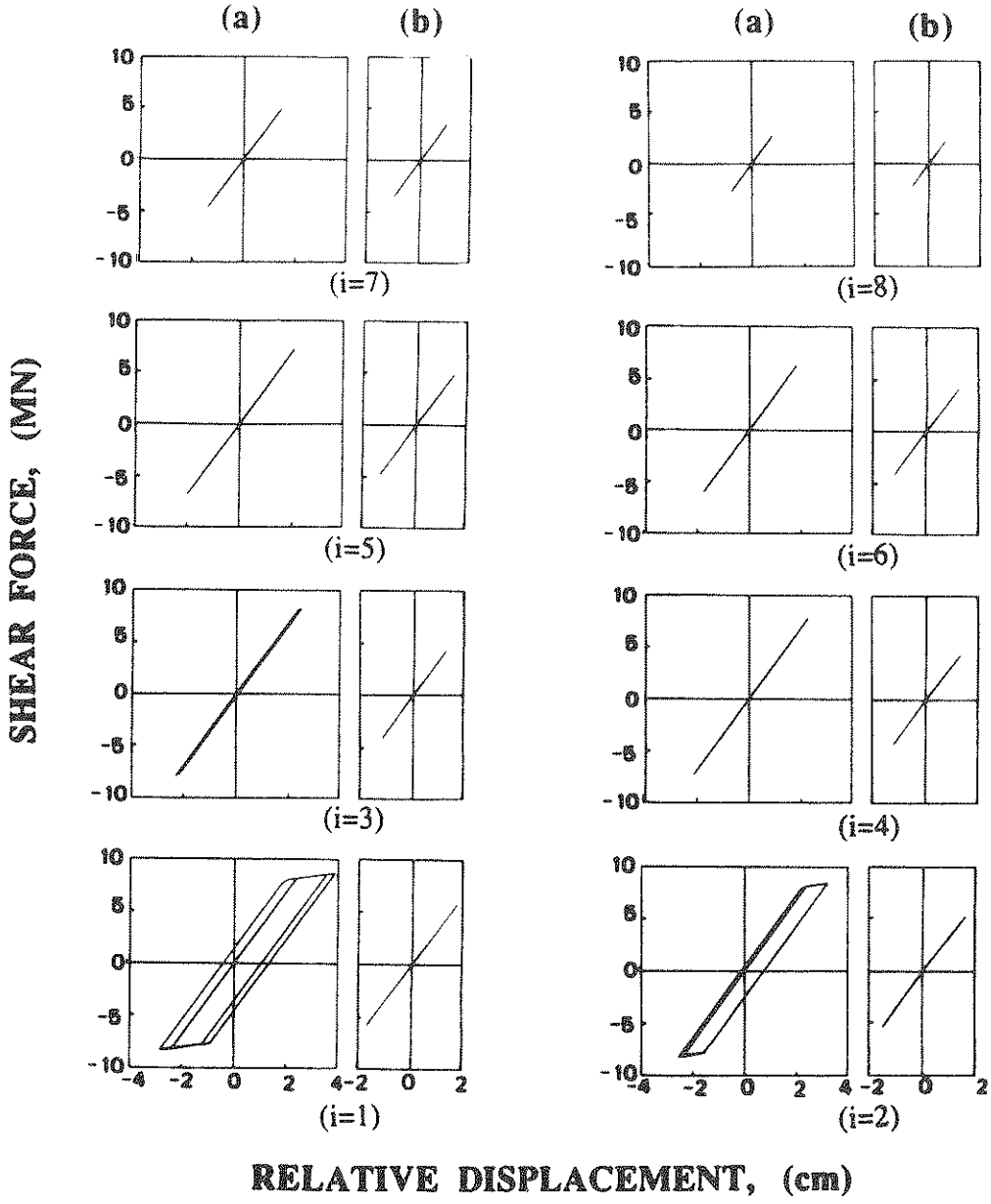

Fig. 32: Hysteresis Loops For Shear Force In Each Story Unit (0.3g Earthquake): (a) Without Control; (b) With Active Tendon Control.

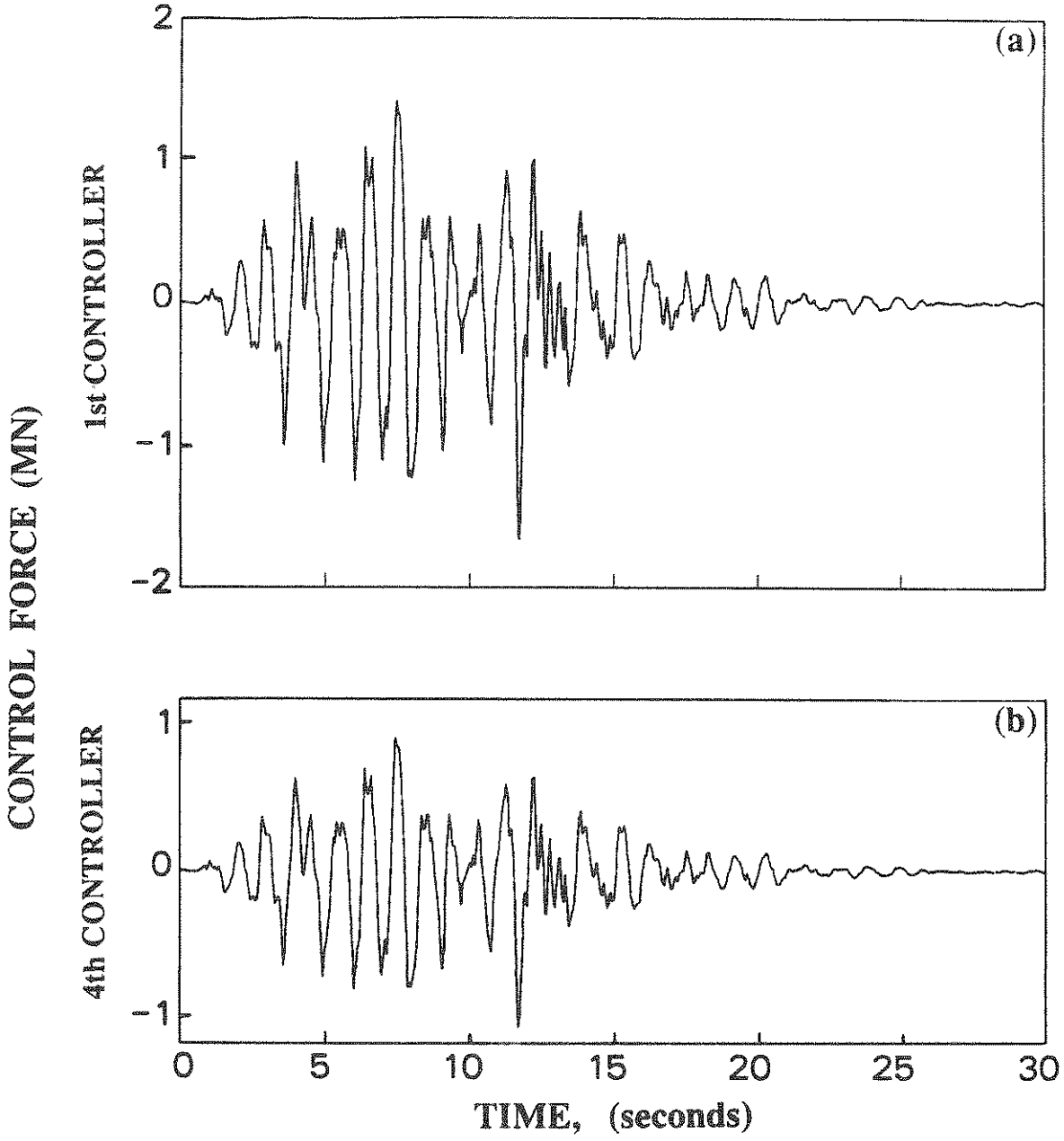

Fig. 33: Required Active Tendon Control Force (0.3g Earthquake): (a) From First Controller; (b) From Fourth Controller.

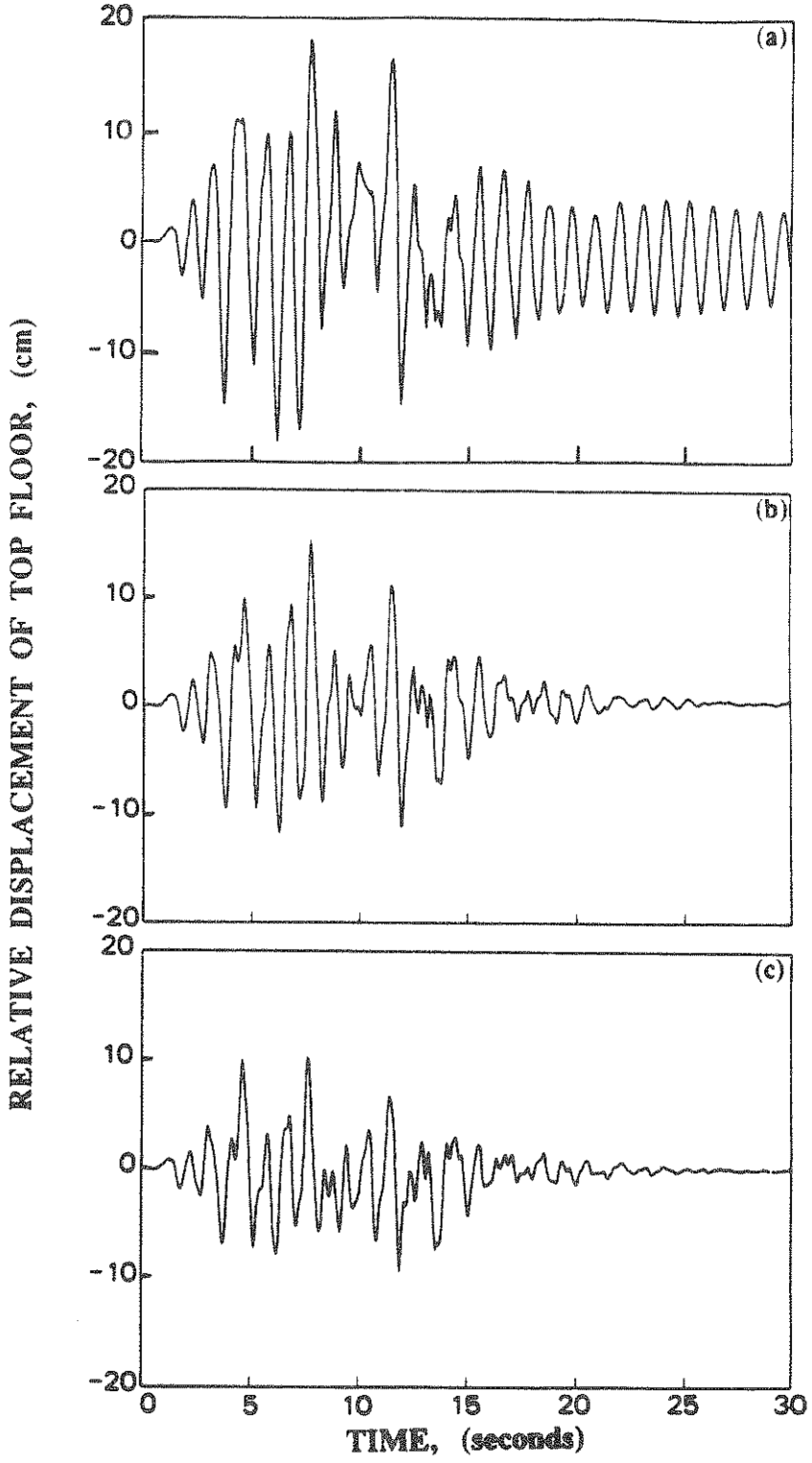

Fig. 34: Top Floor Relative Displacement With Respect to Ground (0.55g Earthquake): (a) Without Control; (b) With Active Tendon Control ($\alpha = 0.25 \times 10^4$); (c) With Active Tendon Control ($\alpha = 0.55 \times 10^4$).

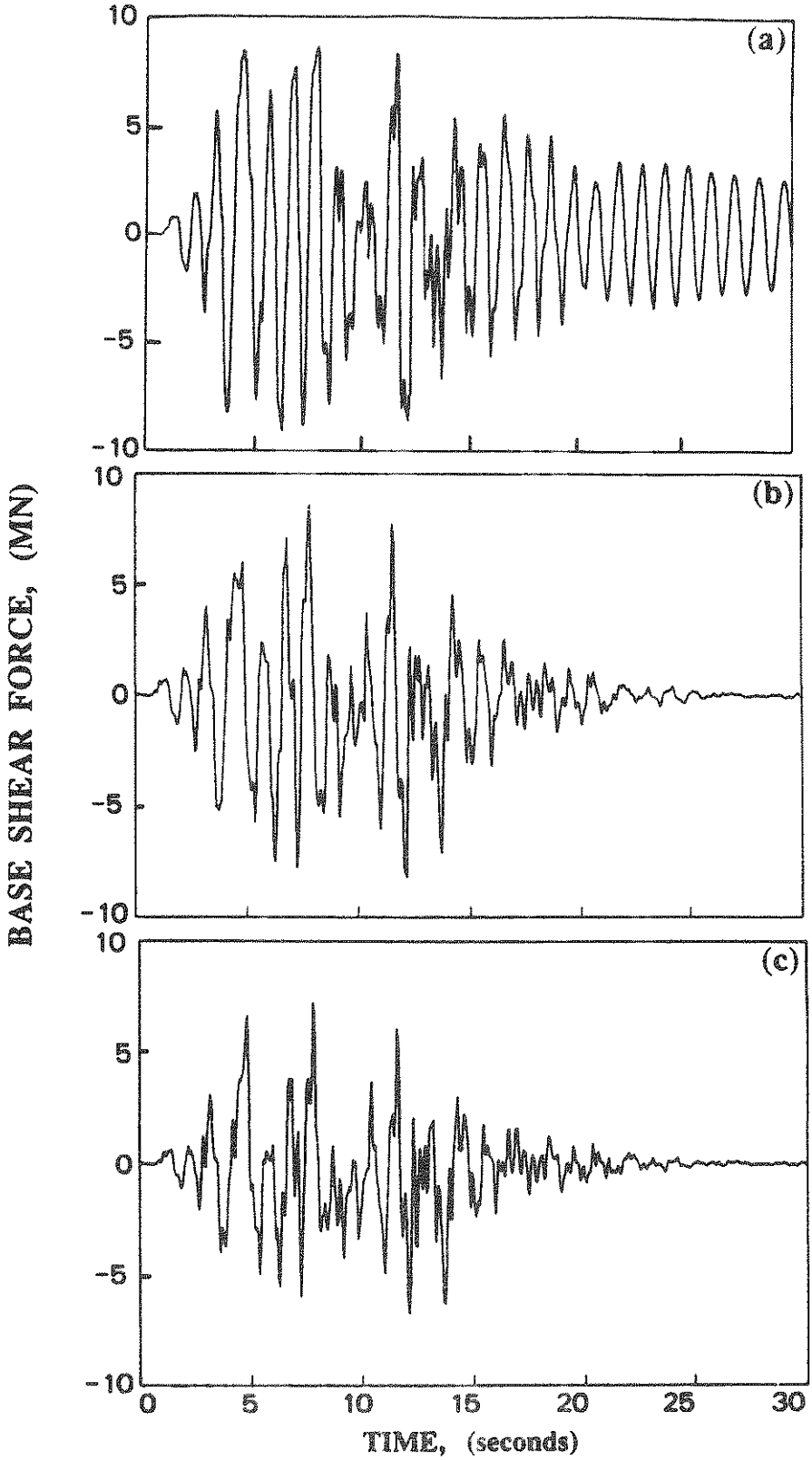

Fig. 35: Base Shear Force (0.55g Earthquake): (a) Without Control; (b) With Active Tendon Control ($\alpha = 0.25 \times 10^4$); (c) With Active Tendon Control ($\alpha = 0.55 \times 10^4$).

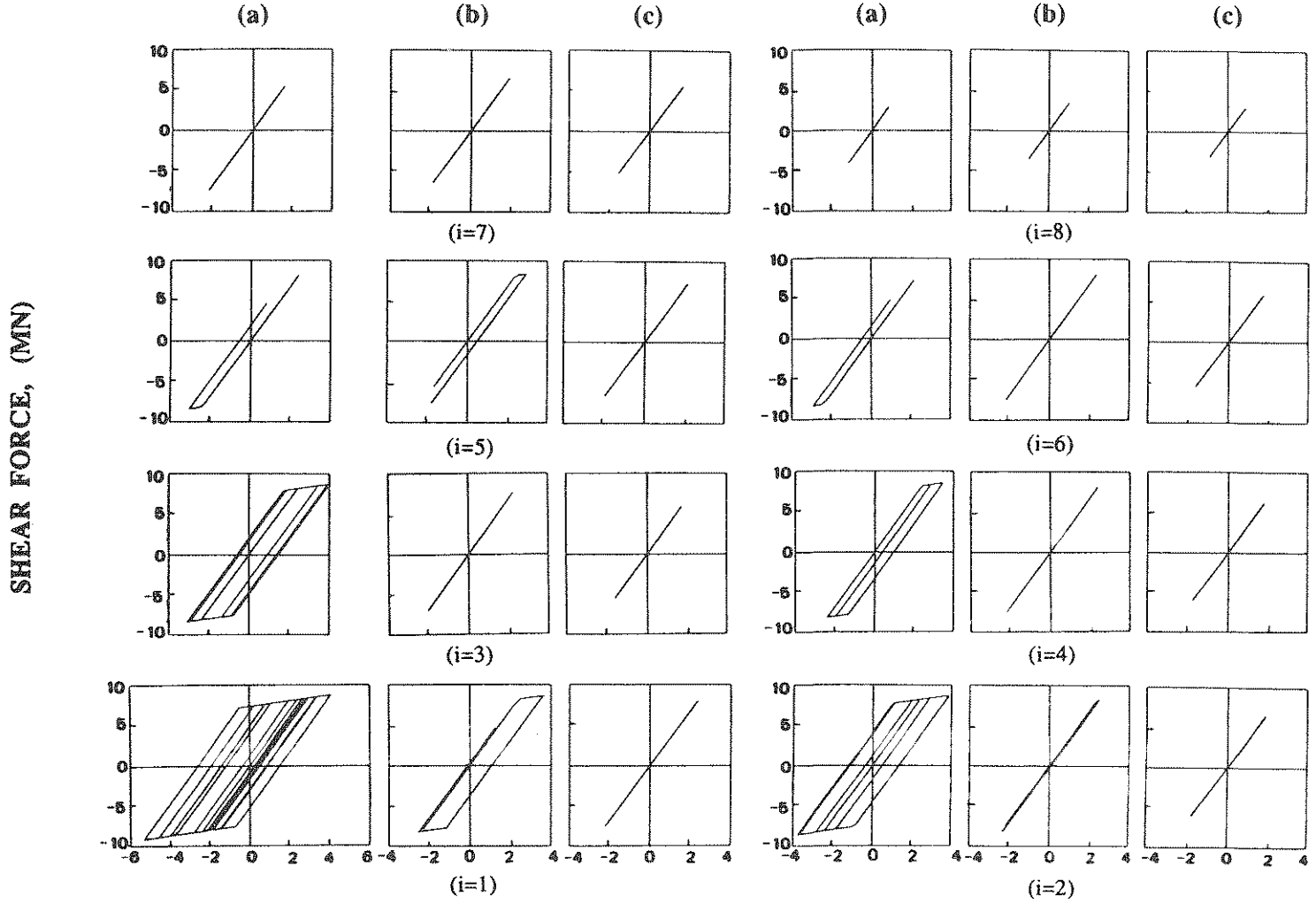

Fig. 36: Hysteresis Loops For Shear Force In Each Story Unit (0.55g Earthquake): (a) Without Control; (b) With Active Tendon Control ($\alpha = 0.25 \times 10^4$); (c) With Active Tendon Control ($\alpha = 0.55 \times 10^4$).

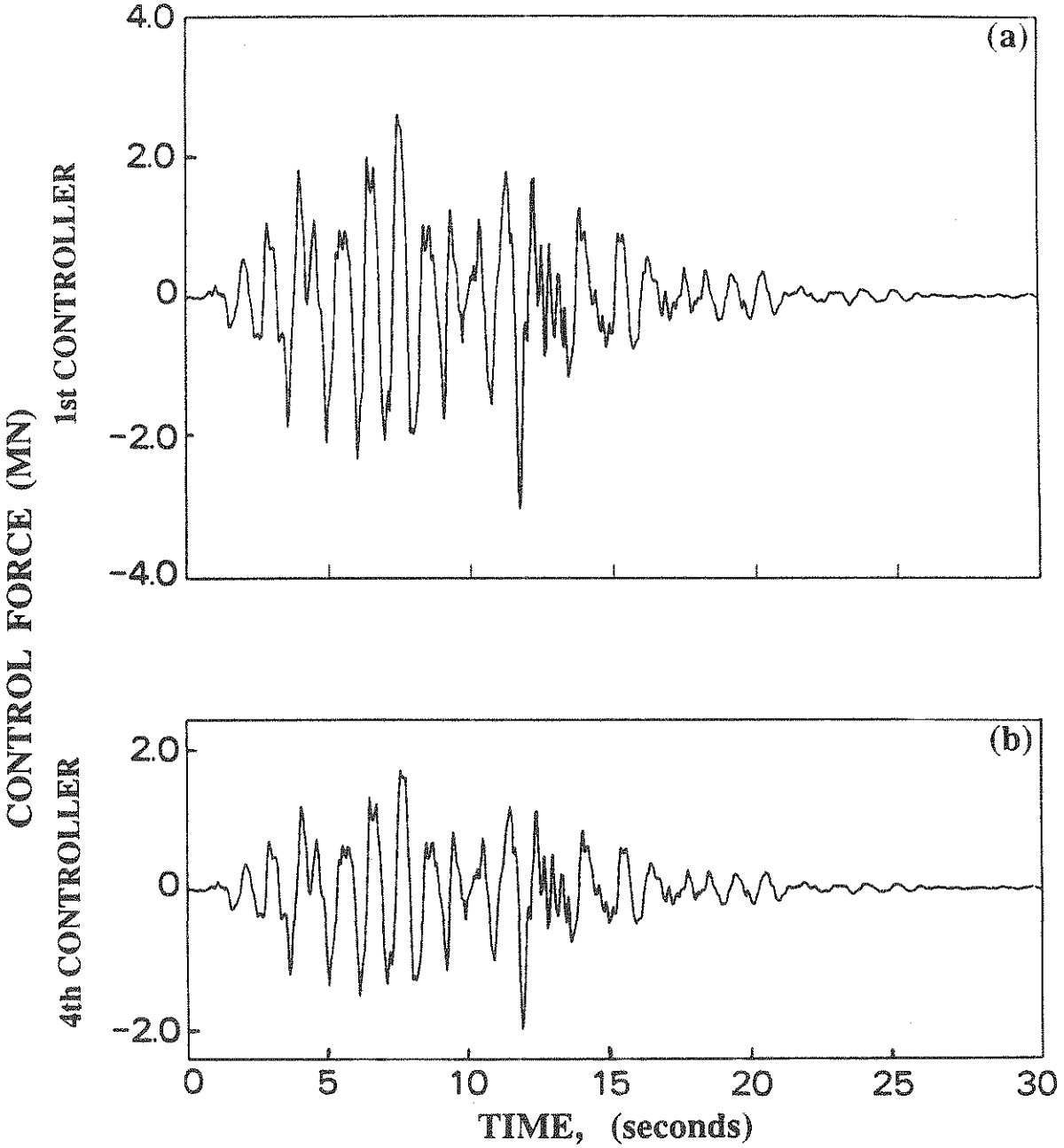

Fig. 37a: Required Active Tendon Control Force for $\alpha = 0.25 \times 10^4$ (0.55g Earthquake): (a) From First Controller; (b) From Fourth Controller.

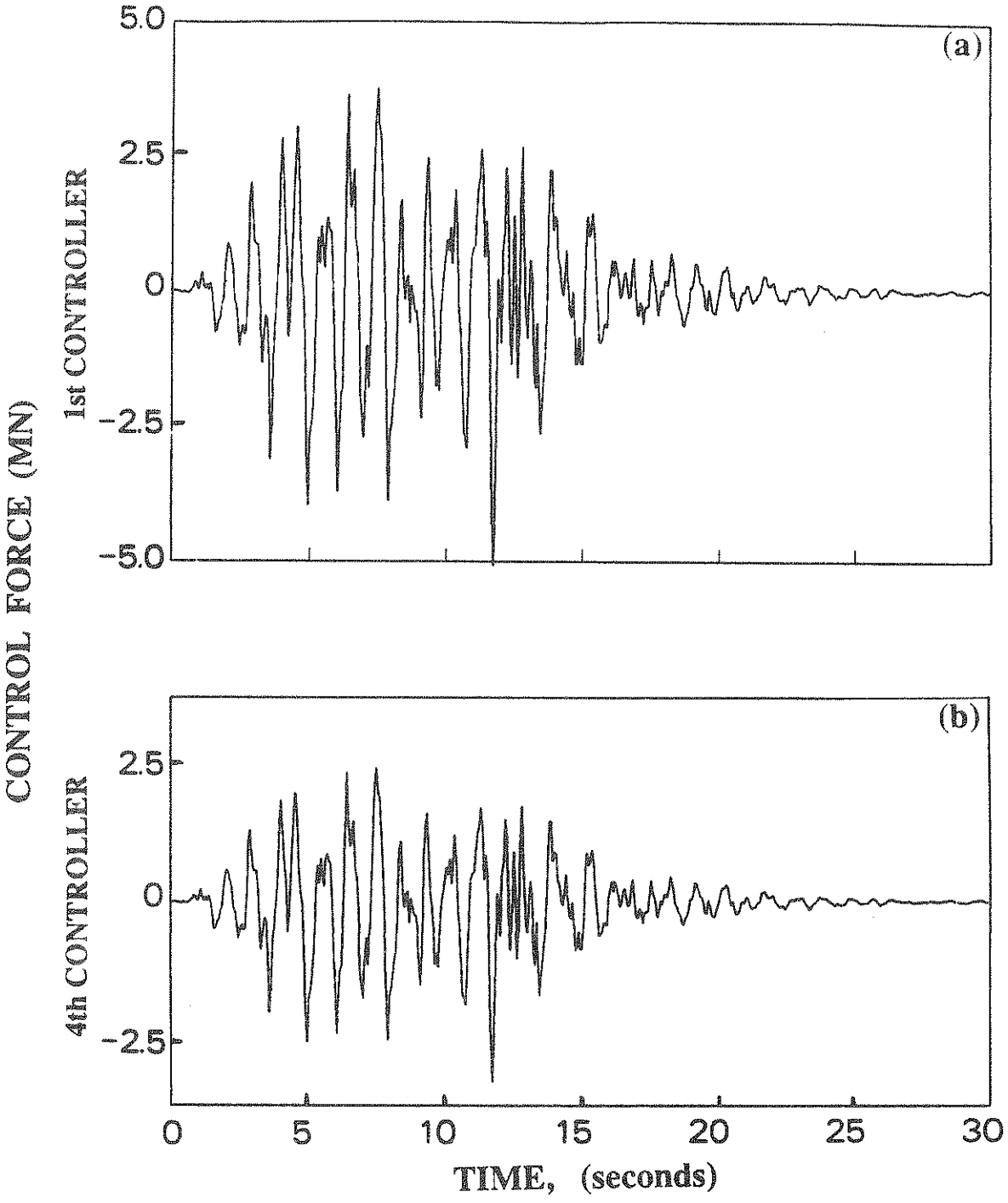

Fig. 37b: Required Active Tendon Control Force for $\alpha = 0.55 \times 10^4$ (0.55g Earthquake): (a) From First Controller; (b) From Fourth Controller.

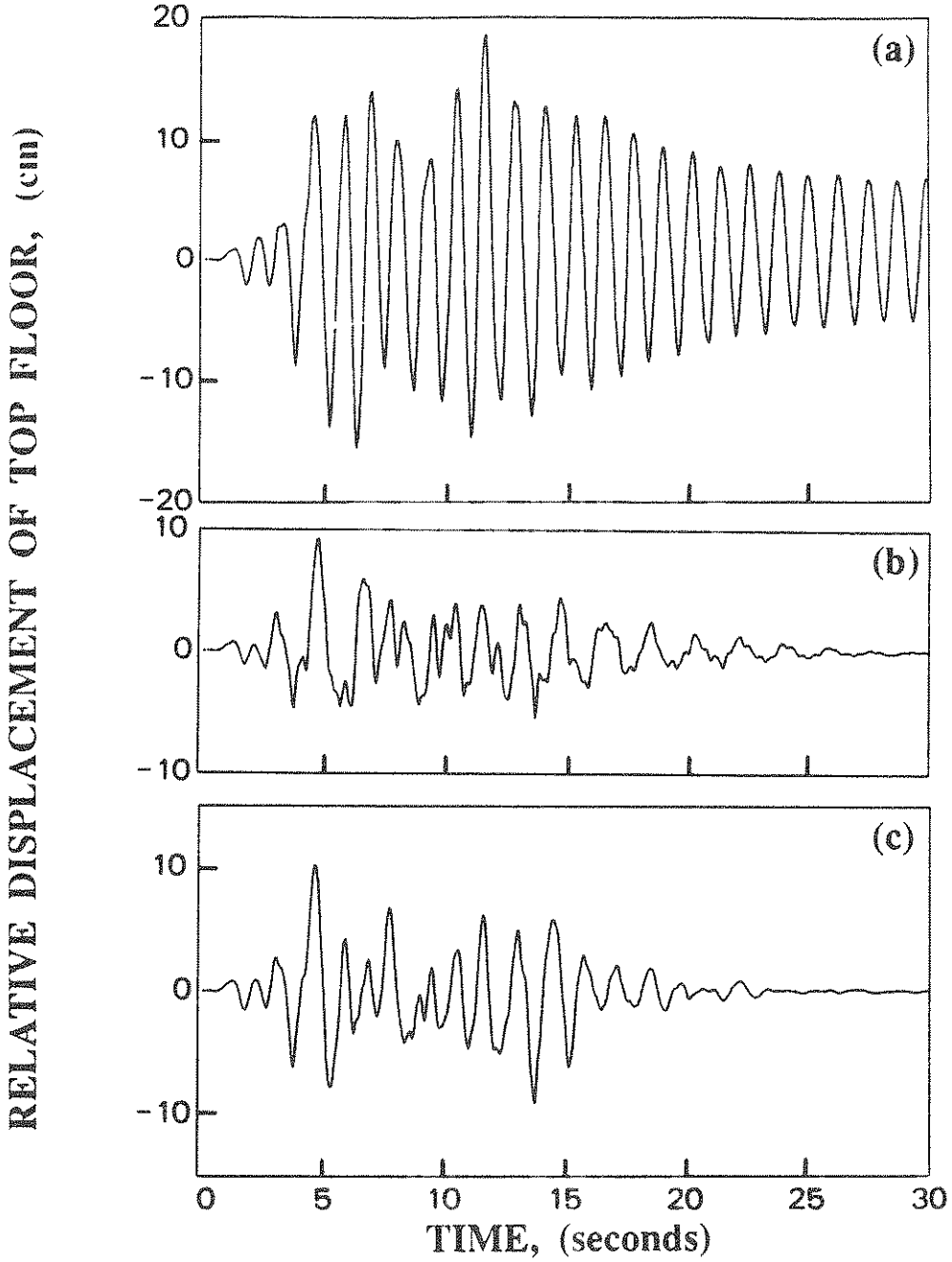

Fig. 38: Top Floor Relative Displacement with Respect to Ground (0.3g Earthquake): (a) Without Control; (b) With Active Mass Damper Using State Variables y_i; (c) With Active Mass Damper Using State Variables x_i.

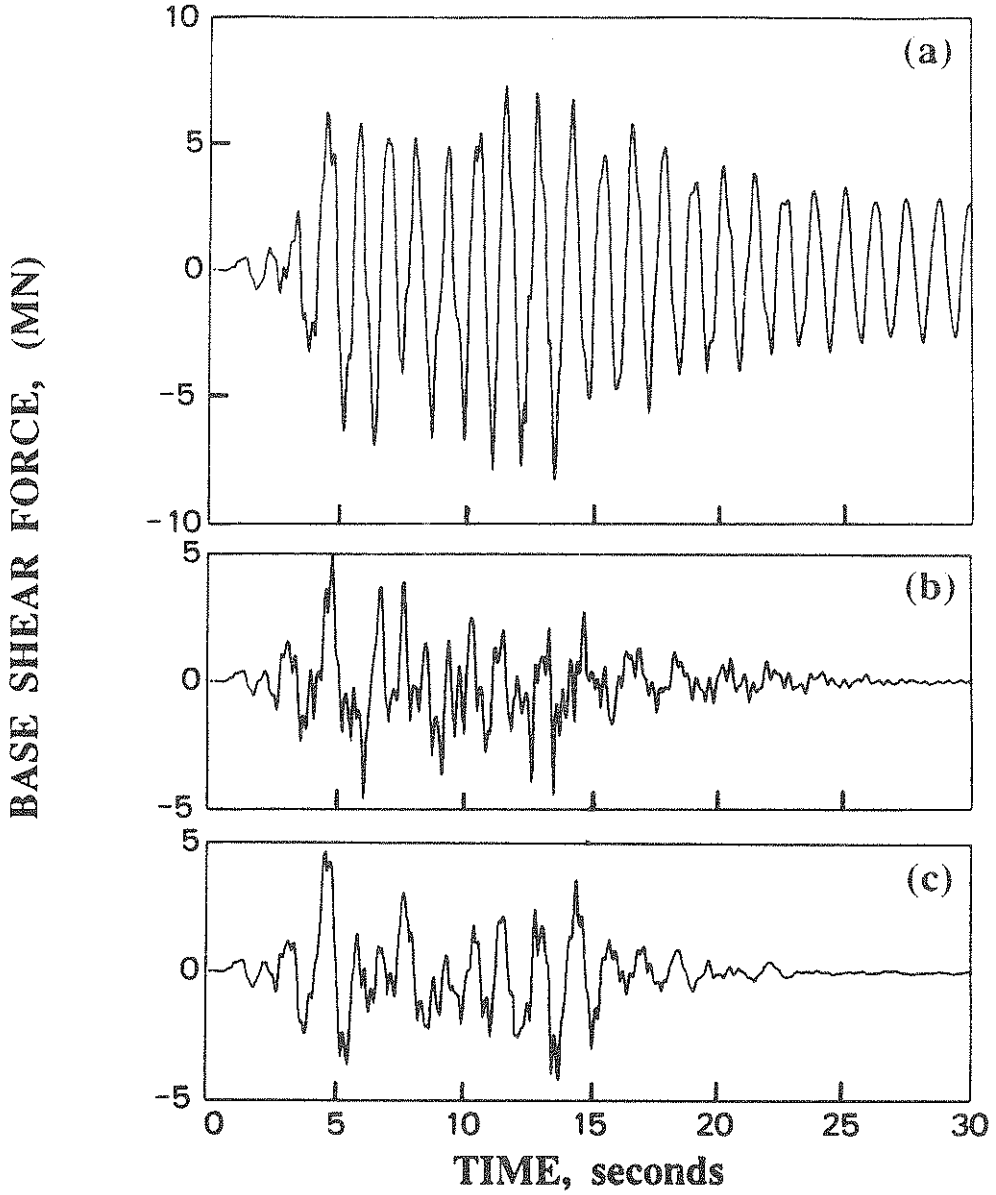

Fig. 39: Base Shear Force (0.3g Earthquake): (a) Without Control; (b) With Active Mass Damper Using State Variables y_i; (c) With Active Mass Damper Using State Variables x_i.

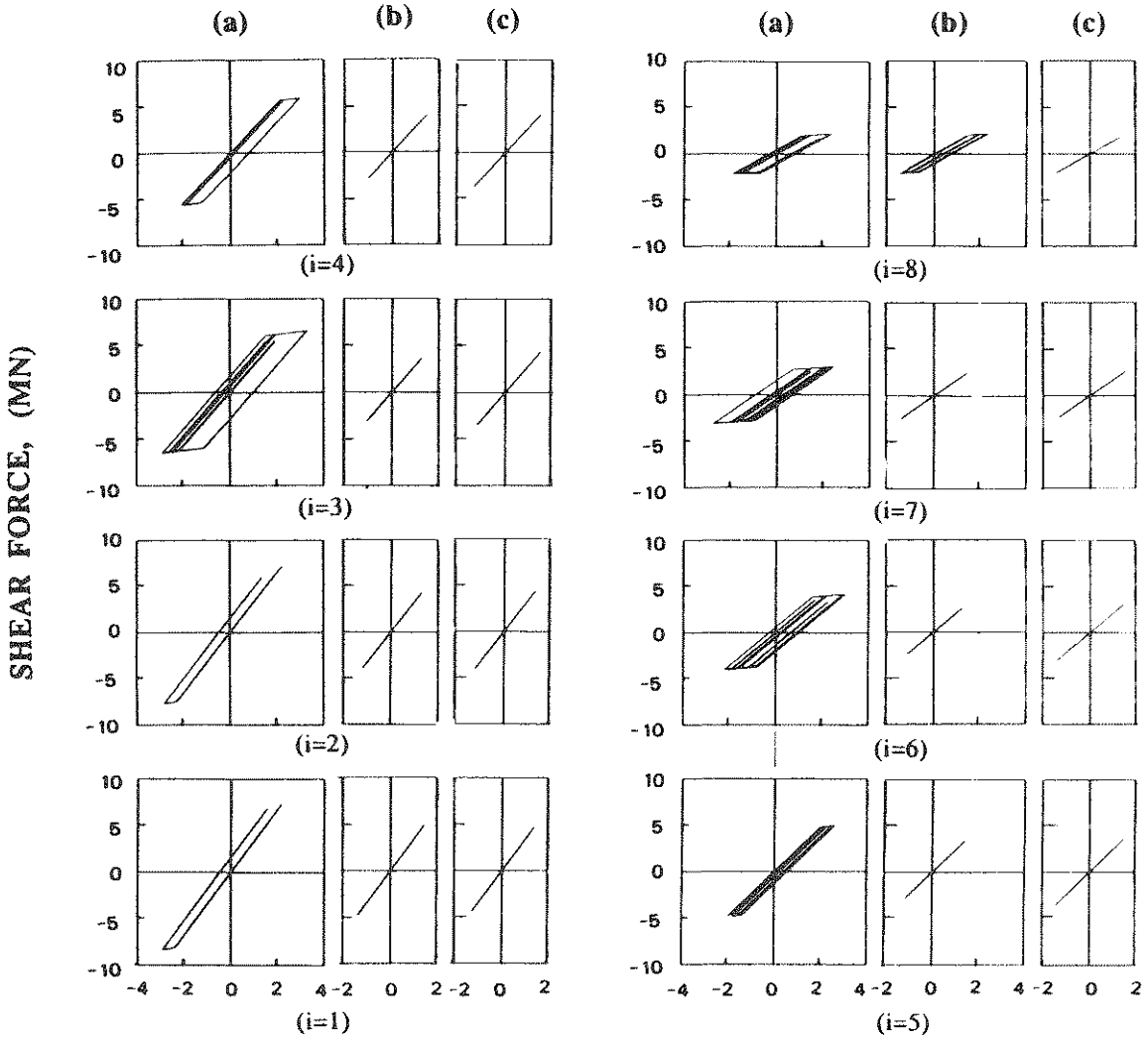

Fig. 40: Hysteresis Loops for Shear Force in Each Story Unit (0.3g Earthquake): (a) Without Control; (b) With Active Mass Damper Using State Variables y_i; (c) With Active Mass Damper Using State Variables x_i.

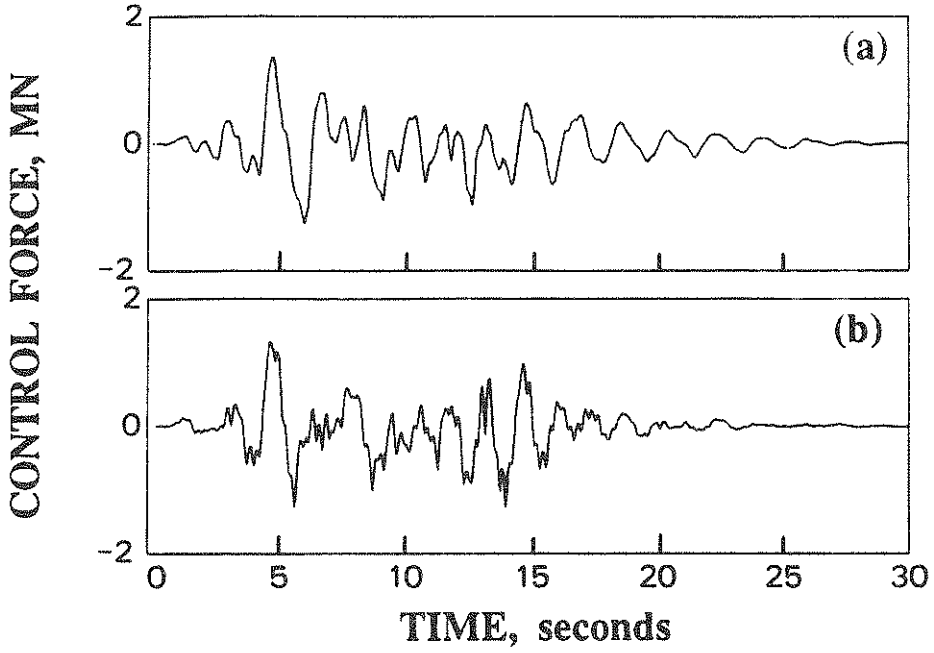

Fig. 41: Required Active Control Force (0.3g Earthquake): (a) With Active Mass Damper Using State Variables y_i; (b) With Active Mass Damper Using State Variables x_i.

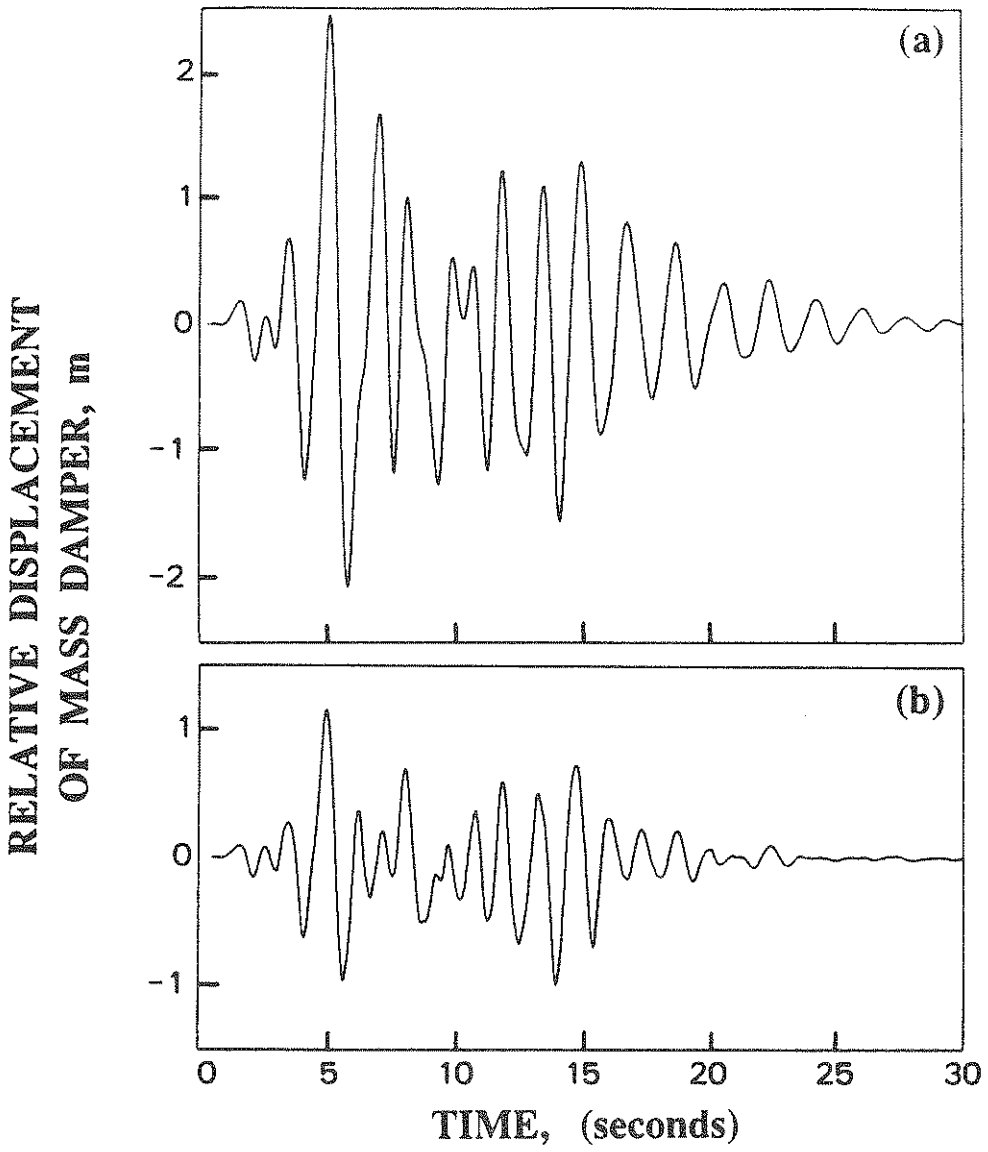

Fig. 42: Relative Displacement of Mass Damper with Respect to Top Floor (0.3g Earthquake): (a) With Active Mass Damper Using State Variables y_i; (b) With Active Mass Damper Using State Variables x_i.

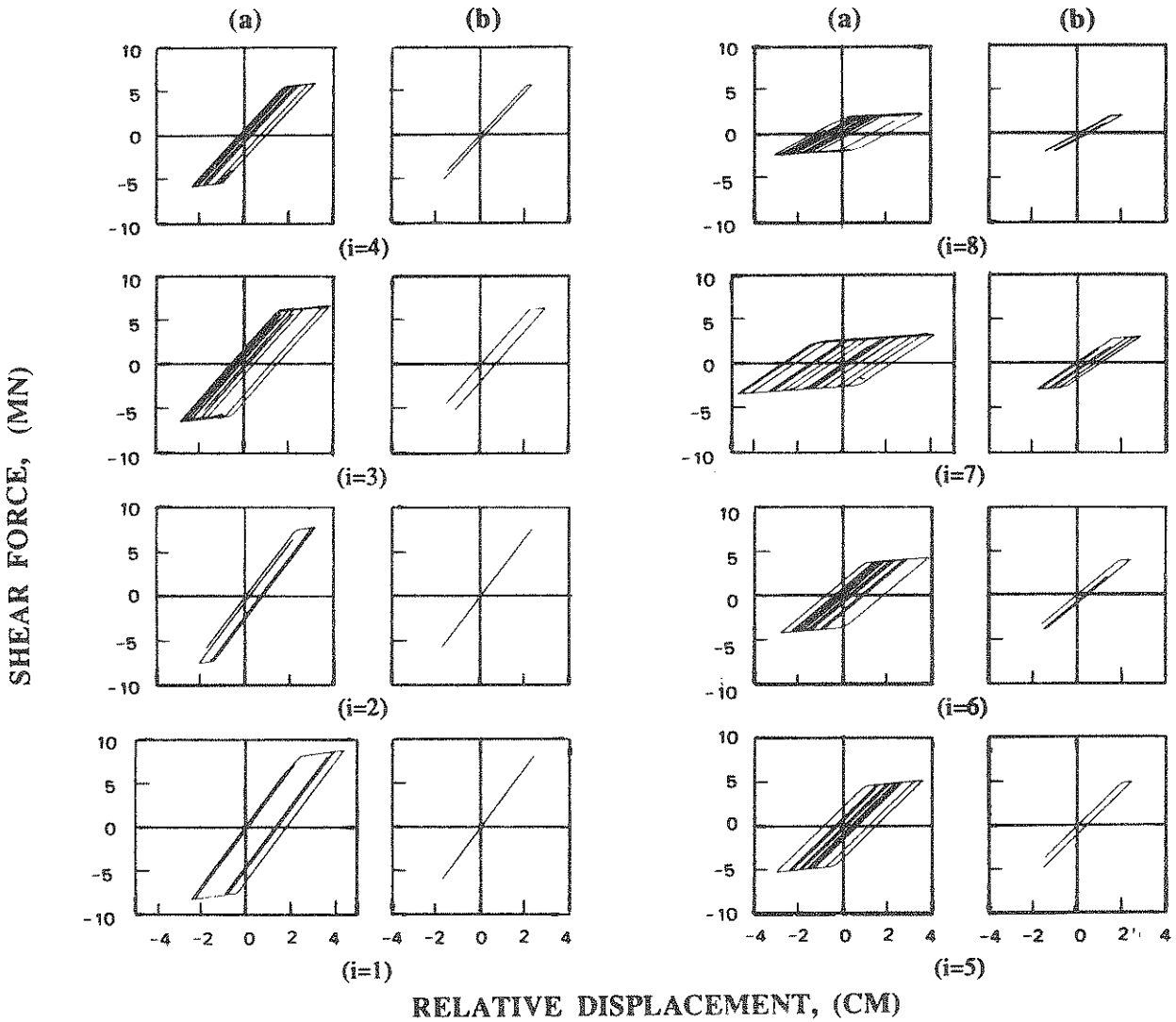

Fig. 43: Hysteresis Loops for Shear Force in Each Story Unit (0.55g Earthquake): (a) Without Control; (b) With Active Mass Damper Using State Variables x_i.

IV. CONCLUSIONS

Three instantaneous optimal algorithms have been developed for active control of nonlinear structures subjected to general dynamic loads. These include the instantaneous optimal closed-loop control algorithm, instantaneous optimal open-loop control algorithm, and instantaneous optimal closed-open-loop control algorithm. Under ideal control environments, these three optimal algorithms yield identical results. Emphasis is placed on applications of active control to inelastic tall buildings subjected to strong earthquake ground motions.

Instantaneous optimal control algorithms are derived by minimizing a time dependent quadratic performance index, whereas nonlinear equations of motion are solved using the Wilson-θ numerical method. These optimal control algorithms are shown to be computational efficient and suitable for on-line implementation of control systems to nonlinear tall buildings under earthquake excitations. While control of inelastic structures has been demonstrated exclusively, these optimal algorithms are equally applicable to structures with other types of nonlinearity, such as the geometric nonlinearity. Likewise, they are applicable to linear structures as a special case.

The following conclusions are obtained from numerical results: (1) Significant yielding of building structures, which generally results in a severe damage, can be mitigated or even eliminated through active control systems using the proposed optimal control algorithms. It is possible and may be practical to keep the structural response well within the elastic limits. (2) The proposed instantaneous optimal control algorithms are reliable and they are capable of consistently mitigating structural response quantities as regulated by the weighting matrices. (3) For the optimal design of building structures implemented by an active control system, the

appropriate choice of state variable for use in the instantaneous optimal control algorithms is important. (4) The combined use of passive/active control systems can be very beneficial. The basic idea behind the use of combined passive/active control devices as an integral protective system is that the structural response can be mitigated mainly by the passive systems, such as base isolators, whereas the damage of passive systems can be alleviated or even eliminated by the active system effectively. Preliminary results obtained in this report are quite encouraging and further research in this regard is being underway. Since base isolators usually exhibit nonlinear behavior, the optimal algorithms developed herein for controlling nonlinear structural systems including buildings with a base isolation system, is quite significant.

Frequently, after yielding occurs resulting from excessive deformation, structural properties may change and degrade thus deviating significantly from the original estimated values. In this connection, the adaptive control algorithm should be developed in conjunction with the instantaneous optimal control algorithms proposed herein. This is a subject of future research. Further, based on the present optimal control algorithms, the control efficiency is regulated at every time instant by the weighting matrices $\underset{\sim}{Q}$ and $\underset{\sim}{R}$. In order to guarantee that the structural response be always within specified limits, weighting matrices should be time dependent and they should be adaptive to the feedback response at every time instant t. This is a subject of research currently underway. Finally, experimental programs will be undertaken in the near future to verify the applicability of these proposed instantaneous optimal control algorithms.

REFERENCES

1. Masri, S.F., Bekey, G.A., and Caughey, T.K., "On-Line Control of Nonlinear Flexible Structures," Journal of Applied Mechanics, ASME, Vol. 49, No. 4, Dec. 1981, pp. 871-884.

2. Masri, S.F., Bekey, G.A., and Caughey, T.K., "Optimal Pulse Control of Flexible Structures," Journal of Applied Mechanics, ASME, Vol. 48, Sept. 1981, pp. 619-626.

3. Reinhorn, A.M., Manolis, G.D., and Wen, C.Y., "Active Control of Inelastic Structures," Journal of Engineering Mechanics, ASCE, Vol. 113, No. 3, March 1987, pp. 315-332.

4. Abdel-Rohman, M., and Nayfeh, A.H., "Active Control of Nonlinear Oscillations in Bridges," Journal of Engineering Mechanics, ASCE, Vol. 113, No. 3, Mar. 1987, pp. 335-334.

5. Dehghanyar, T. J., Masri, S. F., Miller, R. K., and Caughey, T. K., "On-Line Parameter Control of Nonlinear Flexible Structures," Second International Symposium on Structural Control, Univ. of Waterloo, Ontario, Canada, July 15-17, 1985.

6. Hrovat, D., Barak, P., and Robins, M., "Semi-Active vs Passive or Active Tuned Mass Dampers for Structural Control," ASCE, J. Engrg. Mech. Div., 109 (EM3), pp. 691-701, 1983.

7. Leipholz, H. H. (ed.), Structural Control, North-Holland Publishing Company, 1980, Proc. of First International Symposium on Structural Contron, University of Waterloo, Waterloo, Canada, 1980.

8. Leipholz, H.H.E., (ed.), Structural Control, Martinus Nijhoff Publishing Co., Amsterdam, 1987, Proc. of Second International Symposium on Structural Control, University of Waterloo, Waterloo, Canada, July 15-17, 1985.

9. Lin, R.C., Soong, T.T. and Reinhorn, A.M., "Experimental Evaluation of Instantaneous Optimal Algorithms for Structural Control," National Center For Earthquake Engineering Research, Technical Report NCEER-TR-87-0002, 1987.

10. Reinhorn, A.M., and Manolis, G.D., "Current State of Knowledge on Structure Control," The Shock and Vibration Digest, Vol. 17, No. 10, 1985, pp. 35-41.

11. Soong, T. T., and Skinner, G. T., "Experimental Study of Active Structural Control," Journal of the Engineering Mechanics Division, ASCE, Vol. 107, No. EM6, Dec. 1981, pp. 1057-1068.

12. Soong, T. T., Reinhorn, A. M., and Yang, J. N., "A Standardized Mode for Structural Control Experiments and Some Experimental Results," Second International Symposium on Structural Control, Univ. of Waterloo, Ontario, Canada, July 15-17, 1985, in Structural Control, (H.H.E. Leipholz, ed.), Martinus Nijhoff Publishing Co., Amsterdam, 1987, pp. 669-693.

13. Yang, J.N., Akbarpour, A., and Ghaemmaghami, P., "Optimal Control Algorithms For Earthquake Excited Building Structures," in Structural Control, Edited by H.H.E. Leipholz, Martinus, Nijhoff Publisher, 1987, Proc. 2nd International Symposium on Structural Control, University of Waterloo, Canada, July 15-17, 1985, pp. 748-761.

14. Yang, J.N., Akbarpour, and Ghaemmaghami, P., "Instantaneous Optimal Control Laws For Tall Buildings Under Seismic Excitations," National Center For Earthquake Engineering Research Technical Report, NCEER-TR-87-0007, June 10, 1987.

15. Yang, J.N., Akbarpour, A., and Ghaemmaghami, P., "New Optimal Control Algorithms For Structural Control," Journal of Engineering Mechanics, ASCE, Vol. 113, No. 9, Sept. 1987, pp. 1369-1386.

16. Yao, J. T. P., and Soong, T. T., "Importance of Experimental Studies in Structural Control," Reprint 84-010, ASCE, Atlanta Convention, May 14-18, 1984.

17. Yao, J. T. P., and Abdel-Rohman, M., "Research Topics for Practical Implementation of Structural Control," Second International Symposium on Structural Control, Univ. of Waterloo, Ontario, Canada, July 15-17, 1985.

18. Yang, J.N., and Soong, T.T., "Recent Advancement in Active Control of Civil Engineering Structures," paper to appear in Journal of Engineering Probabilistic Mechanics, Dec. 1987.

19. Yang, J.N., and Akbarpour, A., "Practical Considerations of Structural Control -- System Uncertainty, System Time Delay and Truncation of Small Control Forces," National Center For Earthquake Engineering Research Technical Report NCEER-TR-87-0018, Nov. 1987.

20. Kelly, J.M., "Aseismic Base Isolator: Its History and Prospects," Proceedings, World Congress on Joints and Bearing, American Concrete Institute Publication SP-70, Detroit, MI, 1981.

21. Kelly, J.M., "Control Devices for Earthquake Resistant Structural Design," Structural Control, H.H.E. Leipholz, Ed., North Holland, Amsterdam, The Netherlands, 1980, pp. 391-414.

22. Kelly, J.M., and Hudder, S.B., "Experimental Study of Lead and Elastomeric Dampers for Base Isolation System in Laminated Neoprene Bearing," Bulletin New Zealand Society for Earthquake Engineering, Vol. 15, No. 2, June, 1982, pp. 53-67.

23. Megget, L.M., "Analysis and Design of a Base-Isolated Reinforced Concrete Frame Building," Bulletin of New Zealand Society for Earthquake Engineering, Vol. 11, No. 4, Dec. 1978, pp. 245-254.

24. Yang, J.N., "Application of Optimal Control Theory To Civil Engineering Structures," Journal of Engineering Mechanics Division, ASCE, Vol. 101, No. EM-6, Dec. 1975, pp. 818-838.

25. Clough, R.W. and Penzies, J., Dynamics of Structures, Chapters 8 and 15, McGraw-Hill Book Company, New York, 1975.

26. Wilson, E.L., Fahoomand, I., and Bathe, K.J. "Nonlinear Dynamic Analysis of Complex Structures," Journal of Earthquake Engineering and Structural Dynamics, Vol. 1, 1973, pp. 241-252.

APPENDIX: THE WILSON-θ METHOD

The equations of motion of a structural system at any time instant t can be written as, Eq. (2)

$$\underset{\sim}{M}\,\ddot{\underset{\sim}{Y}}(t) + \underset{\sim}{F}_D(t) + \underset{\sim}{F}_s(t) = -\,\underset{\sim}{M}\,\underset{\sim}{v}\,\ddot{X}_0(t) + \underset{\sim}{H}\,\underset{\sim}{U}(t) \qquad \text{(I-1)}$$

in which $\ddot{X}_0(t)$ = earthquake base acceleration, $\underset{\sim}{Y}(t)$ = n-dimensional vector denoting the displacement of the structure relative to the moving base, $\underset{\sim}{M}$ = (nxn) constant mass matrix, $\underset{\sim}{U}(t)$ = r-dimensional control vector, $\underset{\sim}{H}$ = (nxr) matrix denoting the location of r controllers, and $\underset{\sim}{v}$ = unit vector of order n, i.e., $\underset{\sim}{v} = [1,1, \ldots, 1]'$. In Eq. (I-1), $\underset{\sim}{F}_D(t)$ is an n-dimensional damping vector denoting the damping force, and $\underset{\sim}{F}_s(t)$ is an n-dimensional stiffness vector denoting the stiffness restoring force. The equations of motion can be solved by a step-by-step numerical integration in which the response time history is divided into small time interval Δt and the equations of motion are satisfied at discrete time instants $n\Delta t$ for n = 1 ,2, ... At time t-Δt, the matrix equation of motion can be written as

$$\underset{\sim}{M}\,\ddot{\underset{\sim}{Y}}(t-\Delta t) + \underset{\sim}{F}_D(t-\Delta t) + \underset{\sim}{F}_s(t-\Delta t) = -\,\underset{\sim}{M}\,\underset{\sim}{v}\,\ddot{X}_0(t-\Delta t) + \underset{\sim}{H}\,\underset{\sim}{U}(t-\Delta t) \qquad \text{(I-2)}$$

The Wilson-θ method that results in an unconditionally stable solution will be used herein. Based on the Wilson-θ method, the response acceleration is assumed to vary linearly over an extended interval from t-Δt

to $t-\Delta t+\theta\Delta t$ for $\theta \geq 1.37$. The matrix equation of motion at $t-\Delta t+\theta\Delta t$ is given by

$$\underset{\sim}{M}\,\ddot{\underset{\sim}{Y}}(t-\Delta t+\theta\Delta t) + \underset{\sim}{F}_D(t-\Delta t+\theta\Delta t) + \underset{\sim}{F}_s(t-\Delta t+\theta\Delta t) = -\,\underset{\sim}{M}\,\underset{\sim}{v}\,\ddot{X}_0(t-\Delta t+\theta\Delta t) + \underset{\sim}{H}\,\underset{\sim}{U}(t-\Delta t+\theta\Delta t) \qquad (I\text{-}3)$$

Subtracting Eq. (I-2) from Eq. (I-3), one obtains the equation for incremental response from $t-\Delta t$ to $t-\Delta t+\theta\Delta t$,

$$\underset{\sim}{M}\,\hat{\underset{\sim}{\Delta}}\,\ddot{\underset{\sim}{Y}}(t) + \underset{\sim}{C}^*\,\hat{\underset{\sim}{\Delta}}\,\dot{\underset{\sim}{Y}}(t) + \underset{\sim}{K}^*\,\hat{\underset{\sim}{\Delta}}\,\underset{\sim}{Y}(t) = \hat{\underset{\sim}{\Delta}}\,\underset{\sim}{P}(t) \qquad (I\text{-}4)$$

in which

$$\begin{aligned}
\hat{\underset{\sim}{\Delta}}\,\ddot{\underset{\sim}{Y}}(t) &= \ddot{\underset{\sim}{Y}}(t-\Delta t+\theta\Delta t) - \ddot{\underset{\sim}{Y}}(t-\Delta t) \\
\hat{\underset{\sim}{\Delta}}\,\dot{\underset{\sim}{Y}}(t) &= \dot{\underset{\sim}{Y}}(t-\Delta t+\theta\Delta t) - \dot{\underset{\sim}{Y}}(t-\Delta t) \qquad (I\text{-}5) \\
\hat{\underset{\sim}{\Delta}}\,\underset{\sim}{Y}(t) &= \underset{\sim}{Y}(t-\Delta t+\theta\Delta t) - \underset{\sim}{Y}(t-\Delta t)
\end{aligned}$$

are the increments of acceleration, velocity and displacement in the time interval $(t-\Delta t,\ t-\Delta t+\theta\Delta t)$. In Eq. (I-4), the increments of damping force and stiffness restoring force are approximated by the following

$$\left.\begin{aligned}
\underset{\sim}{F}_D(t-\Delta t+\theta\Delta t) - \underset{\sim}{F}_D(t-\Delta t) &= \underset{\sim}{C}^*\,\hat{\underset{\sim}{\Delta}}\,\dot{\underset{\sim}{Y}}(t) \\
\underset{\sim}{F}_s(t-\Delta t+\theta\Delta t) - \underset{\sim}{F}_s(t-\Delta t) &= \underset{\sim}{K}^*\,\hat{\underset{\sim}{\Delta}}\,\underset{\sim}{Y}(t)
\end{aligned}\right\} \qquad (I\text{-}6)$$

in which $\underset{\sim}{C}^* = \underset{\sim}{C}^*(t-\Delta t)$ and $\underset{\sim}{K}^* = \underset{\sim}{K}^*(t-\Delta t)$ are influence coefficient matrices whose i-j elements, denoted by $C^*_{ij}(t-\Delta t)$ and $K^*_{ij}(t-\Delta t)$, respectively, are given as follows

$$C^*_{ij}(t-\Delta t) = \frac{\partial F_{Di}(t-\Delta t)}{\partial \dot{y}_j(t-\Delta t)}$$

$$K^*_{ij}(t-\Delta t) = \frac{\partial F_{si}(t-\Delta t)}{\partial y_j(t-\Delta t)} \qquad \text{(I-7)}$$

where $F_{Di}(t-\Delta t)$ and $F_{si}(t-\Delta t)$ are the ith elements of damping vector $\underset{\sim}{F}_D(t-\Delta t)$ and stiffness vector $\underset{\sim}{F}_s(t-\Delta t)$, respectively. Further, $\dot{y}_j(t-\Delta t)$ and $y_j(t-\Delta t)$ are the jth elements of the response vectors $\underset{\sim}{\dot{Y}}(t-\Delta t)$ and $\underset{\sim}{Y}(t-\Delta t)$, respectively. As observed from Fig. 2, these influence coefficients are tangent damping and tangent stiffness at t-Δt, respectively. Note that the damping vector $\underset{\sim}{F}_D(t-\Delta t)$ and the stiffness vector $\underset{\sim}{F}_s(t-\Delta t)$ are functions of $\underset{\sim}{\dot{Y}}(t-\Delta t)$ and $\underset{\sim}{Y}(t-\Delta t)$, respectively, i.e., $\underset{\sim}{F}_D(t-\Delta t) = \underset{\sim}{F}_D[\underset{\sim}{\dot{Y}}(t-\Delta t)]$ and $\underset{\sim}{F}_s(t-\Delta t) = \underset{\sim}{F}_s[\underset{\sim}{Y}(t-\Delta t)]$.

The incremental loading $\hat{\Delta}\ \underset{\sim}{P}(t)$ is approximated by

$$\hat{\Delta}\ \underset{\sim}{P}(t) = \theta \left\{ - \underset{\sim}{M}\ \underset{\sim}{v} \left[\ddot{X}_0(t) - \ddot{X}_0(t-\Delta t) \right] + \underset{\sim}{H} \left[\underset{\sim}{U}(t) - \underset{\sim}{U}(t-\Delta t) \right] \right\} \qquad \text{(I-8)}$$

Thus, given the response at t-Δt, the responses at t-Δt+$\theta\Delta$t and at t can be derived in the following.

Let τ be the time increment in the time interval $(t-\Delta t,\ t-\Delta t+\theta\Delta t)$, i.e., $0 \le \tau \le \theta\Delta t$. Then, the linear variation of the response acceleration in $(t-\Delta t,\ t-\Delta t+\theta\Delta t)$ can be expressed as

$$\ddot{\underset{\sim}{Y}}(t-\Delta t+\tau) = \ddot{\underset{\sim}{Y}}(t-\Delta t) + \frac{\tau}{\theta\Delta t}\left[\ddot{\underset{\sim}{Y}}(t-\Delta t+\theta\Delta t) - \ddot{\underset{\sim}{Y}}(t-\Delta t)\right] \tag{I-9}$$

Integration of Eq. (I-9) yields

$$\dot{\underset{\sim}{Y}}(t-\Delta t+\tau) = \dot{\underset{\sim}{Y}}(t-\Delta t) + \tau\,\ddot{\underset{\sim}{Y}}(t-\Delta t) + \frac{\tau^2}{2\theta\Delta t}\left[\ddot{\underset{\sim}{Y}}(t-\Delta t+\theta\Delta t) - \ddot{\underset{\sim}{Y}}(t-\Delta t)\right] \tag{I-10}$$

$$\underset{\sim}{Y}(t-\Delta t+\tau) = \underset{\sim}{Y}(t-\Delta t) + \tau\,\dot{\underset{\sim}{Y}}(t-\Delta t) + \frac{\tau^2}{2}\,\ddot{\underset{\sim}{Y}}(t-\Delta t) + \frac{\tau^3}{6\theta\Delta t}\left[\ddot{\underset{\sim}{Y}}(t-\Delta t+\theta\Delta t) - \ddot{\underset{\sim}{Y}}(t-\Delta t)\right] \tag{I-11}$$

For $\tau = \theta\Delta t$, Eqs. (I-10) and (I-11) become

$$\hat{\Delta}\,\dot{\underset{\sim}{Y}}(t) = \theta\,\Delta t\,\ddot{\underset{\sim}{Y}}(t-\Delta t) + \frac{\theta\Delta t}{2}\,\hat{\Delta}\,\ddot{\underset{\sim}{Y}}(t) \tag{I-12}$$

$$\hat{\Delta}\,\underset{\sim}{Y}(t) = \theta\,\Delta t\,\dot{\underset{\sim}{Y}}(t-\Delta t) + \frac{(\theta\Delta t)^2}{2}\,\ddot{\underset{\sim}{Y}}(t-\Delta t) + \frac{(\theta\Delta t)^2}{6}\,\hat{\Delta}\,\ddot{\underset{\sim}{Y}}(t) \tag{I-13}$$

The incremental acceleration $\hat{\Delta}\,\ddot{\underset{\sim}{Y}}(t)$ and incremental velocity $\hat{\Delta}\,\dot{\underset{\sim}{Y}}(t)$ in $(t-\Delta t,\ t-\Delta t+\theta\Delta t)$ can be expressed in terms of the incremental displacement $\hat{\Delta}\,\underset{\sim}{Y}(t)$ using Eqs. (I-12) and (I-13) as follows

$$\hat{\Delta}\,\ddot{\underline{Y}}(t) = \frac{6}{(\theta\Delta t)^2}\,\hat{\Delta}\,\underline{Y}(t) - \frac{6}{(\theta\Delta t)}\,\dot{\underline{Y}}(t-\Delta t) - 3\,\ddot{\underline{Y}}(t-\Delta t) \tag{I-14}$$

$$\hat{\Delta}\,\dot{\underline{Y}}(t) = \frac{3}{\theta\Delta t}\,\hat{\Delta}\,\underline{Y}(t) - 3\,\dot{\underline{Y}}(t-\Delta t) - \frac{\theta\Delta t}{2}\,\ddot{\underline{Y}}(t-\Delta t) \tag{I-15}$$

Substituting $\hat{\Delta}\,\ddot{\underline{Y}}(t)$ and $\hat{\Delta}\,\dot{\underline{Y}}(t)$ given by Eq. (I-14) and (I-15) into the matrix equation for incremental response in $(t-\Delta t,\ t-\Delta t+\theta\Delta t)$, Eq. (I-4), one can solve the only unknown $\hat{\Delta}\,\underline{Y}(t)$ as follows

$$\hat{\Delta}\,\underline{Y}(t) = \underline{G}^{-1}\,\underline{E}_1(t) \tag{I-16}$$

in which

$$\underline{G} = \frac{6}{(\theta\Delta t)^2}\,\underline{M} + \frac{3}{\theta\Delta t}\,\underline{C}^* + \underline{K}^* \tag{I-17}$$

$$\underline{E}_1(t) = \underline{M}\left[\frac{6}{(\theta\Delta t)}\,\dot{\underline{Y}}(t-\Delta t) + 3\,\ddot{\underline{Y}}(t-\Delta t)\right] + \underline{C}^*\left[3\,\dot{\underline{Y}}(t-\Delta t) + \frac{\theta\Delta t}{2}\,\ddot{\underline{Y}}(t-\Delta t)\right]$$

$$- \theta\,\underline{M}\,\underline{v}\left[\ddot{X}_0(t) - \ddot{X}_0(t-\Delta t)\right] + \theta\,\underline{H}\,[\underline{U}(t) - \underline{U}(t-\Delta t)] \tag{I-18}$$

Thus, the incremental responses $\hat{\Delta}\,\ddot{\underline{Y}}(t)$ and $\hat{\Delta}\,\dot{\underline{Y}}(t)$ in $(t-\Delta t,\ t-\Delta t+\theta\Delta t)$ are obtained by substituting Eq. (I-16) into Eqs. (I-14) and (I-15), respectively.

The incremental velocity and displacement vectors in the time interval $(t-\Delta t, t)$, denoted by $\Delta\dot{\underset{\sim}{Y}}(t)$ and $\Delta\underset{\sim}{Y}(t)$, respectively, are obtained from Eqs. (I-10) and (I-11) by setting $\tau=\Delta t$ as follows

$$\Delta\dot{\underset{\sim}{Y}}(t) = \dot{\underset{\sim}{Y}}(t) - \dot{\underset{\sim}{Y}}(t-\Delta t) = \Delta t\, \ddot{\underset{\sim}{Y}}(t-\Delta t) + \frac{\Delta t}{2\theta}\, \hat{\Delta}\, \ddot{\underset{\sim}{Y}}(t) \tag{I-19}$$

$$\Delta\underset{\sim}{Y}(t) = \underset{\sim}{Y}(t) - \underset{\sim}{Y}(t-\Delta t) = \Delta t\, \dot{\underset{\sim}{Y}}(t-\Delta t) + \frac{1}{2}(\Delta t)^2\, \ddot{\underset{\sim}{Y}}(t-\Delta t)$$

$$+ \frac{(\Delta t)^2}{6\theta}\, \hat{\Delta}\, \ddot{\underset{\sim}{Y}}(t) \tag{I-20}$$

in which $\hat{\Delta}\, \ddot{\underset{\sim}{Y}}(t)$ has been obtained in Eqs. (I-14) and (I-16), and $\underset{\sim}{Y}(t-\Delta t)$ and $\dot{\underset{\sim}{Y}}(t-\Delta t)$ are the given initial conditions at $t-\Delta t$. The acceleration response vector $\ddot{\underset{\sim}{Y}}(t-\Delta t)$ at $t-\Delta t$ appearing in Eqs. (I-19) and (I-20) are determined from the matrix equation of motion, Eq. (I-2),

$$\ddot{\underset{\sim}{Y}}(t-\Delta t) = \underset{\sim}{M}^{-1}\left[-\underset{\sim}{M}\ \underset{\sim}{v}\ \ddot{X}_0(t-\Delta t) + \underset{\sim}{H}\ \underset{\sim}{U}(t-\Delta t) - \underset{\sim}{F}_D(t-\Delta t) - \underset{\sim}{F}_s(t-\Delta t)\right] \tag{I-21}$$

Thus, the equations of motion are maintained at time $t-\Delta t$. As the numerical procedures are repeated at each time instant $t+n\Delta t$ for $n=1,2,\ldots$, the equations of motion are preserved at these discrete time points.

Substitution of Eqs. (I-21), (I-14) and (I-16) into Eqs. (I-20) and (I-19) leads to the following expressions for the incremental displacement $\Delta\underset{\sim}{Y}(t)$ and incremental velocity $\Delta\dot{\underset{\sim}{Y}}(t)$.

$$\Delta \underset{\sim}{Y}(t) = \theta^{-2}\, \underset{\sim}{E} \left\{ \underset{\sim}{T}_3\, \dot{\underset{\sim}{Y}}(t-\Delta t) + \underset{\sim}{T}_5 \left[\underset{\sim}{F}_s(t-\Delta t) + \underset{\sim}{F}_D(t-\Delta t) \right] - \underset{\sim}{T}_7 \left[\underset{\sim}{M}\, \underset{\sim}{v}\, \ddot{X}_0(t-\Delta t) \right.\right.$$

$$\left.\left. - \underset{\sim}{H}\, \underset{\sim}{U}\,(t-\Delta t) \right] \right\} + \theta^{-2} \left[\underset{\sim}{T}_1\, \ddot{X}_0(t) + \underset{\sim}{T}_2\, \underset{\sim}{U}(t) \right] \qquad \text{(I-22)}$$

$$\Delta \dot{\underset{\sim}{Y}}(t) = \theta^{-2}\, \underset{\sim}{E} \left\{ \underset{\sim}{T}_4\, \dot{\underset{\sim}{Y}}(t-\Delta t) + \underset{\sim}{T}_6 \left[\underset{\sim}{F}_s(t-\Delta t) + \underset{\sim}{F}_D(t-\Delta t) \right] - \underset{\sim}{T}_8 \left[\underset{\sim}{M}\, \underset{\sim}{v}\, \ddot{X}_0(t-\Delta t) \right.\right.$$

$$\left.\left. - \underset{\sim}{H}\, \underset{\sim}{U}\,(t-\Delta t) \right] \right\} + 3\, \theta^{-2} (\Delta t)^{-1} \left[\underset{\sim}{T}_1\, \ddot{X}_0(t) + \underset{\sim}{T}_2\, \underset{\sim}{U}(t) \right] \qquad \text{(I-23)}$$

in which

$$\left.\begin{aligned}
&\underset{\sim}{T}_1 = -\,\underset{\sim}{E}\,\underset{\sim}{M}\,\underset{\sim}{v}, \quad \underset{\sim}{T}_2 = \underset{\sim}{E}\,\underset{\sim}{H}\,, \quad \underset{\sim}{T}_3 = (6/\Delta t)\underset{\sim}{M} + 3\theta \underset{\sim}{C}^* + \Delta t(\theta^2 - 1)\, \underset{\sim}{K}^* \\
&\underset{\sim}{T}_4 = -\,3\, \underset{\sim}{K}^*, \quad \underset{\sim}{T}_5 = -(3\underset{\sim}{I}_1 + \underset{\sim}{S}_1), \quad \underset{\sim}{T}_6 = -(6/\Delta t)\underset{\sim}{I}_1 - \underset{\sim}{S}_2 \\
&\underset{\sim}{T}_7 = 2\, \underset{\sim}{I}_1 + \underset{\sim}{S}_1, \quad \underset{\sim}{T}_8 = (3/\Delta t)\underset{\sim}{I}_1 + \underset{\sim}{S}_2 \\
&\underset{\sim}{E} = \left[\frac{6}{(\theta \Delta t)^2}\, \underset{\sim}{M} + \frac{3}{\theta \Delta t}\, \underset{\sim}{C}^* + \underset{\sim}{K}^* \right]^{-1} \\
&\underset{\sim}{S}_1 = \left[\Delta t\, (1.5\theta - 1)\, \underset{\sim}{C}^* + 0.5(\Delta t)^2(\theta^2 - \theta)\, \underset{\sim}{K}^* \right] \underset{\sim}{M}^{-1} \\
&\underset{\sim}{S}_2 = \left[3(\theta - 1)\, \underset{\sim}{C}^* + \Delta t \theta (\theta - 1.5)\, \underset{\sim}{K}^* \right] \underset{\sim}{M}^{-1}
\end{aligned}\right\} \qquad \text{(I-24)}$$

The response state vectors $\underset{\sim}{Z}(t)$ and $\underset{\sim}{Z}(t-\Delta t)$ at time t and t-Δt, respectively, are defined as

$$\underset{\sim}{Z}(t) = \begin{bmatrix} \underset{\sim}{Y}(t) \\ \dot{\underset{\sim}{Y}}(t) \end{bmatrix} \quad , \quad \underset{\sim}{Z}(t-\Delta t) = \begin{bmatrix} \underset{\sim}{Y}(t-\Delta t) \\ \dot{\underset{\sim}{Y}}(t-\Delta t) \end{bmatrix} \tag{I-25}$$

and they are related as follows

$$\underset{\sim}{Z}(t) = \underset{\sim}{Z}(t-\Delta t) + \begin{bmatrix} \Delta\underset{\sim}{Y}(t) \\ \Delta\dot{\underset{\sim}{Y}}(t) \end{bmatrix} \tag{I-26}$$

where $\Delta\underset{\sim}{Y}(t)$ and $\Delta\dot{\underset{\sim}{Y}}(t)$ are obtained in Eqs. (I-22) and (I-23), respectively.

Substituting Eqs. (I-22) and (I-23) into Eq. (I-26), one obtains the response state vector $\underset{\sim}{Z}(t)$ as follows

$$\underset{\sim}{Z}(t) = \underset{\sim}{D}^{*}(t-\Delta t) + \underset{\sim}{A}_1 \ddot{X}_0(t) + \underset{\sim}{A}_2\ \underset{\sim}{U}(t) \tag{I-27}$$

in which

$$\underset{\sim}{D}^{*}(t-\Delta t) = \underset{\sim}{A}_3\ \underset{\sim}{Z}(t-\Delta t) + \underset{\sim}{A}_4[\underset{\sim}{F}_D(t-\Delta t) + \underset{\sim}{F}_s(t-\Delta t)]$$
$$+ \underset{\sim}{A}_5\ \ddot{X}_0(t-\Delta t) + \underset{\sim}{A}_6\ \underset{\sim}{U}(t-\Delta t) \tag{I-28}$$

In Eqs. (I-27) and (I-28), $\underset{\sim}{A}_j$ for j=1,2,...,6 are vectors or matrices given in the following

$$\left.\begin{aligned}
&\underset{\sim}{A}_1 = \theta^{-2}\begin{bmatrix} \underset{\sim}{T}_1 \\ \hline \frac{3}{\Delta t}\,\underset{\sim}{T}_1 \end{bmatrix} \quad ; \quad \underset{\sim}{A}_2 = \theta^{-2}\begin{bmatrix} \underset{\sim}{T}_2 \\ \hline \frac{3}{\Delta t}\,\underset{\sim}{T}_2 \end{bmatrix} \\
&\underset{\sim}{A}_3 = \left[\begin{array}{c|c} \underset{\sim}{I}_1 & \theta^{-2}\underset{\sim}{E}\,\underset{\sim}{T}_3 \\ \hline \underset{\sim}{0} & \underset{\sim}{I}_1 + \theta^{-2}\underset{\sim}{E}\,\underset{\sim}{T}_4 \end{array}\right] \quad ; \quad \underset{\sim}{A}_4 = \theta^{-2}\begin{bmatrix} \underset{\sim}{E}\,\underset{\sim}{T}_5 \\ \hline \underset{\sim}{E}\,\underset{\sim}{T}_6 \end{bmatrix} \\
&\underset{\sim}{A}_5 = -\theta^{-2}\begin{bmatrix} \underset{\sim}{E}\,\underset{\sim}{T}_7 \\ \hline \underset{\sim}{E}\,\underset{\sim}{T}_8 \end{bmatrix}\underset{\sim}{M}\,\underset{\sim}{v} \quad ; \quad \underset{\sim}{A}_6 = \theta^{-2}\begin{bmatrix} \underset{\sim}{E}\,\underset{\sim}{T}_7 \\ \hline \underset{\sim}{E}\,\underset{\sim}{T}_8 \end{bmatrix}\underset{\sim}{H}
\end{aligned}\right\} \qquad \text{(I-29)}$$

in which $\underset{\sim}{I}_1$ is an (nxn) identity matrix.

APPENDIX II: BASIC EQUATIONS OF MOTION

With the state variable $y_j(t)$ being defined as the relative displacement of the jth floor with respect to the moving base, the matrix equation of motion for a one-dimensional n-degree-of-freedom shear-beam type tall building implemented by an active control system can be written as

$$\underset{\sim}{M}\,\ddot{\underset{\sim}{Y}}(t) + \underset{\sim}{C}[\dot{\underset{\sim}{Y}}(t)]\,\dot{\underset{\sim}{Y}}(t) + \underset{\sim}{K}[\underset{\sim}{Y}(t)]\,\underset{\sim}{Y}(t) = -\underset{\sim}{M}\,\underset{\sim}{\nu}\,\ddot{X}_0(t) + \underset{\sim}{H}\,\underset{\sim}{U}(t) \qquad \text{(II-1)}$$

For the structure implemented by an active mass damper on the top floor, one obtains the follows matrices and vectors: $\underset{\sim}{Y}(t) = [\, y_1(t), y_2(t), \ldots, y_n(t), y_d(t)\,]'$, $\underset{\sim}{M}$ = a (n+1) by (n+1) diagonal matrix with the jth diagonal element being m_j where $m_{n+1} = m_d$, $\underset{\sim}{\nu}$ = a (n+1) unit vector = $[1,1,\ldots 1]'$, $\underset{\sim}{H}$ = a (n+1) vector = $[0,0,0,\ldots 0, -1,1]'$, $\underset{\sim}{U}(t)$ = a one-component vector, and $\underset{\sim}{C}$ and $\underset{\sim}{K}$ are (n+1) x (n+1) matrices

$$\underset{\sim}{K} = \begin{bmatrix} k_1+k_2 & -k_2 & 0 & & \\ -k_2 & k_2+k_3 & -k_3 & & \\ & \ddots & \ddots & \ddots & \\ & & & k_n+k_d & -k_d \\ & & & -k_d & k_d \end{bmatrix} \qquad \text{(II-2)}$$

$$\underset{\sim}{C} = \begin{bmatrix} c_1+c_2 & -c_2 & 0 & & \\ -c_2 & c_2+c_3 & -c_3 & & \\ & \ddots & \ddots & \ddots & \\ & & & c_n+c_d & -c_d \\ & & & -c_d & c_d \end{bmatrix} \qquad \text{(II-3)}$$

The quantities given above are described in the following: m_j = mass of the jth floor, m_d = mass of the mass damper, k_j = stiffness of the jth story unit, k_d = stiffness of the mass damper, c_j = damping coefficient of the jth story unit, and c_d=damping coefficient of the mass damper.

For a structure implemented by r tendon controllers, one obtains the following: $\underset{\sim}{Y}(t) = [y_1(t), y_2(t),\ldots,y_n(t)]'$, $\underset{\sim}{M}$ = an (nxn) diagonal matrix with the jth diagonal element being m_j, $\underset{\sim}{\nu}$ = an n unit vector = $[1,1,\ldots,1]'$, $\underset{\sim}{U}(t)$ = a r-dimensional vector = $[U_1(t), U_2(t),\ldots,U_r(t)]$ and $\underset{\sim}{C}$ and $\underset{\sim}{K}$ are (nxn) matrices obtained from Eqs. (II-3) and (II-2), respectively, by (i) deleting the last raw and column, and (ii) setting $k_d = c_d = 0$.

$\underset{\sim}{H}$ is an (nxr) location matrix that can be obtained from the (nxn) full-location matrix $\underset{\sim}{H}^*$

$$\underset{\sim}{H}^* = \begin{bmatrix} -1 & 1 & 0 & 0 & 0 & & \\ 0 & -1 & 1 & 0 & 0 & & \\ & 0 & -1 & 1 & 0 & & \\ & & 0 & -1 & 1 & & \\ & & & \ddots & \ddots & \ddots & \\ & & & & 0 & -1 & 1 \\ & & & & & 0 & -1 \end{bmatrix} \qquad \text{(II-4)}$$

When every story unit is installed with a tendon controller, $\underset{\sim}{H}^*$ should be used. With only r (<n) controllers, $\underset{\sim}{H}$ matrix is obtained from $\underset{\sim}{H}^*$ by keeping those columns corresponding to r controllers.

Let $x_j(t)$ be the relative displacement between the j th floor and the j-1 th floor (i.e., the deformation of the jth story unit). With the state variables $[\, x_1(t), x_2(t),\ldots,x_n(t)\,]$, the matrix equation of motion can be written as

$$\underset{\sim}{M}\,\ddot{\underset{\sim}{X}}(t) + \underset{\sim}{C}[\dot{\underset{\sim}{X}}(t)]\,\dot{\underset{\sim}{X}}(t) + \underset{\sim}{K}[\underset{\sim}{X}(t)]\,\underset{\sim}{X}(t) = -\underset{\sim}{V}\ddot{X}_0(t) + \underset{\sim}{H}\,\underset{\sim}{U}(t) \qquad \text{(II-5)}$$

in which the location matrix $\underset{\sim}{H}$ and the control vector $\underset{\sim}{U}(t)$ are identical to those given in Eq. (II-1).

For a structure implemented by an active mass damper on the top floor, the following vectors and matrices are obtained: $\underset{\sim}{X}(t) = [\, x_1(t), x_2(t),\ldots,$

$x_n(t)$, $x_d(t)$]', $\underset{\sim}{V}$ = an (n+1) vector = [m_1, m_2,..., m_n, m_d]', and $\underset{\sim}{M}$, $\underset{\sim}{C}$ and $\underset{\sim}{K}$ are (n+1) x (n+1) matrices given as follows

$$\underset{\sim}{M} = \begin{bmatrix} m_1 & 0 & 0 & 0 & & \\ m_2 & m_2 & 0 & 0 & & \\ m_3 & m_3 & m_3 & 0 & & \\ | & | & | & & & \\ | & | & | & & & \\ | & | & | & & & \\ m_n & m_n & - & - & m_n & 0 \\ m_d & m_d & - & - & m_d & m_d \end{bmatrix} \qquad \text{(II-6)}$$

$$\underset{\sim}{K} = \begin{bmatrix} k_1 & -k_2 & & & \underset{\sim}{0} & \\ & k_2 & -k_3 & & & \\ & & k_3 & -k_4 & & \\ & \underset{\sim}{0} & & \diagdown & \diagdown & \\ & & & & k_n & -k_d \\ & & & & & k_d \end{bmatrix} \qquad \text{(II-7)}$$

$$\underset{\sim}{C} = \begin{bmatrix} c_1 & -c_2 & & & \underset{\sim}{0} & \\ & c_2 & -c_3 & & & \\ & & c_3 & -c_4 & & \\ & \underset{\sim}{0} & & \diagdown & \diagdown & \\ & & & & c_n & -c_d \\ & & & & & c_d \end{bmatrix} \qquad \text{(II-8)}$$

For a structure implemented by r tendon constrollers, one obtains the following: $\underset{\sim}{X}(t) = [x_1(t), x_2(t),..., x_{n(t)}]'$, $\underset{\sim}{V}$ = an n vector = [m_1, m_2,...,m_n]', and $\underset{\sim}{M}$, $\underset{\sim}{K}$ and $\underset{\sim}{C}$ are (nxn) matrices obtained from Eqs. (II-6), (II-7) and (II-8), respectively, by (i) deleting the last raw and column, and (ii) setting $m_d = c_d = k_d = 0$.

NATIONAL CENTER FOR EARTHQUAKE ENGINEERING RESEARCH
LIST OF PUBLISHED TECHNICAL REPORTS

The National Center for Earthquake Engineering Research (NCEER) publishes technical reports on a variety of subjects related to earthquake engineering written by authors funded through NCEER. These reports are available from both NCEER's Publications Department and the National Technical Information Service (NTIS). Requests for reports should be directed to the Publications Department, National Center for Earthquake Engineering Research, State University of New York at Buffalo, Red Jacket Quadrangle, Buffalo, New York 14261. Reports can also be requested through NTIS, 5285 Port Royal Road, Springfield, Virginia 22161. NTIS accession numbers are shown in parenthesis, if available.

NCEER-87-0001 "First-Year Program in Research, Education and Technology Transfer," 3/5/87, (PB88-134275/AS).

NCEER-87-0002 "Experimental Evaluation of Instantaneous Optimal Algorithms for Structural Control," by R.C. Lin, T.T. Soong and A.M. Reinhorn, 4/20/87, (PB88-134341/AS).

NCEER-87-0003 "Experimentation Using the Earthquake Simulation Facilities at University at Buffalo," by A.M. Reinhorn and R.L. Ketter, to be published.

NCEER-87-0004 "The System Characteristics and Performance of a Shaking Table," by J.S. Hwang, K.C. Chang and G.C. Lee, 6/1/87, (PB88-134259/AS).

NCEER-87-0005 "A Finite Element Formulation for Nonlinear Viscoplastic Material Using a Q Model," by O. Gyebi and G. Dasgupta, to be published.

NCEER-87-0006 "SMP - Algebraic Codes for Two and Three Dimensional Finite Element Formulations," by X. Lee and G. Dasgupta, to be published.

NCEER-87-0007 "Instantaneous Optimal Control Laws for Tall Buildings Under Seismic Excitations," by J.N. Yang, A. Akbarpour and P. Ghaemmaghami, 6/10/87, (PB88-134333/AS).

NCEER-87-0008 "IDARC: Inelastic Damage Analysis of Reinforced Concrete-Frame Shear-Wall Structures," by Y.J. Park, A.M. Reinhorn and S.K. Kunnath, 7/20/87, (PB88-134325/AS).

NCEER-87-0009 "Liquefaction Potential for New York State: A Preliminary Report on Sites in Manhattan and Buffalo," by M. Budhu, V. Vijayakumar, R.F. Giese and L. Baumgras, 8/31/87.

NCEER-87-0010 "Vertical and Torsional Vibration of Foundations in Inhomogeneous Media," by A.S. Veletsos and K.W. Dotson, 6/1/87, (PB88-134291/AS).

NCEER-87-0011 "Seismic Probabilistic Risk Assessment and Seismic Margin Studies for Nuclear Power Plants," by Howard H.M. Hwang, 6/15/87, (PB88-134267/AS).

NCEER-87-0012 "Parametric Studies of Frequency Response of Secondary Systems Under Ground-Acceleration Excitations," by Y. Yong and Y.K. Lin, 6/10/87, (PB88-134309/AS).

NCEER-87-0013 "Frequency Response of Secondary Systems Under Seismic Excitations," by J.A. HoLung, J. Cai and Y.K. Lin, 7/31/87, (PB88-134317/AS).

NCEER-87-0014 "Modelling Earthquake Ground Motions in Seismically Active Regions Using Parametric Time Series Methods," G.W. Ellis and A.S. Cakmak, 8/25/87, (PB88-134283/AS).

NCEER-87-0015 "Detection and Assessment of Seismic Structural Damage," by E. DiPasquale and A.S. Cakmak, 8/25/87.

NCEER-87-0016 "Pipeline Experiment at Parkfield, California," by J. Isenberg and E. Richardson, 9/15/87.

NCEER-87-0017 "Digital Simulations of Seismic Ground Motion," by M. Shinozuka, G. Deodatis and T. Harada, 8/31/87, (PB88-155197/AS).

NCEER-87-0018 "Practical Considerations for Structural Control: System Uncertainty, System Time Delay and Truncation of Small Forces," J. Yang and A. Akbarpour, 8/10/87.

NCEER-87-0019 "Modal Analysis of Nonclassically Damped Structural Systems Using Canonical Transformation," by J.N. Yang, S. Sarkani and F.X. Long, 9/27/87.

NCEER-87-0020 "A Nonstationary Solution in Random Vibration Theory," by J.R. Red-Horse and P.D. Spanos, 11/3/87.

NCEER-87-0021 "Horizontal Impedances for Radially Inhomogeneous Viscoelastic Soil Layers," by A.S. Veletsos and K.W. Dotson, 10/15/87, (PB88-150859/AS).

NCEER-87-0022 "Seismic Damage Assessment of Reinforced Concrete Members," by Y.S. Chung, C. Meyer and M. Shinozuka, 10/9/87, (PB88-150867/AS).

NCEER-87-0023 "Active Structural Control in Civil Engineering," by T.T. Soong, 11/11/87.

NCEER-87-0024 Vertical and Torsional Impedances for Radially Inhomogeneous Viscoelastic Soil Layers," by K.W. Dotson and A.S. Veletsos, 12/87.

NCEER-87-0025 "Proceedings from the Symposium on Seismic Hazards, Ground Motions, Soil-Liquefaction and Engineering Practice in Eastern North America, October 20-22, 1987, edited by K.H. Jacob, 12/87.

NCEER-87-0026 "Report on the Whittier-Narrows, California, Earthquake of October 1, 1987," by J. Pantelic and A. Reinhorn, 11/87.

NCEER-87-0027 "Design of a Modular Program for Transient Nonlinear Analysis of Large 3-D Building Structures," by S. Srivastav and J.F. Abel, 12/30/87.

NCEER-88-0001 "Workshop on Seismic Computer Analysis and Design With Interactive Graphics," by J.F. Abel and C.H. Conley, 1/18/88.

NCEER-88-0002 "Optimal Control of Nonlinear Structures," J.N. Yang, F.X. Long and D. Wong, 1/22/88, to be published.

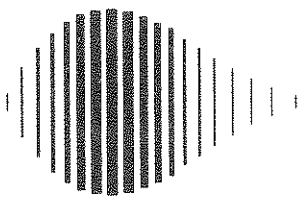

National Center for Earthquake Engineering Research
State University of New York at Buffalo